

# **Biophysical and biochemical analysis of protein-ligand interactions in anti-infective drug discovery**

## **Dissertation**

zur Erlangung des Grades

des Doktors der Naturwissenschaften

der Naturwissenschaftlich-Technischen Fakultät III

Chemie, Pharmazie, Bio- und Werkstoffwissenschaften

der Universität des Saarlandes

von

**Martina Frauke Fruth**

Saarbrücken

2016

Tag des Kolloquiums:	08.07.2016
Dekan:	Prof. Dr. Dirk Bähre
Berichterstatter:	Prof. Dr. Rolf W. Hartmann Prof. Dr. Dr. h.c. Hans H. Maurer
Vorsitz:	Prof. Dr. Claus-Michael Lehr
Akad. Mitarbeiter:	Dr. Stephan Laggai

Die vorliegende Arbeit wurde von Februar 2011 bis Oktober 2015 unter Anleitung von Herrn Univ.-Prof. Dr. Rolf W. Hartmann in der Fachrichtung 8.2 Pharmazeutische und Medizinische Chemie der Naturwissenschaftlich-Technischen Fakultät III der Universität des Saarlandes sowie am Helmholtz-Institut für Pharmazeutische Forschung Saarland (HIPS) angefertigt.

“The great tragedy of science – the slaying of a beautiful hypothesis by an ugly fact.”

Thomas Henry Huxley

## SUMMARY

The increasing number of antibiotic-resistant pathogens has created an urgent demand for novel treatment options to combat infectious diseases. In this thesis, test systems have been established enabling hit identification, lead optimization, and characterization to contribute to the development of potent and innovative anti-infectives, which overcome existing bacterial resistances.

In the first approach, inhibitors of the RNA polymerase ‘switch region’ were studied. Using biochemical and biophysical techniques the exact binding site and ligand binding mode of the ureidothiophene-2-carboxylic acid inhibitors were elucidated. Mode of action studies revealed that congeners of this structural class inhibit the bacterial transcription in the initiation phase. Moreover, the ureidothiophene-2-carboxylic acid inhibitors do not show any cross-resistances with rifampicin or myxopyronin and possess good antibacterial activity in clinically relevant multidrug-resistant MRSA strains.

In the second approach, inhibitors of the CsrA-RNA interaction were discovered by using a screening and a ligand-based approach. CsrA is an mRNA-binding regulatory protein being essential for full virulence of bacteria and thus, it represents an attractive target for anti-infective drug discovery. For this purpose, a test system based on biophysical methods was established, which enabled the identification and characterization of first small molecule and ligand-derived inhibitors of the CsrA-RNA interaction.

## ZUSAMMENFASSUNG

Aufgrund zunehmender Antibiotika-Resistenzen sind neue effiziente Therapiemöglichkeiten dringend erforderlich um eine erfolgreiche Behandlung von Infektionskrankheiten zu gewährleisten. Um die Entwicklung potenter und innovativer Anti-Infektiva zu unterstützen, wurden im Rahmen dieser Arbeit Testsysteme etabliert, welche die Identifizierung von Hitverbindungen sowie die Lead-Optimierung und -Charakterisierung ermöglichen.

Im ersten Ansatz wurden Hemmstoffe der RNA-Polymerase ‘switch region’ untersucht. Unter Anwendung biochemischer und biophysikalischer Methoden konnte deren genaue Bindestelle sowie der Ligandbindungsmodus aufgeklärt werden. Wirkmechanistische Studien haben gezeigt, dass die untersuchten Inhibitoren die Initiationsphase der Transkription hemmen. Die Inhibitoren wiesen keine Kreuzresistenz mit Rifampicin oder Myxopyronin auf und waren zudem wirksam gegen klinisch relevante MRSA Stämme.

Der zweite Ansatz hatte die Entdeckung von Inhibitoren der CsrA-RNA Interaktion zum Ziel, welches mit einem Screening und einem Ligand-basierten Ansatz verfolgt wurde. Bei CsrA handelt es sich um ein mRNA bindendes, regulatorisches Protein, das essentiell für volle bakterielle Virulenz ist und somit ein interessantes Target für die Entwicklung neuer Anti-Infektiva darstellt. Zu diesem Zweck wurde ein auf biophysikalischen Methoden basierendes Testsystem etabliert, mit dem erste ‚Small Molecule‘ sowie Ligand-basierte Hemmstoffe identifiziert und charakterisiert werden konnten.

## PUBLICATIONS INCLUDED IN THIS THESIS

This thesis is divided into three publications, which are referred to in the text by the letters A-C.

**A Binding mode characterization of novel RNA polymerase inhibitors using a combined biochemical and NMR approach**

Martina Fruth, Alberto Plaza, Stefan Hinsberger, J. Henning Sahner, Jörg Haupenthal, Markus Bischoff, Rolf Jansen, Rolf Müller, and Rolf W. Hartmann

*ACS Chem. Biol.*, 2014, **9**, 2656–2663.

**B Expanding the scaffold for bacterial RNA polymerase inhibitors: design, synthesis and structure–activity relationships of ureido-heterocyclic-carboxylic acids**

Walid A. M. Elgaher, Martina Fruth, Matthias Groh, Jörg Haupenthal, and Rolf W. Hartmann

*RSC Adv.*, 2014, **4**, 2177-2194.

**C Discovery of the first small molecule CsrA-RNA interaction inhibitors using biophysical screening technologies**

Christine K. Maurer<sup>‡</sup>, Martina Fruth<sup>‡</sup>, Martin Empting, Olga Avrutina, Jörn Hoßmann, Suvd Nadmid, Jan Gorges, Jennifer Herrmann, Uli Kazmaier, Petra Dersch, Rolf Müller, and Rolf W. Hartmann

<sup>‡</sup> These authors contributed equally to this work.

*Future Med. Chem.*, 2016, **8**, 931-947.

## CONTRIBUTION REPORT

The author wishes to clarify her contributions to the publications **A-C** included in this thesis.

- A** The author significantly contributed to the design of the study, planned, and executed the mutagenesis experiments, the generation of resistant spontaneous mutants, the purification of wild type and mutant *E. coli* RNAP, inhibitor testing in the *in vitro* transcription assay, and assessing their antibacterial activity against *E. coli* TolC wild type and *E. coli* TolC ‘switch region’ mutants. Furthermore, she contributed to the NMR experiments, interpreted the results, and wrote the manuscript.
- B** The author performed the generation of the Rif-resistant *E. coli* TolC mutants. Furthermore, she determined the antibacterial activity of the compounds against *E. coli* TolC wild type and Rif-resistant *E. coli* TolC strains and contributed to writing the correspondent parts of the manuscript.
- C** The author significantly contributed to the design of the study, planned and executed the SPR experiments, and performed the heterologous expression and purification of *Y. pseudotuberculosis* CsrA. Furthermore, she interpreted the results and wrote the manuscript.

## FURTHER PUBLICATION OF THE AUTHOR, WHICH IS NOT PART OF THIS THESIS

**D Peptide-based investigation of the *Escherichia coli* RNA polymerase  $\sigma^{70}$ :core interface as target site**

Kristina Hüsecken, Matthias Negri, Martina Fruth, Stefan Boettcher, Rolf W. Hartmann, and Jörg Haupenthal

*ACS Chem. Biol.*, 2013, **8**, 758-766.

## ABBREVIATIONS

3D	Three-dimensional
CDAD	<i>Clostridium difficile</i> -associated diarrhea
CDC	U.S. Centers of Disease Control and Prevention
CsrA	Carbon storage regulator protein A
dMyx	Desmethyl myxopyronin
DNA	Deoxyribonucleic acid
FDA	US Food and Drug Administration
FP	Fluorescence polarization
HPLC	High performance liquid chromatography
INPHARMA	Interligand NOEs for pharmacophore mapping
MDR	Multidrug-resistant
MIC	Minimal inhibitory concentration
Myx	Myxopyronin
NMR	Nuclear magnetic resonance
NOE	Nuclear Overhauser effect
NOESY	Nuclear Overhauser effect spectroscopy
nts	Nucleotides
PA $\beta$ N	Phenylalanine-arginine $\beta$ -naphthylamide
PCR	Polymerase chain reaction
PoC	Proof of concept
Rif	Rifampicin
RNA	Ribonucleic acid

RNAP	RNA polymerase
RP <sub>c</sub>	Closed RNAP-promoter complex
RP <sub>o</sub>	Open RNAP-promoter complex
Rsm	Regulator of secondary metabolism
RU	Resonance unit
SAR	Structure-activity relationship
SPR	Surface plasmon resonance
STD	Saturation transfer difference
SDM	Site-directed mutagenesis
TB	Tuberculosis
WHO	World Health Organization
XDR	Extensively drug-resistant

## Table of contents

<b>1</b>	<b>Introduction .....</b>	<b>1</b>
1.1	RNA polymerase (RNAP) .....	5
1.1.1	Structure and function .....	5
1.1.2	RNAP as a target for antimicrobial therapy .....	7
1.1.3	The RNAP ‘switch region’ .....	9
1.2	Carbon storage regulator protein A (CsrA).....	12
1.2.1	The Csr system .....	12
1.2.2	Function and structure .....	12
1.2.3	CsrA regulates bacterial virulence.....	14
1.3	Analysis of protein-ligand interactions .....	16
1.3.1	Surface plasmon resonance spectroscopy.....	16
1.3.2	Ligand-based nuclear magnetic resonance (NMR) methods.....	18
1.3.2.1	Saturation transfer difference NMR .....	18
1.3.2.2	Interligand NOE for pharmacophore mapping.....	20
1.3.3	Mutagenesis.....	21
<b>2</b>	<b>Aim of the thesis .....</b>	<b>22</b>
<b>3</b>	<b>Results.....</b>	<b>24</b>
3.1	Binding mode characterization of novel RNA polymerase inhibitors using a combined biochemical and NMR approach.....	24
3.2	Expanding the scaffold for bacterial RNA polymerase inhibitors: design, synthesis and structure–activity relationships of ureido-heterocyclic-carboxylic acids.....	43
3.3	Discovery of the first small molecule CsrA-RNA interaction inhibitors using biophysical screening technologies .....	83
<b>4</b>	<b>Final discussion.....</b>	<b>84</b>
4.1	Characterization of RNAP ‘switch region’ inhibitors.....	84
4.1.1	Aryl-ureido-heterocyclic-carboxylic acids as novel RNAP inhibitors.....	84
4.1.2	Binding site elucidation.....	86
4.1.3	Potential of defeating antibiotic resistance.....	89

4.1.4	Evaluation of the RNAP ‘switch region’ as target for anti-infective drug development ..	90
4.1.5	Outlook.....	91
4.2	Discovery of inhibitors of the CsrA-RNA interaction .....	92
4.2.1	Hit identification and <i>in vitro</i> activity .....	92
4.2.2	Outlook.....	94
<b>5</b>	<b>References .....</b>	<b>96</b>
<b>6</b>	<b>Supporting information .....</b>	<b>107</b>
6.1	Supporting Information for Publication A.....	107
<b>7</b>	<b>Appendix .....</b>	<b>121</b>
7.1	Curriculum Vitae .....	121
7.2	Poster presentations .....	122
<b>8</b>	<b>Acknowledgments.....</b>	<b>123</b>



# 1 Introduction

Throughout history, humankind has recurrently encountered severe bacterial infectious diseases such as typhoid fever, tuberculosis, plague, and cholera leading notably to morbidity and mortality in those days (Tenover, 2006). With the discovery of the first antibiotics and, consequently, the market launches of Prontosil<sup>®</sup> (a sulfonamide antibiotic) and benzylpenicillin in the late 1930's and early 1940's, respectively, the situation drastically improved (Powers, 2004; Bentley, 2009). From this time on, physicians had been able to treat and control a multitude of staphylococcal, streptococcal, pneumococcal, meningococcal, gonococcal as well as *Escherichia coli* and *Corynebacterium diphtheriae*-associated infections (Feldman, 1972). In the following twenty years, referred to as 'the golden era of antibiotic discovery', most of the major antibiotic classes had been discovered such as the aminoglycosides, chloramphenicols, macrolides, cephalosporines, tetracyclines, and quinolones (Lewis, 2013). Accordingly, effective treatments against a broadening spectrum of different bacterial pathogens had become available. The discovery of most antibiotics at that time was based on screening cultures of various microorganisms for antibacterial activity. In addition, semi-synthetic approaches were applied in order to optimize already existing classes of antibiotics resulting for example in the development of penicillinase-resistant penicillins (e.g., methicillin) or the aminopenicillins with activity against Gram-negative bacteria (e.g., ampicillin) (Wright, 1999; Monnet, 2005). Since the 1970's, market launches of new antibiotic substances have declined and most newly approved antibiotics have been derived from already existing antibiotic classes and thus, do not represent novel antibacterial chemical entities.

The discovery of antibiotics was undoubtedly one of the most significant achievements in medicine in the 20<sup>th</sup> century. However, their discovery was accompanied by emergence of resistance against the different classes of antibiotics limiting their efficacy (D'Costa et al., 2011). Antibiotic resistance occurs as a consequence of an evolutionary process driven by natural selection. As some bacteria are intrinsically resistant to certain antibiotics, they can additionally acquire resistance by either spontaneous (de novo) gene mutation or via horizontal transfer of resistance genes from other organisms (Tenover, 2006; Alekshun and Levy, 2007). Due to the widespread use of antibiotics in the past decades, the development of antibiotic resistances has been considerably stimulated resulting in the emergence of numerous single drug-resistant or even multidrug-resistant pathogens (Figure 1) (Tavares et al., 2013).

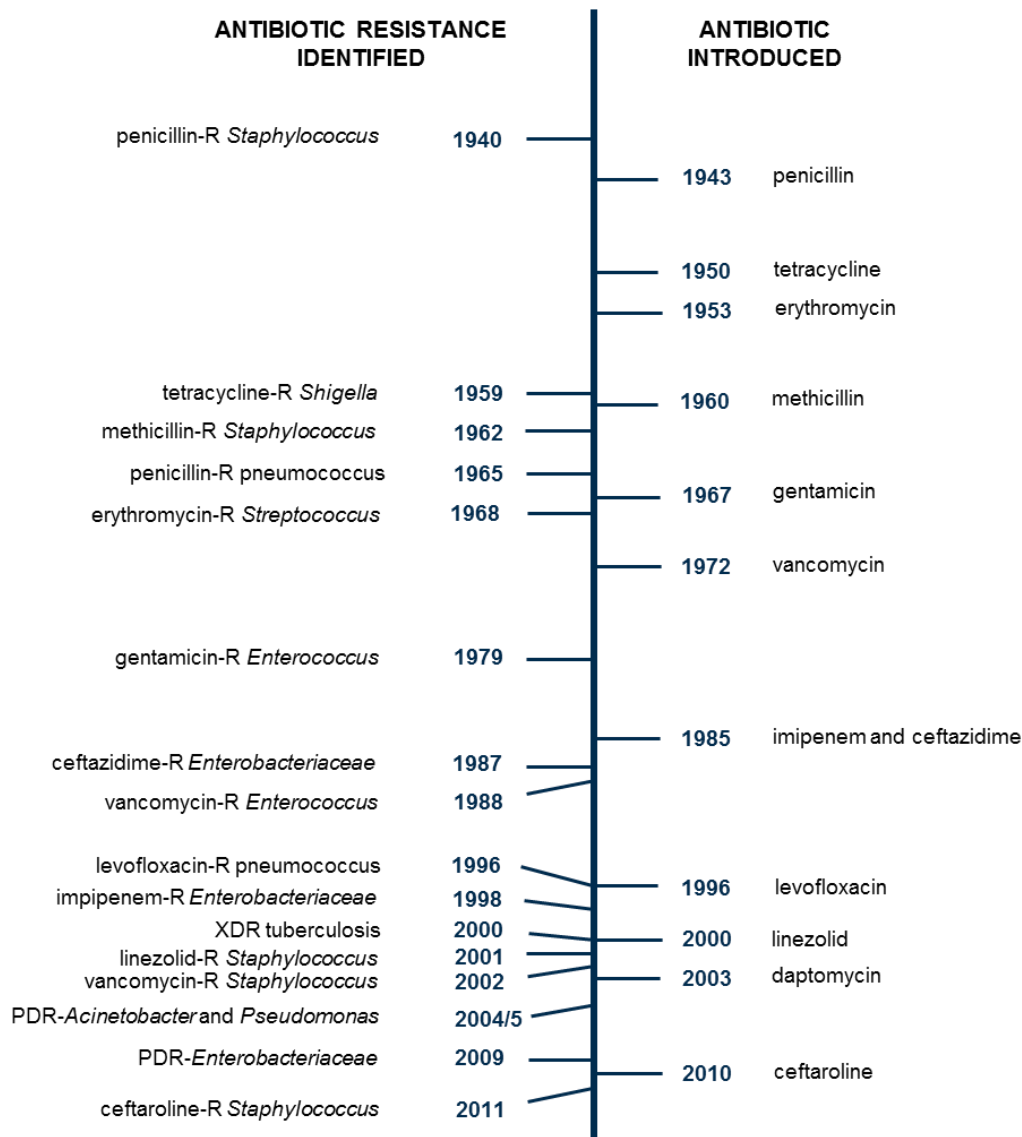


**Figure 1.** Timetable of key antibiotic introduction and resistance events adapted from the U.S. Centers for Disease Control and Prevention report “Antibiotic resistance threats in the United States, 2013”. The abbreviation R stands for resistant, PDR for pan drug-resistant, and XDR for extensively drug-resistant.

Meanwhile, antibiotic resistance has evolved into a serious threat to public health on a global level. Of particular concern in the hospitals are the so-called ‘ESKAPE’ pathogens (*Enterococcus faecium*, *Staphylococcus aureus*, *Klebsiella pneumoniae*, *Acinetobacter baumannii*, *Pseudomonas aeruginosa*, and *Enterobacter species*) that are responsible for two-thirds of all healthcare-associated infections according to the U.S. Centers of Disease Control and Prevention (CDC) (Infectious Diseases Society of America, 2008). These

pathogens are becoming increasingly resistant to single or multiple antibiotics, among them also antibiotics of last-resort, thereby tremendously complicating the treatment of these infections (Rice, 2008). For instance, about 30% of *Enterococcus* healthcare-associated infections are vancomycin-resistant with only few or no remaining treatment options (US Department of Health and Human Services. Centers for Disease Control and Prevention, 2013).

Moreover, infectious diseases that are not predominantly healthcare-associated such as tuberculosis are prone to antimicrobial resistance, too. Tuberculosis, caused by the pathogen *Mycobacterium tuberculosis*, mostly affects the lungs, but can also attack other organs. Globally, it belongs to the most frequent infectious diseases with a third of the world's population being infected. In 2013 alone, about nine million people fell ill with tuberculosis. According to the World Health Organization (WHO) in 2013, an estimated number of 480,000 people developed multidrug-resistant tuberculosis (MDR-TB) and out of these 210,000 people died from the disease. Per definition, MDR-TB is caused by pathogens that are resistant to the first-line antituberculosis agents rifampicin and isoniazid (Matteelli et al., 2014). As stated by the WHO in their "Global Tuberculosis Report 2014", about 9% of the patients with MDR-TB even suffer from extensively drug-resistant tuberculosis (XDR-TB), a form of tuberculosis that, additionally to rifampicin and isoniazid, does not respond to any fluoroquinolone and at least one of the second-line antituberculosis drugs (i.e., kanamycin, capreomycin) (Matteelli et al., 2014).

Antibiotic resistance causes prolonged illness and medical treatment and an increased risk of death and places a tremendous economic burden on society. By way of example, in the European Union multidrug-resistant bacteria cause an estimated economic damage of over 1.5 billion dollar annually (European Centre for Disease prevention and Control/European Medicines Agencies (ECDC/EMA), 2009). However, along with increasing prevalence of antibiotic resistance, the number of new antibacterial agents reaching the market is decreasing, which is further exacerbating the situation. This is partially attributable to the fact that most pharmaceutical companies have abandoned their antibiotic research and development programs over the past decades (Spellberg et al., 2004). Compared to drugs for the treatment of chronic diseases such as diabetes and hypertension, antibiotics provide a poor return of investment since they are generally used for a curative short-course therapy. Additionally, novel agents are mostly restricted to last-resort treatment (Davies, 2006). Another reason that can be accounted for the decline of market launches of antibacterial

agents is more of scientific nature. According to Brad Spellberg, “the low-hanging fruit have been plucked” and “thus, discovery and development of antibiotics has become scientifically more complex, more expensive, and more time consuming over time” (Spellberg, 2012).

However, considering the severe impact of antimicrobial resistance on global health, it is of prime importance to preserve the efficacy of existing antibacterial agents and also to develop novel treatment options. For this purpose, it is important to gain a better understanding of the molecular basis of host-pathogen interactions and resistance development. Identifying anti-infectives with novel modes of action represents a promising strategy to circumvent target-specific resistances (Black and Hodgson, 2005). Furthermore, addressing novel sites on currently exploited targets provides another opportunity to escape existing resistance mechanisms. An alternative approach for antimicrobial drug development is based on targeting bacterial virulence, i.e., the ability of bacteria to damage the host and cause disease (Clatworthy et al., 2007). Compared to traditional antibiotics, anti-virulence therapeutics ‘disarm’ the bacteria instead of inhibiting their growth or killing them. Hence, it is hypothesized that an anti-virulence strategy exerts less evolutionary pressure for the development of resistances (Rasko and Sperandio, 2010).

Beyond doubt, fighting antibiotic resistance is a challenging task and requires concerted action. Aware of the threatening situation government and leading healthcare organizations on a national and global level tailored initiatives to secure a prudent use of antibiotics and to improve surveillance systems in order to curtail the development and spread of antibiotic resistances (Tamma and Cosgrove, 2011). Importantly, also incentives were provided to restart research into novel antimicrobial agents, which are urgently required (Boucher et al., 2009; Tamma and Cosgrove, 2011).

## 1.1 RNA polymerase (RNAP)

### 1.1.1 Structure and function

The RNA polymerase (RNAP) catalyzes the transcription of deoxyribonucleic acid (DNA) into ribonucleic acid (RNA) and, accordingly, is a key enzyme in gene expression that is present in all living organisms (Ebright, 2000; Vassylyev et al., 2002). The prokaryotic RNAP is a large multi-subunit enzyme. The core enzyme (~ 400 kDa) consists of five subunits: two alpha ( $\alpha_2$ ), one beta ( $\beta$ ), one beta prime ( $\beta'$ ), and one omega ( $\omega$ ) subunit (Landick and Geszvain, 2005) (Figure 2). Due to the structural organization of the subunits, the core enzyme resembles the shape of a crab claw. The two pincers of the claw are formed by the two largest subunits,  $\beta$  and  $\beta'$ . Together, they account for the catalytic activity of the enzyme. In between the two pincers, there is a large cleft with a diameter of around 27 Å. At the base of the cleft, the active site channel is located containing a  $Mg^{2+}$  ion chelated by three aspartates of the  $\beta'$  subunit (Landick and Geszvain, 2005). During transcription, the pincers open and close by a ~ 30° rotation of the  $\beta'$  pincer, which is also referred to as the 'clamp' (Häbich and Nussbaum, 2009; Chakraborty et al., 2012). 'Clamp' opening allows the entry of template DNA to the active center and 'clamp' closing retains the DNA inside the active center cleft enabling an efficient transcription (see Figure 5). Both  $\alpha$  subunits are required for the assembly of the subunits to a functional core enzyme. Besides, they are involved in promoter recognition (Igarashi and Ishihama, 1991; Ross et al., 2001). The function of the  $\omega$  subunit is to promote the RNAP assembly and increase its stability (Minakhin et al., 2001). The core enzyme accommodates several channels allowing the template DNA, RNA, and nucleotides to move inside and outside the active center (see Figure 2).

Together with a dissociable accessory protein, the sigma ( $\sigma$ ) factor, the RNAP holo enzyme is formed. The  $\sigma$  factor in complex with the core enzyme is essential for specific promoter recognition and efficient transcription initiation. In response to their environment, bacteria produce various kinds of  $\sigma$  factors, whereby the number of  $\sigma$  factors differs among bacterial species. The predominant  $\sigma$  factor in *E. coli* is  $\sigma^{70}$ , also referred to as the housekeeping  $\sigma$  factor, which transcribes most genes in growing cells. Once bacteria are exposed to changing conditions such as heat or lack of nutrients, they adapt their gene expression to respond to the altered environment by producing alternative  $\sigma$  factors (e.g.  $\sigma^E$ ,  $\sigma^S$ ,  $\sigma^H$ ,  $\sigma^N$  in *E. coli*) (Jishage M, Iwata A, Ueda S, Ishihama A, 1996; Gourse et al., 2006).

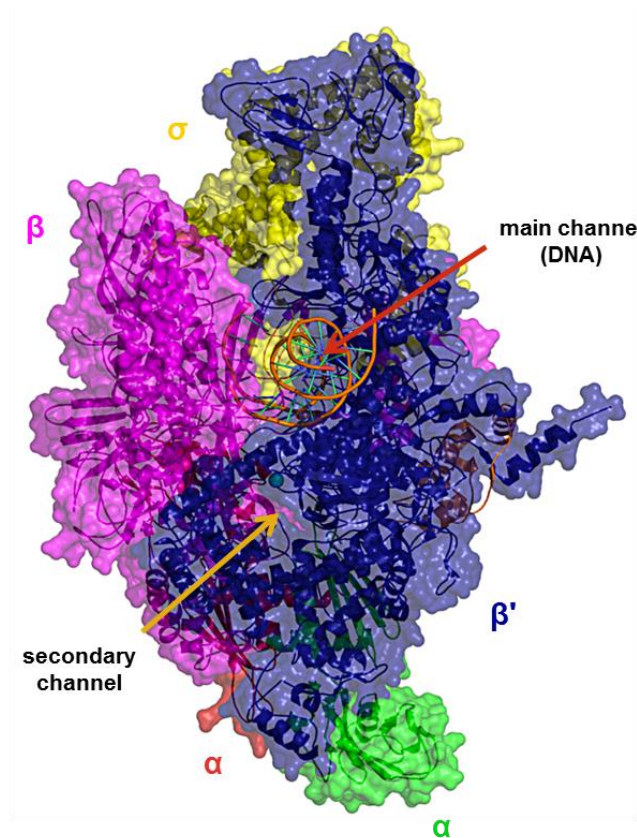


**Figure 2.** Structural organization of the *E. coli* RNAP holo enzyme with bound DNA in the main channel (homology model created by Matthias Negri, unpublished).

The transcription process can be divided into three stages: initiation, elongation, and termination. The first step of the transcription initiation implies the formation of the holo enzyme. The dissociable  $\sigma$  factor enables the RNAP to specifically recognize and bind to the promoter site. Upon binding to the promoter, the closed promoter-polymerase complex ( $RP_c$ ) is formed (Chamberlin, 1974; McClure, 1985). Subsequent promoter melting induces the formation of the open complex ( $RP_o$ ). This involves the unwinding of the double-stranded DNA at the transcription site forming the so-called transcription bubble (Figure 3). The RNA synthesis takes place in 5' to 3' direction. First, the complex undergoes several cycles of abortive transcription, synthesizing and releasing short RNA transcripts usually ranging from 2–12 nucleotides (nts) (Hsu, 2002). At this stage, the RNAP is still bound to the promoter DNA. As soon as the transcripts reach a length of  $\sim 13$ –15 nts, the transcription process is transitioned into the elongation phase. This is accompanied by the promoter clearance and the release of the  $\sigma$  factor from the RNAP. The RNAP-DNA hybrid forms a stable transcription elongation complex that effectively transcribes DNA in RNA with an average rate of

30–100 nts/s (Landick and Geszvain, 2005). RNA synthesis proceeds along the DNA template strand until the RNAP recognizes a signal for chain termination. The termination mechanism can be either direct (Rho-independent termination) or mediated by the termination factor Rho (Rho-dependent termination) (Henkin, 1996). The transcription termination implicates the release of the transcript and the uncoupling of the RNAP from the DNA template. During the transcription process, the RNA polymerase undergoes multiple conformational changes to optimally adapt to the single steps of transcription.

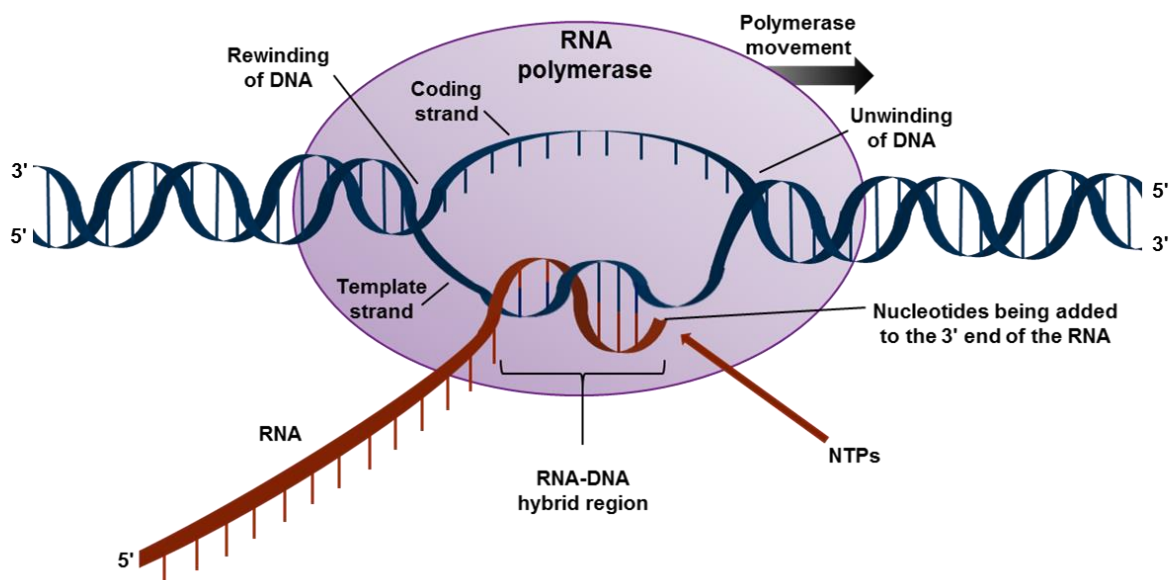


**Figure 3.** Schematic illustration of the transcription bubble (adapted from 2012 Pearson Education, Inc.). Double-stranded DNA is separated and, subsequently, the RNA polymerase synthesizes an RNA strand complementary to the template strand in 5' to 3' direction.

### 1.1.2 RNAP as a target for antimicrobial therapy

Since the RNAP is essential for growth and survival of bacteria, it represents an attractive target for antimicrobial therapy. Despite similarity in the structural organization and functionality, prokaryotic and eukaryotic RNAP sequences are not highly conserved, sharing only partially homologous sequences in the core enzyme (Cramer, 2002, Artsimovitch and Vassilyev, 2006, 2006) In contrast, the RNAP is highly conserved among bacteria. Accordingly, targeting the bacterial RNAP enables the development of efficient antibacterial agents with broad-spectrum activity combined with therapeutic selectivity (Chopra, 2007).

RNAP is a large protein with various cavities and channels offering multiple target sites to interfere with its catalytic activity. Consequently, several classes of bacterial RNAP inhibitors, among them natural products, small molecules, and peptides, targeting different sites of this enzyme have already been identified (Darst, 2004; Chopra, 2007; Villain-Guillot et al., 2007; Mariani and Maffioli, 2009; Hüsecken et al., 2013).

The only RNAP inhibitors currently approved for clinical use are the rifamycins (rifampicin, rifabutin, rifapentine, rifamixin) and fidaxomicin, making the RNAP a clinically validated but still underexploited target (Figure 4a) (Floss and Yu, 2005; Rivkin and Gim, 2011; Venugopal and Johnson, 2012).

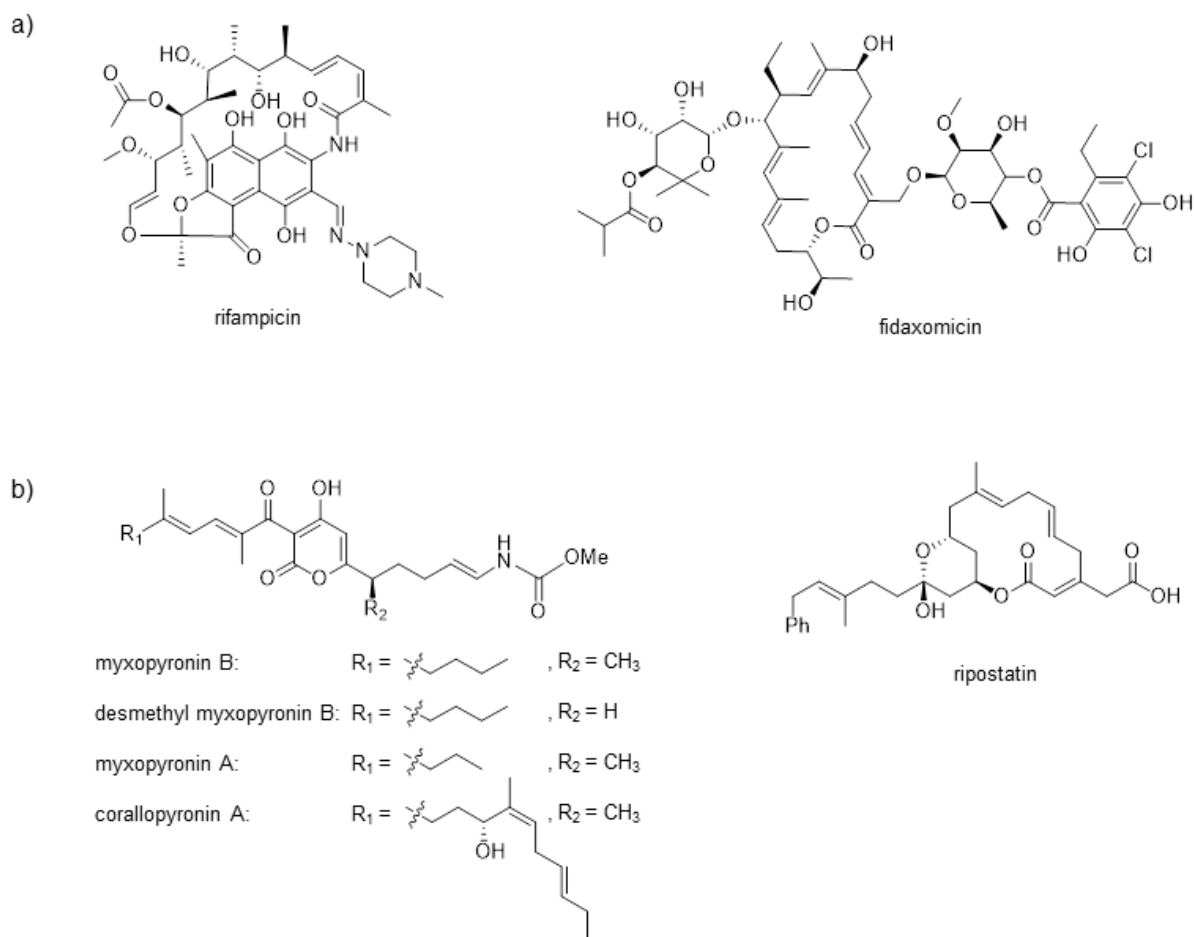


**Figure 4.** Structures of RNAP inhibitors. a) Clinically approved RNAP inhibitors. b) RNAP ‘switch region’ binders.

Rifamycins inhibit the transcription beyond a transcript length of 2 to 3 nts presumably by sterically blocking the elongation process (McClure WR, 1978; Campbell et al., 2001; Feklistov et al., 2008). As disclosed from the crystal structure of *Thermus aquaticus* core RNAP in complex with rifampicin (Rif), its binding site is located 12 Å distant from the active center in the RNAP  $\beta$  subunit deep inside the RNA-DNA channel (Campbell et al., 2001). Rifamycin antibiotics are used in the clinics for the treatment of both Gram-positive and Gram-negative bacterial infections and play an important role in the first-line treatment of tuberculosis. However, their medical value is limited owing to the emergence of Rif-resistant strains. Resistance to the class of rifamycins arises from point mutations in the *rpoB* gene encoding the RNAP  $\beta$  subunit (Jin and Gross, 1988; Severinov et al., 1994).

A further clinically used RNAP inhibitor, fidaxomicin, was approved in 2011 by the US Food and Drug Administration (FDA) for *Clostridium difficile*-associated diarrhea (CDAD). Fidaxomicin binds to the RNAP ‘switch region’, a target site distinct to the that of the rifamycins, and, thereby, inhibits transcription initiation (Artsimovitch et al., 2012). It is poorly absorbed in the gastrointestinal tract after oral administration and displays a narrow spectrum of antimicrobial activity (Venugopal and Johnson, 2012; Sears et al., 2013). Moreover, fidaxomicin does not exhibit any cross-resistance with other antibacterial agents, including the rifamycins. According to this, the RNAP ‘switch region’ represents a promising target site for the development of RNAP inhibitors, which are also effective against Rif-resistant bacteria.

### 1.1.3 The RNAP ‘switch region’

The ‘switch region’ is situated at the base of the RNAP ‘clamp’ ( $\beta$  subunit) and acts as a hinge, which coordinates the opening and closing of the RNAP ‘clamp’ during transcription (Figure 5). The ‘switch region’ does not overlap with the rifamycins’ binding site and is highly conserved in Gram-positive and Gram-negative bacteria making it an interesting target for inhibitor design with broad-spectrum antibacterial activity.

In 2008, Mukhopadhyay et al. identified the ‘switch region’ as the binding site of the described RNAP inhibitors myxopyronin (Myx), corallopyronin (Cor) and ripostatin (Rip) (Figure 4) (Mukhopadhyay et al., 2008). Several years before, Irschik et al. isolated these natural products from myxobacteria and discovered their potent and selective inhibitory activity against bacterial RNAP (Irschik et al., 1983; Irschik et al., 1985; Irschik et al., 1995).

Rip is a macrocyclic lactone, whereas Myx and Cor are both  $\alpha$ -pyrone antibiotics. Cor is structurally closely related to Myx, differing only by an additional seven-carbon extension of the dienone side chain (see Figure 4). The mode of action of these natural product inhibitors is based on preventing entry of double-stranded promoter DNA into the active-center cleft by locking the clamp in a closed or partially closed position (Figure 5). Nonetheless, they exhibit slight differences in their inhibitory profile. In contrast to Myx, which is not capable of completely inhibiting the catalytic activity of the RNAP, Cor and Rip are able to fully prevent RNA synthesis (Irschik et al., 1985; Irschik et al., 1995). According to the crystal structure of *Thermus thermophilus* RNAP in complex with Myx and desmethyl myxopyronin B (dMyx), this inhibitor class binds in an almost entirely enclosed and predominantly hydrophobic ‘crescent-shaped’ binding pocket within the ‘switch region’ (Mukhopadhyay et al., 2008; Belogurov et al., 2009).

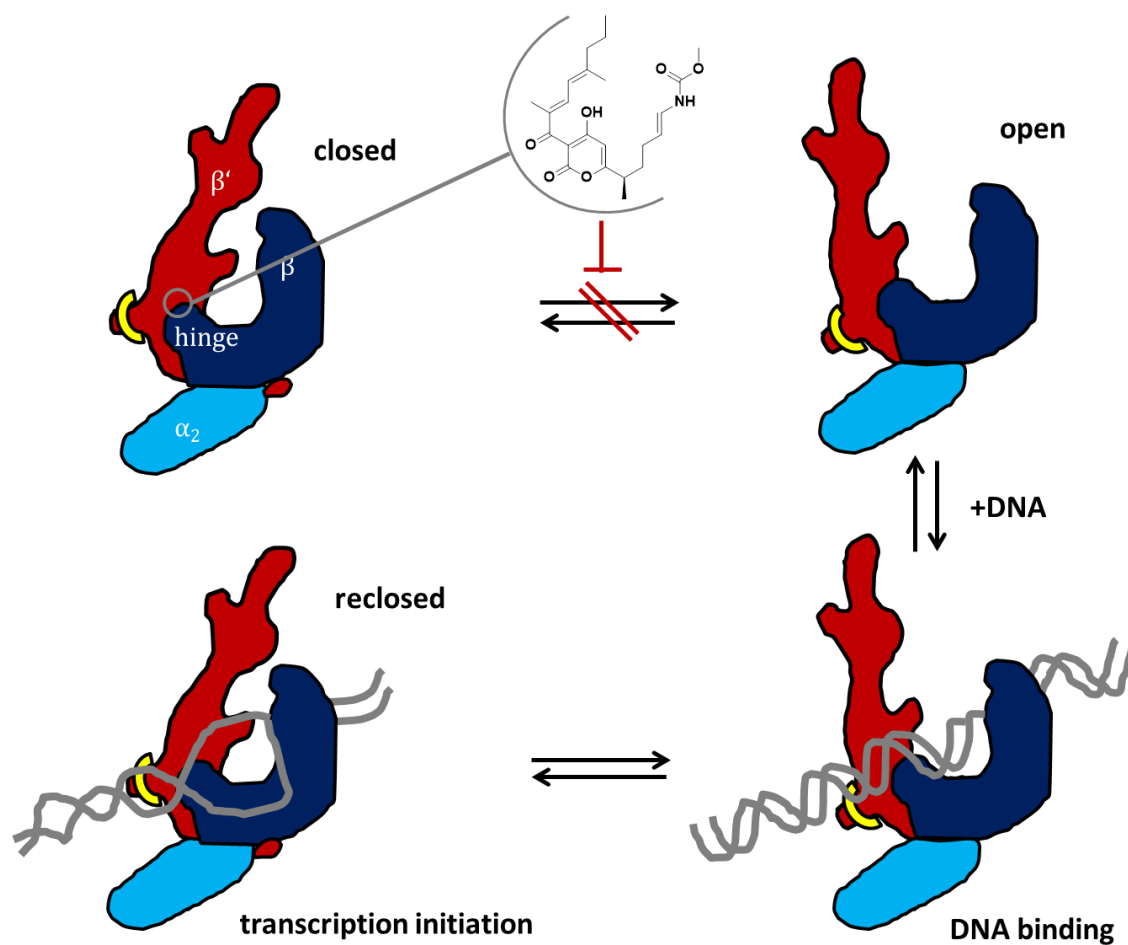


**Figure 5.** Schematic illustration of the mode of action of myxopyronin (adapted from Häbich and Nussbaum, 2009).

According to isolation and sequencing of Myx-, Cor-, and Rip-resistant *E. coli* mutants, the target of Cor and Rip completely overlaps with the Myx binding site (Mukhopadhyay et al., 2008). In contrast, the target of the approved drug fidaxomicin, also referred to as lipiarmycin, tiacumicin, or Difucid®, only minimally overlaps with the Myx binding pocket (Srivastava et al., 2011).

Myx, Cor, and Rip display potent *in vitro* activity against bacterial RNAP (IC<sub>50</sub> values ranging from 1–4 µM) (Häbich and Nussbaum, 2009). These antibiotics are primarily active against Gram-positive bacteria but ineffective against many Gram-negative pathogens most probably due to penetration barriers and efflux (Häbich and Nussbaum, 2009; Srivastava et al., 2011). Furthermore, they possess no acute toxicity in mice and, in analogy to fidaxomicin, no cross-resistances with rifamycins. Nevertheless, these antibiotics cannot be considered as candidates for clinical use because of deficient physicochemical properties including low stability, high lipophilicity, high serum protein binding, and, consequently, confined *in vivo* efficacy (Häbich and Nussbaum, 2009; Moy et al., 2011). Some efforts have already been made in the synthesis of Myx analogs. However, apart from desmethyl myxopyronin B, the biological activity could not be improved so far (Doundoulakis et al., 2004; Lira et al., 2007).

Following the validation of the RNAP ‘switch region’ as an antimicrobial drug target and the availability of the co-crystal structure of *Thermus thermophilus* RNAP in complex with Myx, the discovery of two synthetic inhibitor classes binding to the ‘switch region’, the pyridyl-benzamides and the squaramides, have been reported (McPhillie et al., 2011; Buurman et al., 2012). Both classes display good inhibitory activity against *E. coli* RNAP but no significant antibacterial activity.

## 1.2 Carbon storage regulator protein A (CsrA)

### 1.2.1 The Csr system

Bacteria use complex regulatory networks to adapt gene expression in response to environmental changes (Aertsen and Michiels, 2004; van Assche et al., 2015). A representative of such a network is the posttranscriptional carbon storage regulator (Csr) system, which controls multiple physiological and metabolic adaptive mechanisms (Revelles et al., 2013). The Csr system and its homologs (e.g., the regulator of secondary metabolism (Rsm) system in *P. aeruginosa*) have been found in numerous bacterial species, predominantly in Gram-negative pathogens (Yakhnin et al., 2007). Csr-like systems consist of several molecular components and are based on an autoregulatory feedback mechanism (reviewed in (Babitzke and Romeo, 2007)). The main player of the Csr network is the RNA-binding protein CsrA, which affects translation and stability of mRNA targets by binding to their 5' untranslated region (Romeo, 1998; Babitzke and Romeo, 2007). CsrA activity is antagonized by non-coding small RNAs (sRNAs), such as CsrB and CsrC in *Yersinia pseudotuberculosis* and *E. coli*, which both possess multiple binding sites for CsrA (Timmermans and van Melderren, 2010). Through binding of several CsrA dimers to CsrB or CsrC, interaction of CsrA with its target mRNAs is impeded. In turn, in some bacteria such as *E. coli*, activity of CsrB and CsrC is negatively regulated by CsrD, a membrane-bound protein that triggers their RNase E-mediated degradation (Suzuki et al., 2006). Conversely, CsrA activates expression of *csrB* and *csrC* via the BarA/UvrY system and negatively regulates CsrD (Suzuki et al., 2002; Jonas et al., 2010).

### 1.2.2 Function and structure

CsrA is a global, posttranscriptional regulator protein that controls multiple unrelated physiological processes involved, amongst others, in metabolism, motility, and biofilm formation (Timmermans and van Melderren, 2010). Primarily, CsrA triggers a negative regulation by competing with ribosome binding and, thereby, inhibiting target translation (Baker et al., 2002; Dubey et al., 2003). Nevertheless, some cases of positive regulation have been described in literature but the exact molecular mechanism of action remains to be determined. As an example, CsrA activates the expression of *E. coli flhDC*, which is the master operon for flagellum biosynthesis. It is assumed that binding of CsrA to the leader region of *flhDC* transcripts results in the stabilization of the mRNA and, thereby, impedes its degradation by RNase E (Wei et al., 2001; Yakhnin et al., 2013).

CsrA and its homologs such as RsmA/RsmE in *Pseudomonas* species are highly conserved in many bacteria (Schubert et al., 2007; Heroven et al., 2012). The three-dimensional (3D) structures of CsrA and its homologs, determined by solution NMR (Gutiérrez et al., 2005) and X-ray crystallography studies (Rife et al., 2005; Heeb et al., 2006; Marden et al., 2013), reveal a homodimeric organization (Figure 6). The two CsrA monomers consist each of five  $\beta$ -strands and one  $\alpha$ -helix. The five-stranded antiparallel  $\beta$ -sheets of two monomers intertwine and form a hydrophobic core.

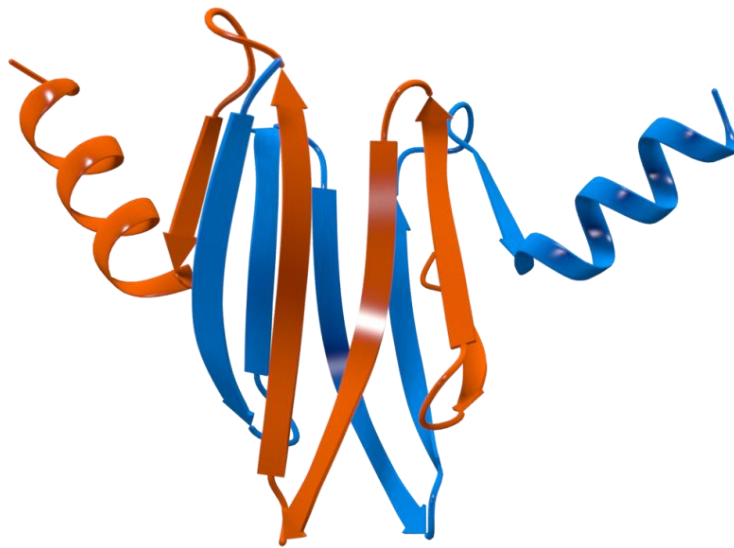


**Figure 6.** Ribbon diagram of the crystal structure of CsrA homodimer from *Yersinia enterocolitica* (PDB: 2BTI). The individual CsrA monomers are colored red and blue.

The two identical RNA-binding sites of the dimer are each located at the interface of the  $\beta_1$ -strand of one monomer and the  $\beta_5$ -strand of the antiparallel monomer. Mutagenesis studies have shown that Arg44 is the most important amino acid for RNA binding (Heeb et al., 2006). In addition, *in vitro* selection and NMR studies indicated that CsrA binds with high affinity to mRNAs containing a conserved 5'-ACANGGANGU-3' core motif preferentially with the GGA motif located in a hairpin loop (Dubey et al., 2005; Schubert et al., 2007). However, the number of CsrA-binding sites varies among different target mRNAs.

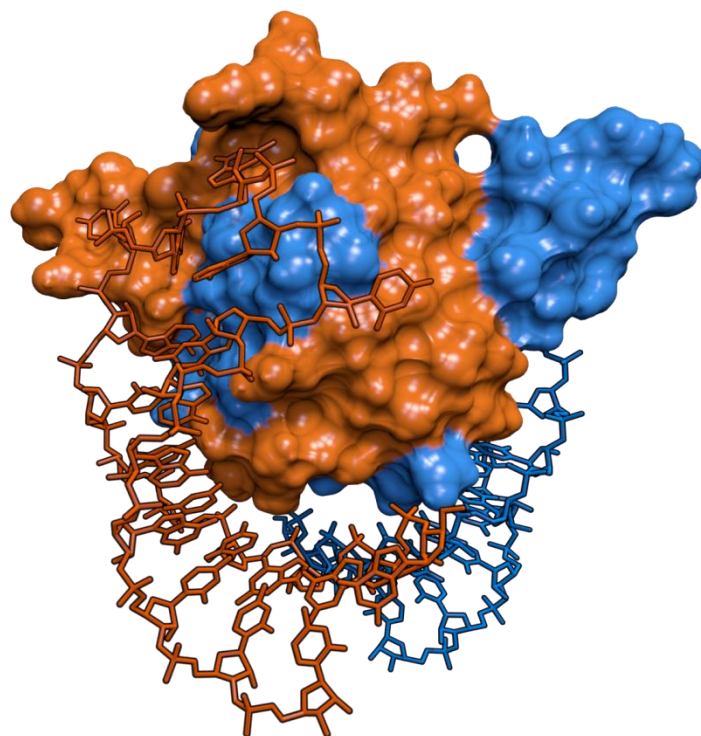


**Figure 7.** Solution NMR structure of the CsrA homolog RsmE from *Pseudomonas fluorescens* (PDB: 2JPP) in complex with the 20 nts *hcnA* mRNA (2:2 complex) (Schubert et al., 2007).

### 1.2.3 CsrA regulates bacterial virulence

Comprehensive studies have proven that CsrA is an important component of bacterial virulence networks and essential for successfully establishing an infection in the host organism. It regulates the expression of various virulence factors required for host cell adhesion and invasion in several pathogens such as enteropathogenic *E. coli* (EPEC), *Y. pseudotuberculosis*, *Helicobacter pylori*, and *Salmonella enterica* serovar Typhimurium (Altier et al., 2000; Barnard et al., 2004; Heroven et al., 2008; Bhatt et al., 2009).

In some bacterial species such as *Y. pseudotuberculosis* and *P. aeruginosa* CsrA mediates the switch between acute and chronic stages of infection. Hence, expression of virulence factors involved in early stages of infection (e.g., motility, cell attachment, host invasion) are upregulated whereas such involved in persistent infection (e.g., biofilm formation) are downregulated (Heurlier et al., 2004; Heroven et al., 2008; Heroven et al., 2012).

Remarkably, first discovered in *S. enterica*, CsrA can function both as activator and as repressor of certain virulence factors depending on the CsrA protein levels (Altier et al., 2000). Accordingly, CsrA excess and deficiency inhibited the expression of virulence factors

involved in invasion of epithelial cells. This so-called 'see-saw' regulation mechanism was also observed for EPEC and might enable an optimal adaptation of virulence gene expression tailored to prevailing conditions during host infection (Bhatt et al., 2009).

Notably, recent studies have demonstrated that lack of CsrA or its ortholog RsmA results in considerable virulence attenuation in mouse models of *P. aeruginosa* (Mulcahy et al., 2008), *H. pylori* (Barnard et al., 2004), and *Y. pseudotuberculosis* (Heroven & Dersch, unpublished results) infection, predominantly due to reduced host colonization.

Taken together, a number of studies proved that CsrA is crucial for bacterial virulence. Accordingly, it represents an attractive target for anti-infective drug development.

### 1.3 Analysis of protein-ligand interactions

Binding of a drug to its target molecule, usually a protein, is the prerequisite for developing its pharmacological effect. Hence, a detailed analysis of protein-ligand interactions is essential for understanding pharmacodynamic processes and provides the basis for rational drug design. Structural characterization tools (X-ray crystallography, NMR), *in silico* methods, and various biophysical techniques play an important role for the selection of suitable target molecules as well as for the identification, characterization, and optimization of lead compounds that modulate the target's activity (Holdgate et al., 2010; Fang, 2012; Cala et al., 2014). The methods deployed for protein-ligand interaction studies within the scope of this work are described below.

#### 1.3.1 Surface plasmon resonance spectroscopy

Surface plasmon resonance (SPR) is an optical phenomenon that allows monitoring of biomolecular interactions in real-time. It occurs, when plane polarized light encounters an electrically conducting metal layer at the interface of two media with different optical densities under the condition of total internal reflection (Figure 8a). Energy of the absorbed photons of the incident light is transferred to free electrons in the metal surface, which, in response, start to oscillate and are converted to surface plasmons. Thereby, an evanescent wave is generated and, concomitantly, the intensity of the reflected light is decreased, which is measured by an optical detection unit. The angle, at which the reflection reaches a minimum, is called the resonance angle that is dependent on the refractive index at the sensor surface.

In an SPR spectroscopy based binding experiment, a molecule (ligand), mostly a protein, is immobilized on the sensor surface, over which a potential interaction partner (analyte) is flushed. Binding of the analyte to the immobilized ligand alters the refractive index at the sensor surface and causes a shift of the resonance angle. The resulting shift is directly proportional to the mass increase at the sensor surface due to the bound analyte and can therefore be used to determine binding constants. SPR signals are commonly described as resonance or response units (RU), whereby 1 RU correlates with a change in the SPR angle by approximately  $0.0001^\circ$  (Thillaivinayagalingam et al., 2010). Time-dependent changes in the SPR signal are recorded in an SPR sensorgram, in which the association and dissociation phase of a binding event can be monitored (Figure 8b).

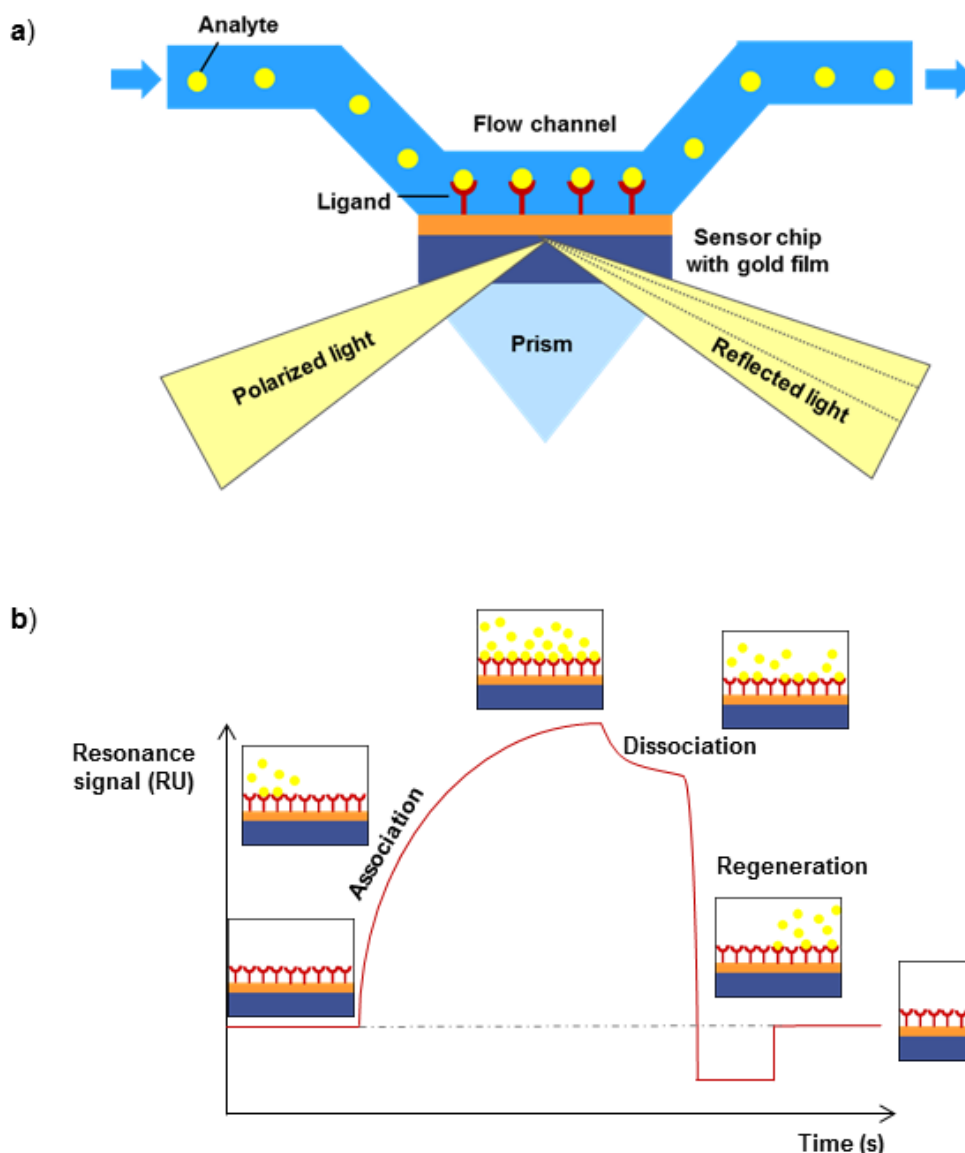


**Figure 8.** Adapted from Figure 1 and Figure 2 in reference (Campbell, 2016). a) Typical set-up for an SPR biosensing instrument. b) SPR sensorgram showing the optical response versus time of a typical binding cycle. Upon injection of the analyte and subsequent binding to the ligand (association), the resonance signal increases due to a change in the refractive index. After completed injection time, the analyte is displaced with buffer and dissociation of the analyte molecules can be monitored. In case of incomplete dissociation, the surface is recovered by injecting a regeneration solution to regain baseline level.

SPR spectroscopy does not necessarily require labeling of the interaction partners and is characterized by a low analyte and particularly low ligand consumption. Furthermore, it is a highly sensitive technique amenable to high throughput application and enables the detection of a variety of biomolecular interactions such as ligand-protein, protein-protein, nucleic acid-protein, and nucleic acid-nucleic acid interactions (Cooper, 2002). An SPR experiment generates data with high information content, as binding stoichiometry, affinity, and kinetic

constants can be determined simultaneously. Due to these aspects, SPR biosensors have found wide application in numerous areas in industry and academia. For instance, SPR technology is applied during almost all stages of the drug discovery process, from target identification, screening procedures aiming at hit identification and characterization, hit to lead optimization as well as preclinical and clinical studies (Cooper, 2002).

Due to continuous advancements, SPR-based sensors will most likely maintain or even expand their role in areas such as drug development, clinical diagnostics, or food analysis. A tremendous gain in high-throughput, for example, has been achieved by SPR imaging technique (SPRi). SPRi enables the simultaneous analysis of numerous different biomolecular interactions by operating in a microarray format and using a CCD-camera for signal detection (Scarano et al., 2010; Spoto and Minunni, 2012).

### **1.3.2 Ligand-based nuclear magnetic resonance (NMR) methods**

Due to recent instrumental and methodological improvements, nuclear magnetic resonance (NMR) spectroscopy has become a powerful tool in drug discovery (Pellecchia et al., 2008). It allows the detection and characterization of ligand binding as well as mapping the binding site in solution under nearly physiological conditions. These methods are either based on the observation of resonance signals derived from the protein or the ligands. The application of protein-based methods including chemical shift mapping are restricted by the size of the receptor (< 50 kDa) and require isotopic labelling of the receptor as well as typically long acquisition times (Moore, 1999; Skjærven et al., 2013). In comparison, ligand-based NMR methods do not impose a size limitation regarding the receptor and, particularly, require a smaller amount of unlabeled protein, which makes them amenable for application in high-throughput format. In the following, the principles of two ligand-based NMR methods used in this thesis, saturation transfer difference (STD) NMR and interligand NOE for pharmacophore mapping (INPHARMA), are explained in more detail.

#### **1.3.2.1 Saturation transfer difference NMR**

STD NMR spectroscopy was invented as a screening technique for the detection of protein-binding molecules and, furthermore, for the identification of ligand moieties being significantly involved in the binding process (Mayer and Meyer, 1999).

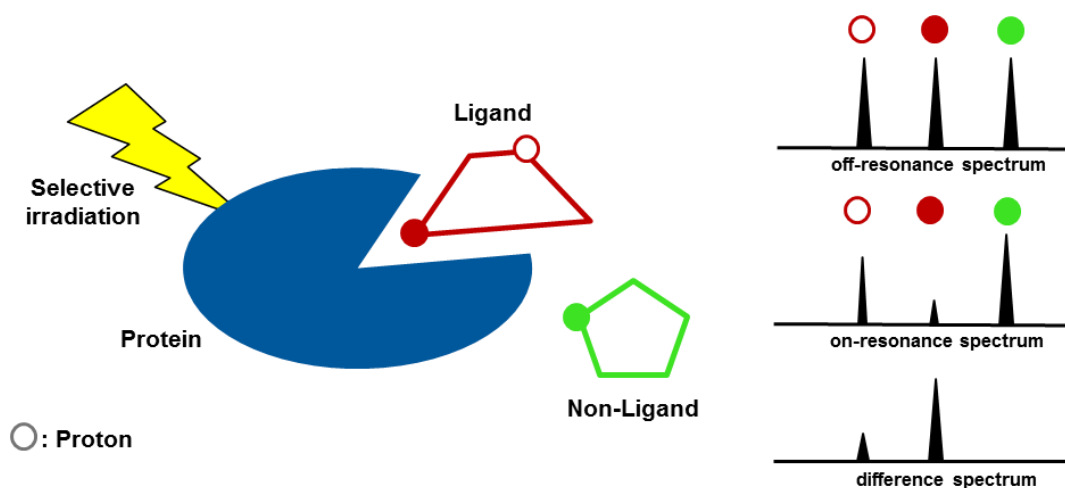


**Figure 9.** Schematic illustration of an STD NMR experiment (modified from Hiraishi et al., 2013).

The principle of STD experiments is illustrated in Figure 9. These experiments involve the record of two different 1D  $^1\text{H}$  NMR spectra (on-resonance and off-resonance spectrum) of a sample containing the receptor and a large molar excess of the ligand. In the on-resonance experiment, receptor protons are selectively irradiated with a frequency that saturates only protons of the receptor but not those of the ligands. Due to spin-diffusion, the saturation spreads rapidly throughout the entire receptor. If binding occurs, saturation is transferred from the protein to protons of the bound ligand that are in close proximity to the protein via the intermolecular nuclear Overhauser effect (NOE). After dissociation of the ligand, the saturation is transferred to the solution, where it is detected. In the off-resonance experiment, a reference 1D  $^1\text{H}$  NMR spectrum is recorded applying a saturation pulse at a frequency, at which neither receptor nor ligand protons resonate, usually around +30 ppm (Ludwig and Günther, 2009). Subtraction of the on-resonance spectrum from the off-resonance spectrum results in the difference spectrum (STD spectrum), in which only signals from binding molecules that received saturation from the protein are visible. The intensity of the signals correlates to the distance between ligand and protein protons. The closer the protons of the ligand to the protein, the more intense is the correspondent signal in the STD spectrum due to a more efficient magnetization transfer. In this way, the binding epitope of ligands can be identified. In contrast, the signals of non-binders are erased in the difference spectrum. Owing to the functional principle of this method, only ligands with a fast exchange and dissociation constants in the micromolar to millimolar range can be detected but not tight or covalent binders (Mayer and Meyer, 1999). Nevertheless, high-affinity ligands can be monitored indirectly, when low-affinity ligands are available that bind competitively to the same binding

site. In that case, a reduction of STD signals belonging to the low-affinity reference discloses the presence of a high-affinity ligand upon titration to the analyzed sample (Wang et al., 2004).

### 1.3.2.2 Interligand NOE for pharmacophore mapping

The term INPHARMA stands for interligand NOE for pharmacophore mapping. This NMR technique is based on the observation of protein-mediated interligand NOEs that originate from ligands binding competitively to the same target site (Sánchez-Pedregal et al., 2005). If the binding mode of one of the ligands is known, the INPHARMA method can be applied to determine the relative orientation of the ligands compared to the reference ligand within the receptor binding site (Sánchez-Pedregal et al., 2005; Orts et al., 2008; Bartoschek et al., 2010). INPHARMA represents a promising technique for rational drug design as it provides valuable information about the ligands' binding mode and their bioactive conformation. Furthermore, this information can be used for the establishment of a binding pharmacophore, which enables virtual screening.

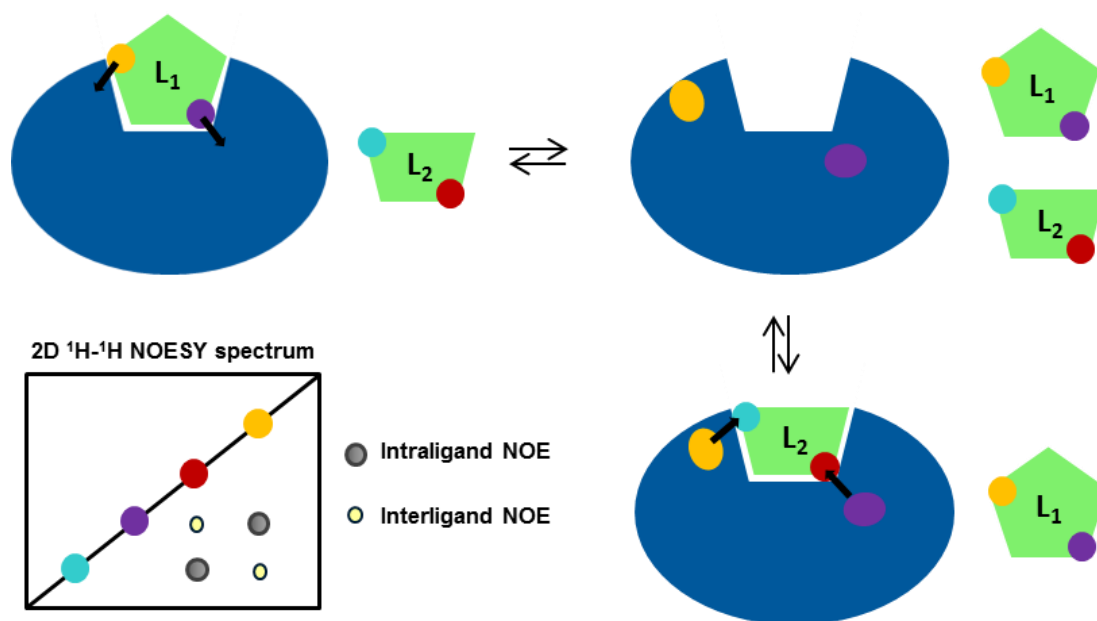


**Figure 10.** Scheme of an INPHARMA experiment (adapted from Carlomagno, 2012).

The principle of the protein-mediated transfer of magnetization is depicted in Figure 10. A NOESY spectrum is recorded of a sample containing the macromolecular receptor and an excess of competitive ligands with similar affinity constants under fast exchange conditions

( $k_{\text{off}}$ : 100–1000 Hz) (Sánchez-Pedregal et al., 2005). Ligand 1 ( $L_1$ ) binds to the protein and the binding protons of  $L_1$  transfer their magnetization via spin-diffusion to protons of the receptor. After dissociation of  $L_1$ , ligand 2 ( $L_2$ ) binds to the receptor within the mixing time of the NOESY experiment. Provided that  $L_2$  binds competitively to the same binding site than  $L_1$ , the magnetization that was transferred from  $L_1$  to the protein is then transferred from receptor protons to protons of  $L_2$ . This results in interligand NOE signals in the recorded spectrum. Interligand NOE peaks only appear between protons of  $L_1$  and  $L_2$  being in immediate vicinity to the protein and occupying the same area within the binding pocket. Analysis of a series of such intermolecular crosspeaks discloses the relative orientation of the competitive ligands bound to the receptor.

### 1.3.3 Mutagenesis

Mutagenesis is the process of generating an alteration in the DNA sequence resulting in a genetic mutation. This can occur naturally (spontaneous mutations) provoked by errors in the DNA replication process or can be induced by chemical or physical mutagens (induced mutations). Furthermore, the genetic information of an organism can also be intentionally changed in the laboratory using molecular biology methods, which is referred to as *in vitro* mutagenesis (Ling and Robinson, 1997; Tee and Wong, 2013). Thereby, the DNA sequence can either be modified randomly or in a predefined way (Cormack, 2001; Wilson and Keefe, 2001). A well established method in this field is ‘site-directed mutagenesis’ (SDM) (Costa et al., 1996; Zheng et al., 2004; Edelheit et al., 2009). This technique allows a site-specific substitution, insertion, or deletion of DNA bases within the gene of interest. Prevalent SDM methods employ polymerase chain reaction (PCR) using synthetic oligonucleotide primers containing the desired mutation. During PCR, the mutation is incorporated into the target sequence at a predefined site. The mutated gene inserted into a vector is then introduced into the recipient, where it is propagated and expressed. Thereupon, the impact of the generated gene mutation on its biological function can be investigated. SDM is widely applied for ‘protein engineering’ and for studying protein structure-function relationships including identifying catalytic residues of a protein or mapping ligand-receptor interaction sites.

## 2 Aim of the thesis

The discovery of novel anti-infectives intended to secure an effective treatment of infectious diseases is of major significance due to the emergence and persistence of drug-resistant bacterial strains. A promising strategy to counteract antibiotic resistances is to develop anti-infective agents addressing new target sites of validated antibiotic targets and/or displaying alternative mechanisms of action. The main objective of this thesis was to identify and to characterize novel anti-infective compounds that overcome existing resistances utilizing various biochemical and biophysical methodologies. This work was focussed on two different bacterial targets for anti-infective drug design, RNAP and CsrA.

The first part of this thesis is devoted to the characterization of RNAP inhibitors targeting the ‘switch region’. The previously identified ‘switch region’ is distinct to the target site of the clinically relevant RNAP inhibitors of the rifamycin class and, thus, represents a promising target for the development of potent broad-spectrum antibiotics sharing no cross-resistances with the rifamycins or other antibacterial agents. Recently, within a rational drug design strategy, we developed small molecule RNAP inhibitors containing a ureidothiophene-2-carboxylic acid core that were proposed to bind to the ‘switch region’ (Sahner et al., 2013b). To enable lead optimization towards enhanced affinity and efficacy, a detailed knowledge of the ligand-protein interactions are of primary importance. Therefore, this work aimed at the elucidation of the binding site and binding mode of these inhibitors to promote structure-based inhibitor design and optimization. To achieve this goal, mutagenesis studies and ligand-based NMR methods should be employed in order to determine the binding epitope as well as the binding pose and orientation of the ligands within the target site. Additionally, the mode of action as well as the pharmacological profile against several drug-resistant bacterial strains of this inhibitor class should be investigated.

In the second part, we aimed at the discovery of CsrA-RNA interaction inhibitors. CsrA is a posttranscriptional regulator protein that binds to mRNA and, thereby, affects its stability and translation. Decisively, CsrA is essential for full virulence of bacteria and hence, can be considered as an attractive target for anti-infective drug development. Inhibitors of the CsrA-RNA interaction are supposed to attenuate CsrA-dependent virulence without killing the bacteria and thus, exerting less selection pressure for the development of bacterial resistances. For the discovery of CsrA-binding molecules, an SPR-based test system ought to be established. Subsequently, identified hit compounds should be tested for their ability to

disrupt the CsrA-RNA interaction utilizing an FP-based competition assay and their binding profile should be investigated by SPR.

## 3 Results

### 3.1 Binding mode characterization of novel RNA polymerase inhibitors using a combined biochemical and NMR approach

Martina Fruth, Alberto Plaza, Stefan Hinsberger, Jan Henning Sahner, Jörg Haupenthal, Markus Bischoff, Rolf Jansen, Rolf Müller, and Rolf W. Hartmann

Reprinted with permission from *ACS Chem. Biol.*, 2014, **9**, 2656–2663.  
DOI: 10.1021/cb5005433

Copyright: © 2014 American Chemical Society.

#### Publication A

#### ABSTRACT

The bacterial RNA polymerase (RNAP) represents a validated target for the development of broad-spectrum antibiotics. However, the medical value of RNAP inhibitors in clinical use is limited by the prevalence of resistant strains. To overcome this problem, we focused on the exploration of alternative target sites within the RNAP. Previously, we described the discovery of a novel RNAP inhibitor class containing an ureidothiophene-2-carboxylic acid core structure. Herein, we demonstrate that these compounds are potent against a set of methicillin-resistant *Staphylococcus aureus* (MRSA) strains (MIC: 2–16  $\mu\text{g ml}^{-1}$ ) and rifampicin-resistant *Escherichia coli* TolC strains (MIC: 12.5–50  $\mu\text{g ml}^{-1}$ ). Additionally, an abortive transcription assay revealed that these compounds inhibit the bacterial transcription process during the initiation phase. Furthermore, the binding mode of the ureidothiophene-2-carboxylic acids was characterized by mutagenesis studies and ligand-based NMR spectroscopy. Competition saturation transfer difference (STD) NMR experiments with the described RNAP inhibitor myxopyronin A (**Myx**) suggest that the ureidothiophene-2-carboxylic acids compete with **Myx** for the same binding site in the RNAP switch region. INPHARMA (interligand NOE for pharmacophore mapping) experiments and molecular docking simulations provided a binding model in which the ureidothiophene-2-carboxylic acids occupy the region of the **Myx** western chain binding site and slightly occlude that of the

eastern chain. These results demonstrate that the ureidothiophene-2-carboxylic acids are a highly attractive new class of RNAP inhibitors that can avoid the problem of resistance.

## INTRODUCTION

Antimicrobial resistance has become a global health concern due to the widening gap between the rapid spread of resistant pathogens (1) and the shortage of effective treatment options (2, 3). Thus, the development of novel and potent anti-infectives is urgently needed. A validated but hitherto underexploited target for the development of broad-spectrum antibiotics is the bacterial RNA polymerase (RNAP). Up to date, rifamycins and fidaxomicin are the only RNAP inhibitors used in clinical practice (4–8). Rifampicin (**Rif**) (Figure 1), a member of the rifamycin family, plays a fundamental role in tuberculosis treatment as a first-line agent in combination with isoniazid (9). However, its use is limited due to the prevalence of **Rif**-resistant *Mycobacterium tuberculosis* (MTB) strains (10, 11). Resistance to the class of rifamycins arises from point mutations in the *rpoB* gene encoding for the RNAP  $\beta$  subunit (12).

A strategy to overcome the problem of resistance is to explore alternative target sites, which are distant from the **Rif** binding pocket. Therefore, we applied a virtual screening approach addressing the RNAP switch region (18). This target site resides at the base of the RNAP clamp, a domain of the  $\beta'$  subunit and coordinates the opening and closing of the RNAP active centre cleft. The switch region is not overlapping with the **Rif** binding site and is highly conserved among Gram-positive and Gram-negative bacteria grading it as an attractive target for the identification of novel broad-spectrum antibiotics (13–15). Using a homology model of *E. coli* RNAP a 3D-pharmacophore model was established, which incorporates protein-derived properties of the switch region as well as ligand features from **Myx**, a well-known switch region binder (16–18) (Figure 1). The virtual screening based on this model identified a hit compound containing an ureidothiophene-2-carboxylic acid core, which served as starting point for activity-guided optimization (18). This class of compounds (Figure 1) showed promising *in vitro* RNAP transcription inhibition and antibacterial activity against Gram-positive bacteria (*S. aureus*, *B. subtilis*) and *E. coli* TolC. Moreover, they possessed a significantly lower resistance frequency compared to **Rif** or **Myx** (18). Present work described here revealed that the ureidothiophene-2-carboxylic acids are also active against several clinical MRSA isolates and **Rif**-resistant spontaneous *E. coli* TolC mutants. Thus, the ureidothiophenes are considered promising candidates for further development.

Here, we established the mode of binding of the ureidothiophenes by using a combination of site-directed mutagenesis and ligand-based NMR methods including STD NMR and INPHARMA. As common methods like SPR or protein based NMR approaches are not feasible to detect binding of small molecules to RNAP due to its large size (core enzyme: ~ 380 kDa), the two ligand-based NMR spectroscopic methods applied herein represent excellent alternatives as they do not impose restrictions on the size of the target protein (19, 20). Besides, to gain deeper insight into the mode of action of the ureidothiophene-2-carboxylic acids an abortive transcription assay was performed.

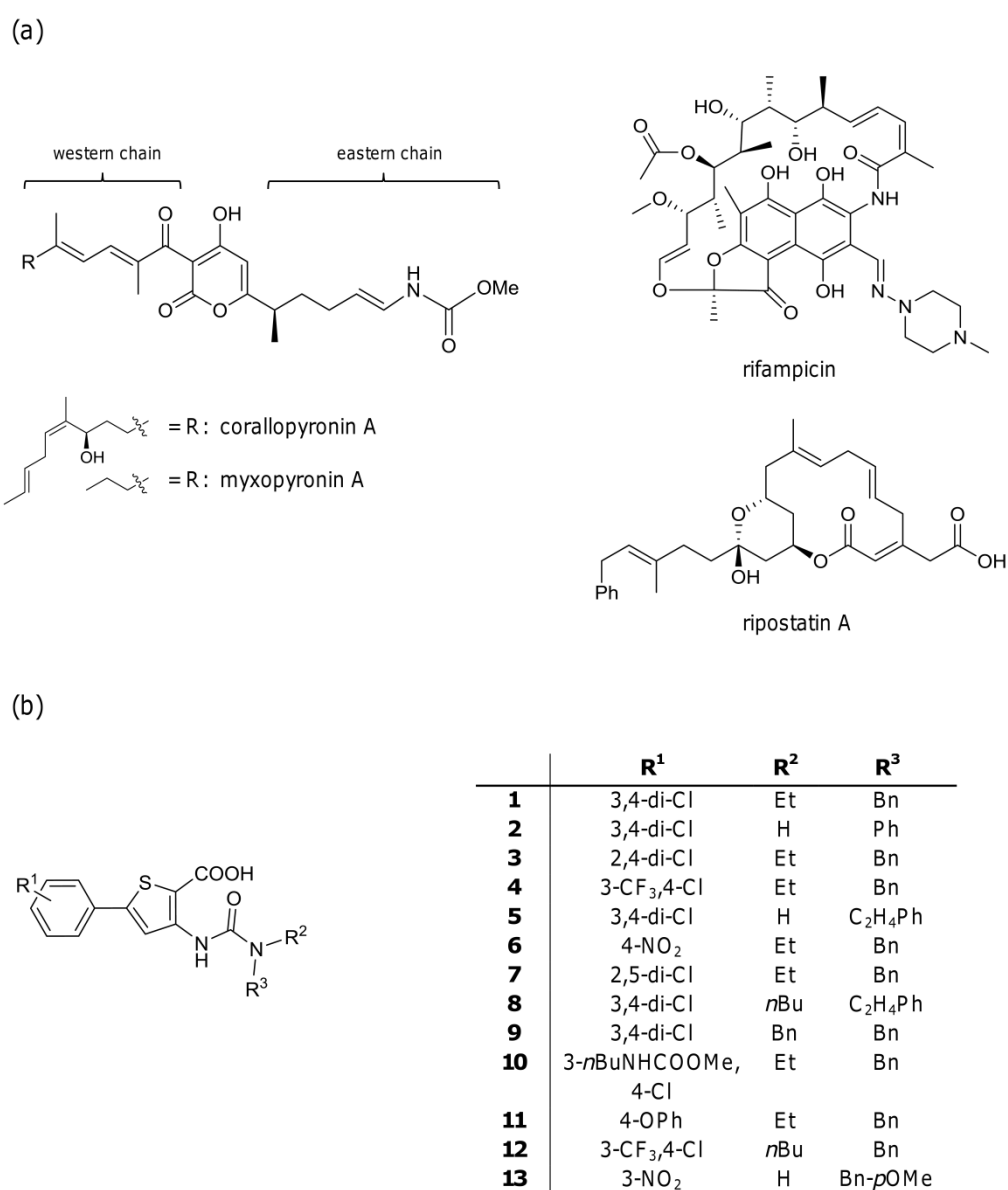


**Figure 1.** (a) RNAP-inhibiting natural products, (b) ureidothiophene-2-carboxylic acid derivatives.

## RESULTS & DISCUSSION

**Antibacterial Activity.** First of all, the activity of the ureidothiophene-2-carboxylic acid derivatives against resistant strains, including **Rif**-resistant *E. coli* TolC and multidrug-resistant *S. aureus*, was assessed by broth microdilution methods (Table 1a and 1b).

**Table 1.** (a) MIC value determination in clinical *Staphylococcus aureus* (MRSA) isolates; (b) MIC value determination in **Rif**-resistant *E. coli* TolC mutants

(a)

MRSA		MIC [ $\mu\text{g ml}^{-1}$ ]			
Isolate	Type <sup>a</sup>	2	9	Myx	Rif
USA300 Lac	CA-MRSA	8	2	1	0.0156
COL	HA-MRSA	16	2	1	0.0078–0.0156
5191	LA-MRSA	16	2	0.5–1	0.0078–0.0156
R44	LA-MRSA	8	2	1	0.0156

<sup>a</sup> CA-MRSA, community acquired MRSA; HA-MRSA, hospital acquired MRSA; LA-MRSA, livestock-associated MRSA

(b)

Strain	MIC [ $\mu\text{g ml}^{-1}$ ]							Myx	Rif
	1	3	4	5	6	7			
<i>Ec</i> TolC	12.5–25	12.5–25	25	12.5	25	25	1.25	8	
<i>Ec</i> TolC $\beta$ Q513L <sup>b</sup>	12.5	12.5–25	25	12.5	25–50	25	1.25	>100	
<i>Ec</i> TolC $\beta$ H526Y <sup>b</sup>	12.5	12.5–25	25	12.5	50	25	1.25	>100	

<sup>b</sup> **Rif**-resistant *E. coli* TolC strains with mutations in the *rpoB* gene encoding for the RNAP  $\beta$  subunit.

Spontaneous **Rif**-resistant *E. coli* TolC mutants with single point mutations in the *rpoB* gene causing high level resistance to **Rif**, were still susceptible towards the ureidothiophene-2-carboxylic acids. These results indicate that the ureidothiophenes show no cross-resistance with **Rif** as intended by our approach to address the RNAP switch region. Moreover, the compounds display potent activity against a set of methicillin-resistant *Staphylococcus aureus*

(MRSA) isolates with differing antimicrobial resistance patterns (Table S1), such as the community acquired MRSA strain USA300 Lac (21), the early hospital acquired MRSA strain COL (22) and the livestock-associated MRSA CC398 isolates 5191 (23) and R44 (24). Compound **9** (Figure 1) was found to be the most potent. It exhibited a MIC value of  $2 \mu\text{g ml}^{-1}$  in all screened MRSA strains, which is similar to that of the reference compound **Myx** (Table 1a).

**Abortive Transcription Assay.** It has been shown that **Myx** inhibits the transcription initiation (14). Since the ureidothiophene-2-carboxylic acids were designed to bind to the same binding site than **Myx**, it can be assumed that these compounds may also inhibit the initiation of the transcription cycle. To confirm this hypothesis, an HPLC-based abortive transcription assay (25) was performed. Inhibition of transcription initiation was measured by quantification of abortive transcripts that are usually formed during the initiation phase (26, 27). As illustrated in Figure 2, compounds **1** and **6** (Figure 1) induced a drastic reduction of abortive transcript formation. As expected, this data demonstrate that the ureidothiophenes interfere with the transcription process during the initiation phase.

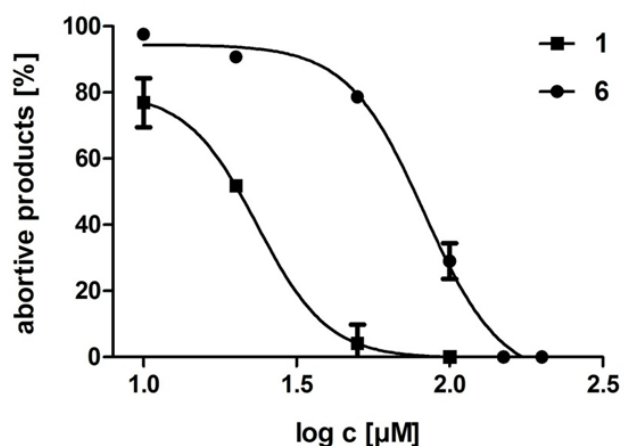


**Figure 2.** Abortive Transcription Assay. Dose-dependent inhibition of **1** and **6** on abortive product formation (ApUp<sup>3</sup>H-C) using ApU and <sup>3</sup>H-CTP as substrates. Standard deviations from two independent experiments are indicated by error bars.

**Mutagenesis Studies.** The ureidothiophene-2-carboxylic acids were designed as RNAP inhibitors that bind into the switch region. Recent docking studies suggest that these compounds bind in a tilted conformation overlapping with the **Myx** western chain but do not

extend in the binding region of the eastern chain (18). To corroborate these findings, several amino acid substitutions in the switch region were introduced (Figure S1). Subsequently, the effects of these mutations on both the RNAP transcription inhibition and the antibacterial activity were examined. As expected, mutations in the binding pocket of the **Myx** eastern chain including RNAP  $\beta$  V1275M and  $\beta$  E1279K, did not impair the antibacterial activity of the ureidothiophene-2-carboxylic acid series against *E. coli* TolC (Table S2). Surprisingly, substitution of amino acids located in the proposed binding site such as RNAP  $\beta$  S1322,  $\beta$  L1291,  $\beta'$  K345,  $\beta'$  K334 and  $\beta'$   $\Delta$ 334–5 neither had a significant effect on the antibacterial activity against *E. coli* TolC nor on the *in vitro* activity (Table S2, S3).

**Characterization of the Binding Mode by STD NMR, INPHARMA and Molecular Docking.** All together, the above mentioned results raise the question whether the RNAP switch region is indeed the binding site of the ureidothiophene compound series as obtained from our molecular docking experiments. Thus, we performed competition STD NMR (28) experiments where the representative compound **6** (Figure 1) was titrated into a 100:1 complex of **Myx**/RNAP. Difference spectra were monitored for a change in intensity of signals belonging to either **6** or **Myx** during the titration. As shown in Figure 3, stepwise addition of **6** to the complex **Myx**/RNAP diminished the signal intensities of **Myx** concomitant with steady increases in signal intensities belonging to **6**. In fact, addition of three equivalents of **6** resulted in a ~70% uniform decrease in intensity for signals belonging to **Myx** (see Figure 3C). By addition of five equivalents of **6** the signals of **Myx** were almost unnoticeable. Consequently, **6** and **Myx** bind the switch region of RNAP in a competitive manner.

Additionally, competition STD NMR experiments were performed between **6** and two other described switch region binders, corallopyronin A (**Cor**) and ripostatin A (**Rip**) (29, 30) (Figure 1). **Cor** is a structural analog of **Myx** whereas **Rip** is a cyclic macrolide. So far no crystal structures for these natural products have been reported. Nevertheless, isolation and sequencing of **Cor**- and **Rip**-resistant mutants show that the binding pocket of **Rip** and **Cor** overlap with that of **Myx** (14). As illustrated in Figure S2, an overall reduction of the **Cor** and **Rip** STD signals is observed upon the addition of **6**, further indicating that **6** binds into the RNAP switch region.

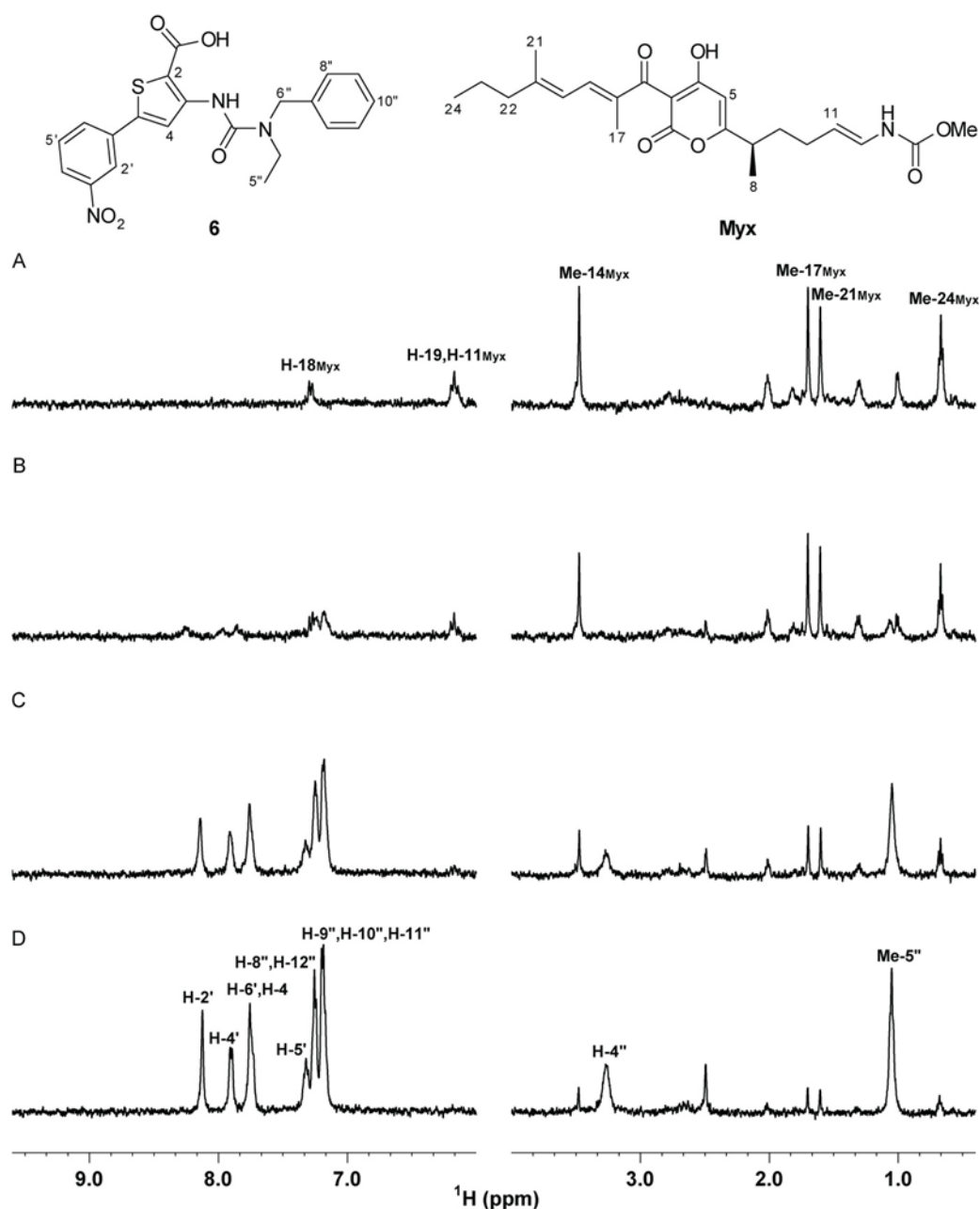


**Figure 3.** STD NMR competition experiments of **6** and **Myx** binding to core RNAP. (A) Expanded  $^1\text{H}$  STD NMR spectrum of **Myx** (250  $\mu\text{M}$ ) in the presence of core RNAP (2.5  $\mu\text{M}$ ). (B-D) STD NMR spectra of the same sample upon addition of (B) 1, (C) 3 and (D) 5 equivalents of **6**.

The INPHARMA method was used to exclude allosteric effects on the displacement of **Myx** by **6** (31). This method is based on the observation of protein-mediated NOE transfer between two ligands binding competitively to the same protein binding pocket. Additionally, we qualitatively analyzed the INPHARMA correlations (32, 33) to determine the binding orientation of **6** in the switch region of RNAP relative to that of **Myx**. To this respect, 2D-NOESY experiments were performed for a mixture of RNAP/**Myx**/**6** in a concentration

ratio of 1:150:150 at mixing times ranging from 20 to 600 ms. Interligand NOE signals were not detected between **6** and **Myx** in absence of RNAP at mixing times as high as 200 ms, thus excluding a direct interaction between **6** and **Myx**. Due to the size of the receptor (~380 kDa) and to avoid “long” spin-diffusion pathways contributing to the interligand signals, 2D NOESY experiments acquired with a mixing time of 70 ms were chosen to analyze spin-diffusion-mediated interligand NOE interactions (34). In particular, INPHARMA correlations of different intensities were observed between protons of the aromatic rings of **6** and protons Me-24, H-23, H-22, Me-21, Me-17, and H-10 of **Myx** (Figure 4 and Table 2).

Interestingly, besides the weak INPHARMA correlations from H-10 no other signals were observed from protons belonging to the eastern chain of **Myx**. These results corroborate that **6** and **Myx** bind competitively to the switch region of RNAP, and furthermore indicate that **6** occupies the region of the **Myx** western chain binding site and slightly occludes that of the eastern chain. Additionally, the strongest INPHARMA correlations were observed from Me-24<sub>Myx</sub> to the protons of both, phenyl and benzyl rings of **6** (Figure 4), suggesting that these two rings and Me-24<sub>Myx</sub> occupy the same area in the binding site. This can only be accomplished if **6** binds to the RNAP switch region in two different poses. In one pose, the phenyl ring is residing at a similar site to that of Me-24<sub>Myx</sub> while in the second pose the benzyl moiety is placed at the Me-24<sub>Myx</sub> position. Unfortunately, overlapping of proton signals for Me-5'' of **6** and Me-8<sub>Myx</sub> prevents us from using diagnostic INPHARMA correlations from the latter to further corroborate this hypothesis. To circumvent this problem, an ureidothiophene analogue (**13**) without the ethyl group at the position of R<sup>2</sup> (Figure 1) was synthesized. Additionally, a methoxy group was introduced to the benzyl ring of **13** to avoid the signal overlap of H-18<sub>Myx</sub> with H-8''/H-12'' of **6**. As a matter of fact, a 2D NOESY spectrum of the mixture RNAP/**13**/**Myx** clearly showed strong interligand NOE interactions from Me-8<sub>Myx</sub> to the protons of the phenyl ring and benzyl moiety indicating that all these three residues are located near the same protein protons (Figure 4b and Table 2). Also, Me-24<sub>Myx</sub> showed strong INPHARMA correlations to protons of both aromatic rings of **13**. Taken together, these results suggest that both, **6** and **13**, can bind to the switch region of RNAP in two different poses with inverted orientations (*vide supra*). Moreover, the INPHARMA data indicate that **6** and **13** partially occlude the **Myx** binding site in a region that ranges from Me-24<sub>Myx</sub> to Me-8<sub>Myx</sub>.

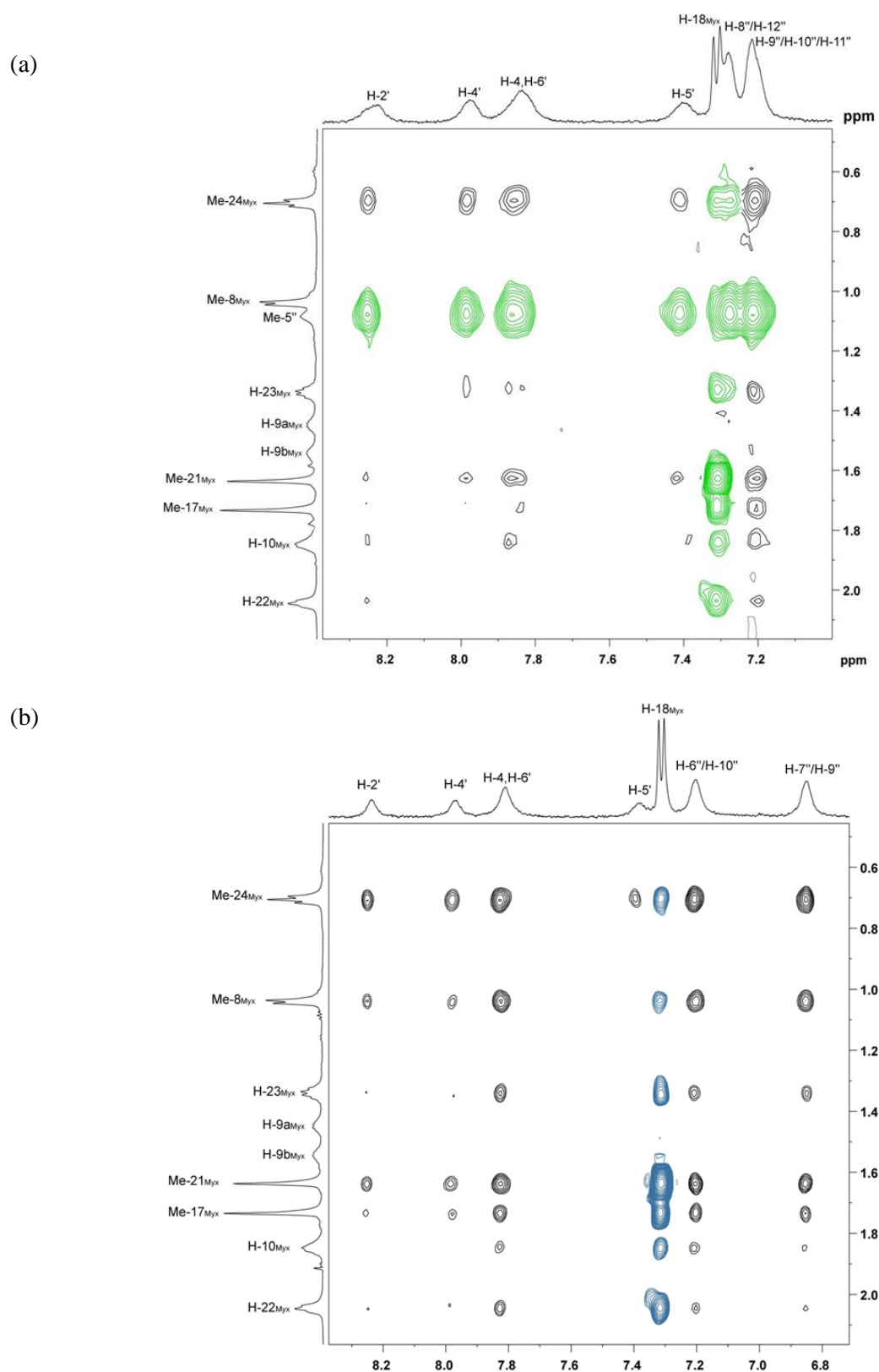


**Figure 4.** NOESY spectra (a) of a mixture of RNAP (2.5  $\mu\text{M}$ ), **Myx** (375  $\mu\text{M}$ ) and **6** (375  $\mu\text{M}$ ) and (b) of a mixture of RNAP (2.5  $\mu\text{M}$ ), **Myx** (375  $\mu\text{M}$ ) and **13** (375  $\mu\text{M}$ ). Signals are assigned in the 1D spectra. The numbering of the atoms of **Myx** and **6** corresponds to that shown in Figure 3, numbering of **13** is shown in the SI (Figure S4). Black peaks represent the interligand transferred NOEs

(INPHARMA NOEs) mediated by the hydrogen atoms of RNAP. Overlapping signals are colored in green and intramolecular transferred NOEs from **13** are colored in blue.

**Table 2.** Observed INPHARMA signals between the hydrogen atoms of **Myx** and **6** and **13**, respectively.

<b>Myx</b>	<b>Compound 6</b>	<b>Compound 13</b>
<b>Me-24</b>	H-2', H-4', H-5', H-4/6' <sup>a</sup> , H-4'', H-9''-11''	H-2', H-4', H-5', H-4/6' <sup>a</sup> , H-6''/10'', H-7''/9'', MeO-8''
<b>H-23</b>	H-4', H-4/6' <sup>a</sup> , H-9''-11''	H-2', H-4', H-4/6' <sup>a</sup> , H-6''/10'', H-7''/9'', 8''MeO-8''
<b>H-22</b>	H-2', H-4/6' <sup>a</sup> , H-9''-11''	H-2', H-4', H-4/6' <sup>a</sup> , H-6''/10'', H-7''/9'', MeO-8''
<b>Me-21</b>	H-2', H-4', H-5', H-4/6' <sup>a</sup> , H-9''-11''	H-2', H-4', H-4/6' <sup>a</sup> , H-6''/10'', H-7''/9'', MeO-8''
<b>Me-17</b>	H-4/6' <sup>a</sup> , H-9''-11''	H-2', H-4', H-4/6' <sup>a</sup> , H-6''/10'', H-7''/9'', MeO-8''
<b>H-10</b>	H-2', H-4/6' <sup>a</sup> , H-8''-12''	H-4/6' <sup>a</sup> , H-6''/10'', H-7''/9'', MeO-8''
<b>Me-8</b>	–	H-2', H-4', H-4/6' <sup>a</sup> , H-6''/10'', H-7''/9'', MeO-8''

<sup>a</sup> indicates overlapping signals

To further evaluate the binding mode of **6** and **13** in the switch region of RNAP, we performed molecular docking studies using MOE (*Molecular Operating Environment*) (31) based on the INPHARMA results. The obtained docking poses with inverted orientations for **6** and **13** that correlated best with the STD and INPHARMA results are illustrated in Figure 5.

In poses A and C the NO<sub>2</sub>-substituted phenyl ring is positioned in the upper hydrophobic region of the **Myx** western chain pocket whereas the benzyl ring occupies the lower part of the eastern chain pocket of **Myx**. In docking poses B and D the same area of the switch region is occupied by **6** and **13**, but the benzyl and the phenyl ring bind in inverted orientations compared to poses A and C.

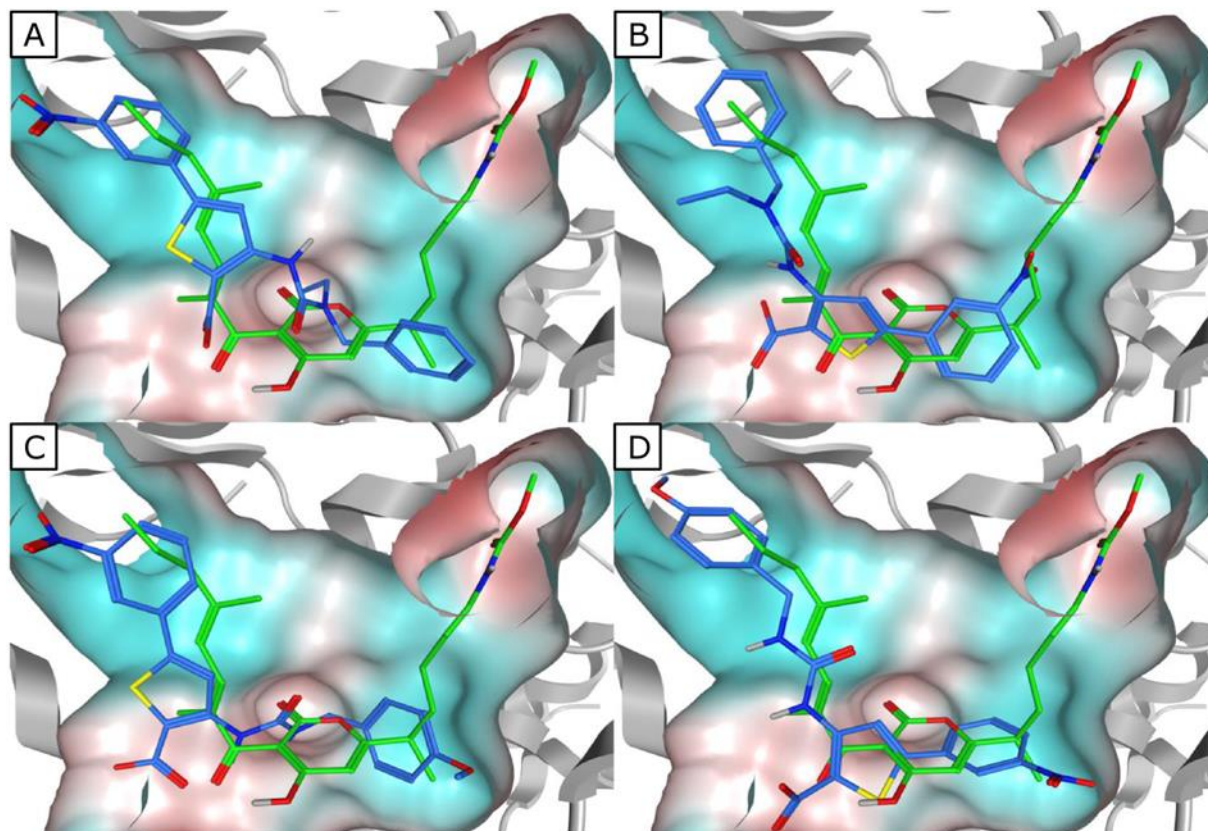


**Figure 5.** Proposed binding modes of **6** (A, B) and **13** (C, D) in the RNAP switch region. Since there is no high-resolution crystal structure of the *E. coli* RNAP switch region available, an *E. coli* homology model (18) was used. The binding mode of **Myx** (green) is shown to illustrate its relative orientation to **6** and **13** (blue). Hydrophobic and hydrophilic areas of the pocket are colored turquoise and red, respectively.

Recently we could demonstrate that the ureidothiophene-2-carboxylic acids are capable of inhibiting the  $\sigma$ :core assembly which would indicate that these compounds could also bind to the  $\sigma$ :core interface (36). Existence of a second binding site is also supported by the fact that titrating **Myx** into a **6**/RNAP complex did not result in the displacement of the STD signals of **6** (data not shown). Further evidence of a second binding site for the ureidothiophenes was achieved by monitoring the dose-dependent effect of **6** to quench the intrinsic fluorescence of RNAP core enzyme. Graphical representation of the results displayed a monophasic curve progression for **Myx** (14) and **Rif** whereas **6** showed a biphasic character of the curve indicating that **6** can bind to more than one binding site. Besides that these compounds can bind in two orientations, a second binding site within RNAP could also contribute to the fact, that amino acid substitutions in the switch region do not impair the inhibitory activity of the ureidothiophene-2-carboxylic acids.

## CONCLUSION

In summary, we have shown that the ureidothiophene-2-carboxylic acids possess good antibacterial activity against different clinically relevant MRSA isolates and **Rif**-resistant *E. coli* TolC strains indicating the absence of cross-resistance with existing antibiotics. On the basis of the STD NMR and INPHARMA data, these compounds bind competitively to **Myx** in the RNAP switch region. The structural information provided by the transfer NOE experiments along with molecular docking studies allowed us to propose a plausible binding mode for the ureidothiophene-2-carboxylic acids, which occupy the same area of the switch region as the **Myx** western chain and the 2-pyrone core. Moreover, our results confirm that our pharmacophore-based virtual screening approach has been successful in identifying easily accessible small molecule RNAP inhibitors that bind to the intended target site, the RNAP switch region, thus providing the potential to avoid the problem of resistance. In closing, these results provide useful insights into the structural requirements for optimized interactions with the target site and may thus facilitate structure-based optimization of this inhibitor class.

## METHODS

**Plasmids.** For purification of *E. coli* wild type core RNAP the plasmid pVS10 was used which encodes the *E. coli* *rpoA-rpoB-rpoC* [His6] and *rpoZ* ORFs under control of a T7 promoter (37). Amino acid substitutions in the *E. coli* RNAP subunits were constructed by site-directed mutagenesis on the basis of pVS10, pRL663 and pIA458 containing a fragment from  $\beta$  *SdaI* to  $\beta'$  *BsmI* (17) and were verified by sequencing. Detailed information about the plasmids are provided in the SI.

**Selection of Rif- and Myx-resistant *E. coli* TolC Spontaneous Mutants.** The procedure was performed as described earlier (38).

**Protein Purification.** Wild type and altered RNAP core enzymes were purified as described previously (37) without the DNA-affinity chromatography step.

**MIC Determination.** 3–4 isolated colonies of *E. coli* TolC transformed with a pRL663 or pRL706 derivative or colonies of spontaneous myxopyronin-resistant *E. coli* TolC mutants were transferred into 5 ml MHB containing 200  $\mu\text{g ml}^{-1}$  ampicillin and incubated over night at 37 °C with shaking. The turbidity of the bacterial suspension was adjusted to that of a McFarland standard 0.5 (OD 600  $\sim$  0,1 for  $10^8$  cfu  $\text{ml}^{-1}$ ) and was then diluted by a factor of 1:100 with sterile MHB ( $10^6$  cfu  $\text{ml}^{-1}$ ). Aliquots of 100  $\mu\text{l}$  bacterial suspension were

subcultured in 100  $\mu\text{L}$  MHB containing the compounds dissolved in DMSO in different concentrations in a 96-well plate in triplicates and incubated at 37 °C for 18 h with shaking (50 rpm). Final DMSO concentration in the experiment was 1 %. For testing *E. coli* TolC transformed with a pRL663 and pRL706 derivative, the MHB was supplemented with IPTG (1 mM). Given MIC values are means of at least two independent determinations (three if  $\text{MIC} < 10 \text{ mg mL}^{-1}$ ) and are defined as the lowest concentration of the compounds that inhibit visible growth of the tested isolates.

MICs for MRSA isolates were determined by broth microdilution as recommended by the Clinical and Laboratory Standards Institute (39). Antibiotic resistance profiles of the MRSA isolates were determined using the Vitek 2 automated antimicrobial susceptibility testing system (bioMérieux, Marcy l'Étoile, France).

**Transcription Assay.** The assay was performed as described previously (18, 40, 41) with minor modifications. Final concentrations in a total volume of 30  $\mu\text{L}$  were 56 nM wild type or mutant core RNAP, respectively. An equimolar amount of  $\sigma^{70}$  was used along with 60 nCi of [5,6- $^3\text{H}$ ]-UTP, 400  $\mu\text{M}$  ATP, CTP and GTP as well as 100  $\mu\text{M}$  of UTP, 20 units of RNase inhibitor (RiboLock, Fermentas), 10 mM DTT, 40 mM tris-HCl (pH 7.5), 150 mM KCl, 10 mM  $\text{MgCl}_2$  and 0.1% CHAPS. As a DNA template 3500 ng of religated pcDNA3.1/V5-His-TOPO was used per reaction. Prior to starting the experiment, core enzyme was preincubated with  $\sigma^{70}$  for 10 min at 25 °C to allow formation of the holo enzyme. Subsequent steps are performed as described previously (18).

**HPLC-based Abortive Transcription Assay.** The assay was performed as described previously (42).

**NMR Spectroscopy.** STD NMR data were recorded at 290 K on a Bruker Avance 500 NMR instrument equipped with a cryogenically cooled 5 mm inverse triple resonance gradient probe. Experiments were recorded with the carrier set at  $-2 \text{ ppm}$  for on-resonance irradiation and 40 ppm for off-resonance irradiation. Control spectra were recorded under identical conditions. Selective protein saturation (2 s) was accomplished using a train of 50 ms Gauss-shaped pulses, each separated by a 1 ms delay, at an experimentally determined optimal power (50 dB on our probe); a T1 $\rho$  filter (15 ms) was incorporated to suppress protein resonances. Experiments were recorded using a minimum of 256 scans and 32 K points. On- and off-resonance spectra were processed independently and subtracted to provide a difference spectrum. 2D NOESY (INPHARMA) experiments were recorded at 290 K on a

Bruker Ascend 700 NMR instrument equipped with a cryogenically cooled 5 mm inverse triple resonance gradient probe. Samples containing 150:150:1 **Myx/6**/core RNAP and **Myx/13**/core RNAP were prepared in deuterated buffer (20 mM NaPO<sub>4</sub> and 50 mM NaCl, pH 6.8). 2D NOESY experiments were acquired using standard pulse sequences with water suppression (WATERGATE), 96 scans as 2048x400 data points at mixing times ranging from 20–800 ms.

**Computational Chemistry.** The virtual binding modes of compounds **6** and **13** were created using MOE (*Molecular Operating Environment*). The model of *E. coli* RNAP in complex with myxopyronin A, which was used as receptor in the following docking experiments, was created by superposition of 3DXJ (*T. thermophilus* RNAP in complex with myxopyronin A) (14) and an *E. coli* RNAP homology model (18). After removal of the *T. thermophilus* protein the remaining receptor-ligand complex was energy minimized using the LigX module of MOE (standard settings) tethering receptor and ligand (strength: 10). Employing the docking module of MOE, compounds **6** and **13** were docked into the myxopyronin binding site. “Triangle Matcher” was chosen as placement method and “London dG” was selected as scoring function. “Rotate bonds” and “Remove duplicates” functions were switched on and 30 hits were retained. Implying the results of the NMR experiments a pharmacophore containing two aromatic features (radius F1: 2 Å, F2: 1.5 Å) was used to guide the docking. Furthermore the same docking was performed with an additional forcefield refinement. The docking results were searched for the poses which correlated best with the NMR results. These were further refined using the LigX module (standard settings) tethering the receptor (strength: 5000) to afford the final binding modes.

## ACKNOWLEDGMENTS

The authors thank R.-H. Ebright for providing pRL663 and pRL706 derivatives and I. Artsimovitch for providing pVS10 and pIA derivatives. Furthermore, we thank J. Jung, J. Ludwig and K. Hilgert for excellent technical support.

## REFERENCES

1. Mattelli, A., Roggi, A., and Carvalho, A. (2014) Extensively drug-resistant tuberculosis: epidemiology and management. *Clin. Epidemiol.* 6, 111–118.
2. Conly, J.-M., and Johnston, B.-L. (2005) Where are all the new antibiotics? The new antibiotic paradox. *Can. J. Infect. Dis. Med. Microbiol.* 16, 159–160.
3. EDCD/EMA Joint Technical Report. The bacterial challenge: time to react. (2009) EMA/576176/2009.
4. Artsimovitch, I., and Vassylyev, D.-G. (2006) Is it easy to stop RNA polymerase? *Cell Cycle* 5, 399–404.
5. Chopra, I. (2007) Bacterial RNA polymerase: a promising target for the discovery of new antimicrobial agents. *Curr. Opin. Invest. Drugs* 8, 600–607.
6. Villain-Guillot, P., Bastide, L., Gualtieri, M., and Leonetti, J.-P. (2007) Progress in targeting bacterial transcription. *Drug Discov. Today* 12, 200–208.
7. Mariani, R., and Maffioli, S.-J. (2009) Bacterial RNA polymerase inhibitors: an organized overview of their structure, derivatives, biological activity and current clinical development status. *Curr. Med. Chem.* 16, 430–454.
8. Venugopal, A.-A., and Johnson, S. (2012) Fidaxomicin: A Novel Macrocyclic Antibiotic Approved for Treatment of *Clostridium difficile* Infection. *Clin. Infect. Dis.* 54, 568–574.
9. Mitchison, D. (2000) Role of individual drugs in the chemotherapy of tuberculosis. *Int. J. Tuberc. Lung Dis.* 4, 796–806.
10. Espinal, M.-A., Laszlo, A., Simonsen, L., Boulahbal, F., Kim, S.-J., Reniero, A., Hoffner, S., Rieder, H.-L., Binkin, N., Dye, C., Williams, R., and Raviglione, M.-C. (2001) Global trends in resistance to antituberculosis drugs. World Health Organization-International Union against tuberculosis and lung disease working group on anti-tuberculosis drug resistance surveillance. *N. Engl. J. Med.* 344, 1294–1303.
11. Mukinda, F.-K., Theron, D., van der Spuy, G.-D., Jacobson, K.-R., Roscher, M., Streicher, E.-M., Musekiwa, A., Coetzee, G.-J., Victor, T.-C., Marais, B.-J., Nachega, J.-B., Warren, R.-M., and Schaaf, H.-S. (2012) Rise in rifampicin-monoresistant tuberculosis in Western Cape, South Africa. *Int. J. Tuberc. Lung Dis.* 16, 196–202.

12. Jin, D.-J., and Gross, C.-A. (1988) Mapping and Sequencing of Mutations in the *Escherichia coli* rpoB Gene that Lead to Rifampicin Resistance. *J. Mol. Biol.* 202, 45–58.
13. Chopra, I. (2007) Bacterial RNA polymerase: a promising target for the discovery of new antimicrobial agents. *Curr. Opin. Invest. Drugs* 8, 600–607.
14. Mukhopadhyay, J., Das, K., Ismail, S., Koppstein, D., Jang, M., Hudson, B., Sarafianos, S., Tuske, S., Patel, J., Jansen, R., Irschik, H., Arnold, E., and Ebright, R.-H. (2008) The RNA polymerase ‘‘switch region’’ is a target for inhibitors. *Cell* 135, 295–307.
15. Srivastava, A., Talaue, M., Liu, S., Degen, D., Ebright, R.-Y., Sineva, E., Chakraborty, A., Druzhinin, S.-Y., Chatterjee, S., Mukhopadhyay, J., Ebright, Y.-W., Zozula, A., Shen, J., Sengupta, S., Niedfeldt, R.-R., Xin, C., Kaneko, T., Irschik, H., Jansen, R., Donadio, S., Connell, N., and Ebright, R.-H. (2011) New target for inhibition of bacterial RNA polymerase: ‘switch region’. *Curr. Opin. Microbiol.* 14, 532–543.
16. Irschik, H., Gerth, K., Hofle, G., Kohl, W., and Reichenbach, H. (1983) The myxopyronins, new inhibitors of bacterial RNA synthesis from *Myxococcus fulvus* (Myxobacteriales). *J. Antibiot.* 36, 1651–1658.
17. Belogurov, G., Vassylyeva, M., Sevostyanova, A., Appleman, J., Xiang, A., Lira, R., Webber, S., Klyuyev, S., Nudler, E., Artsimovitch, I., and Vassylyev, D. (2009) Transcription inactivation through local refolding of the RNA polymerase structure. *Nature* 45, 332–335.
18. Sahner, J.-H., Groh, M., Negri, M., Hauptenthal, J., and Hartmann, R.-W. (2013) Novel small molecule inhibitors targeting the ‘‘switch region’’ of bacterial RNAP: structure-based optimization of a virtual screening hit. *Eur. J. Med. Chem.* 65, 223–231.
19. Fejzo, J., Lepre, C., and Xie, X. (2003) Application of NMR Screening in Drug Discovery. *Curr. Top. Med. Chem.* 3, 81–97.
20. Meyer, B., and Peters, T. (2003) NMR Spectroscopy Techniques for Screening and Identifying Ligand Binding to Protein Receptors. *Angew. Chem. Int. Ed.* 42, 864–890.
21. Voyich, J.-M., Braughton, K.-R., Sturdevant, D.-E., Whitney A.-R., Saïd-Salim, B., Porcella, S.-F., Long, R.-D., Dorward, D.-W., Gardner, D.-J., Kreiswirth, B.-N., Musser, J.-M., and DeLeo, F.-R. (2005) Insights into mechanisms used by *Staphylococcus aureus* to avoid destruction by human neutrophils. *J. Immunol.* 175, 3907–3919.

22. Kornblum, J., Hartman, B.-J., Novick, R.-P., and Tomasz, A. (1986) Conversion of a homogeneously methicillin-resistant strain of *Staphylococcus aureus* to heterogeneous resistance by Tn551-mediated insertional inactivation. *Eur. J. Clin. Microbiol.* 5, 714–8.
23. Ballhausen, B., Jung, P., Kriegeskorte, A., Makgotlho, P.-A., Ruffing, U., von Müller, L., Köck, R., Peters, G., Herrmann, M., Ziebuhr, W., Becker, K., and Bischoff, M. (2014) LA-MRSA CC398 differ from classical community acquired-MRSA and hospital acquired-MRSA lineages: functional analysis of infection and colonization processes. *Int. J. Med. Microbiol.* Epub Jun 27, 2014. DOI: 10.1016/j.ijmm.2014.06.006.
24. Ruffing, U., Akulenko, R., Bischoff, M., Helms, V., Herrmann, M., and von Müller, L. (2012) Matched-cohort DNA microarray diversity analysis of methicillin sensitive and methicillin resistant *Staphylococcus aureus* isolates from hospital admission patients. *PLoS One* 7, e52487.
25. Hüsecken, K., Negri, M., Fruth, M., Boettcher, S., Hartmann, R.-W., and Hauptenthal, J. (2013) Peptide-based investigation of the *Escherichia coli* RNA polymerase  $\sigma^{70}$ : core interface as target site. *ACS Chem. Biol.* 8, 758–766.
26. McClure, W.-R., Cech, C.-L., and Johnston, D.-E. (1978) A steady state assay for the RNA polymerase initiation reaction. *J. Biol. Chem.* 253, 8941.
27. Vo, N.-V., Hsu, L.-M., Kane, C.-M., and Chamberlin, M.-J. (2003) *In Vitro* Studies of Transcript Initiation by *Escherichia coli* RNA Polymerase. 2. Formation and Characterization of Two Distinct Classes of Initial Transcribing Complexes. *Biochemistry* 42, 3787–3797.
28. Mayer, M., and Meyer, B. (2001) Group Epitope Mapping by Saturation Transfer Difference NMR To Identify Segments of a Ligand in Direct Contact with a Protein Receptor. *J. Am. Chem. Soc.* 123, 6108–6117.
29. Irschik, H., Jansen, R., Höfle, G., Gerth, K., and Reichenbach, H. (1985) The coralopyronins, new inhibitors of bacterial RNA synthesis from *Myxobacteria*. *J. Antibiot.* 38, 145–152.
30. Irschik, H., Augustiniak, H., Gerth, K., Höfle, G., and Reichenbach, H. (1995) The Ripostatins, Novel Inhibitors of Eubacterial RNA Polymerase Isolated from *Myxobacteria*. *J. Antibiot.* 48, 787–792.

31. Sánchez-Pedregal, V.-M., Reese, M., Meiler, J., Blommers, M.-J.-J., Griesinger, C., and Carlomagno, T. (2005) The INPHARMA Method: Protein-Mediated Interligand NOEs for Pharmacophore Mapping. *Angew. Chem.* 117, 4244–4247.
32. Bartoschek, S., Klabunde, T., Defossa, E., Dietrich, V., Stengelin, S., Griesinger, C., Carlomagno, T., Focken, I., and Wendt, K.-U. (2010) Drug Design for G-Protein-Coupled Receptors by a Ligand-Based NMR-Method. *Angew. Chem.* 49, 1426–1429.
33. Krimm, I. (2012) INPHARMA-based identification of ligand binding site in fragment-based drug design. *Med. Chem. Commun.* 3, 605–610.
34. Orts, J., Griesinger, C., and Carlomagno, T. (2009) The INPHARMA technique for pharmacophore mapping: A theoretical guide to the method. *J. Mag. Res.* 200, 64–73.
35. *Molecular Operating Environment*, 2010.10; Chemical Computing Group Inc., 1010 Sherbooke St. West, Suite #910, Montreal, QC, Canada, H3A 2R7, (2010).
36. Hüsecken, K., unpublished results.
37. Belogurov, G.-A., Vassilyeva, M.-N., Svetlov, V., Klyuyev, S., Grishin, N.-V., Vassilyev, D.-G., and Artsimovitch, I. (2007) Structural Basis for Converting a General Transcription Factor into an Operon-Specific Virulence Regulator. *Mol. Cell* 26, 117–129.
38. Elgaher, W.-A.-M., Fruth, M., Groh, M., Haupenthal, J., and Hartmann, R.-W. (2014) Expanding the scaffold for bacterial RNA polymerase inhibitors: design, synthesis and structure–activity relationships of ureidoheterocyclic-carboxylic acids. *RSC Adv.* 4, 2177–2194.
39. Methods for Dilution Antimicrobial Susceptibility Tests for Bacteria That Grow Aerobically. Approved standard - Ninth edition. CLSI document M07-A9. Clinical and Laboratory Standards Institute, 950 West Valley Road, Suite 2500, Wayne, PA 19087, USA, 2012.
40. Haupenthal, J., Hüsecken, K., Negri, M., Maurer, C.-K., and Hartmann, R.-W. (2012) Influence of DNA Template Choice on Transcription and Inhibition of *Escherichia coli* RNA Polymerase. *Antimicrob. Agents Chemother.* 56, 4536–4539.
41. Hinsberger, S., Hüsecken, K., Groh, M., Negri, M., Haupenthal, J., and Hartmann, R.-W. (2013) Discovery of Novel Bacterial RNA Polymerase Inhibitors: Pharmacophore-Based Virtual Screening and Hit Optimization. *J. Med. Chem.* 56, 8332–8338.

42. Hüsecken, K., Negri, M., Fruth, M., Boettcher, S., Hartmann, R.-W. and Hauptenthal, J. (2013) Peptide-Based Investigation of the *Escherichia coli* RNA Polymerase  $\sigma^{70}$ :Core Interface As Target Site. *ACS Chem. Biol.* 8, 758–766.

### 3.2 Expanding the scaffold for bacterial RNA polymerase inhibitors: design, synthesis and structure–activity relationships of ureido-heterocyclic-carboxylic acids

Walid A. M. Elgaher, Martina Fruth, Matthias Groh, Jörg Haupenthal, and Rolf W. Hartmann

Reprinted with permission from *RSC Adv.*, 2014, 4, 2177-2194. DOI: 10.1039/c3ra45820b  
Copyright: © 2014 Royal Society of Chemistry.

#### Publication B

#### ABSTRACT

The emergence of bacterial resistance requires the development of new antibiotics with alternative mode of action. Based on class I, developed in our previous study, a new series of RNA polymerase (RNAP) inhibitors targeting the switch region was designed. Feasible synthetic procedures of the aryl-ureido-heterocyclic-carboxylic acids were developed including three regioisomeric thiophene classes (II–IV), as well as three isosteric furan (V, VI) and thiazole (VII) classes. Biological evaluation using a RNAP transcription inhibition assay revealed that class II compounds possess the same activity as the parent class I, whereas classes III, V–VII were active, however with lower potency. Structure activity relationship (SAR) studies, supported by molecular modeling, elucidated the structural requirements necessary for interaction with the binding site. Beside the RNAP inhibitory effects, the new compounds displayed good antibacterial activities against Gram positive bacteria and the Gram negative *E. coli* TolC strain. Moreover, they showed no cross resistance with the clinically used RNAP inhibitor rifampicin (Rif) and a lower rate of resistance compared to Rif.

#### INTRODUCTION

The eternal battle against pathogenic bacteria demands the discovery and development of new weapons aiming vital targets, since the prevalence of antibiotic resistance poses a real threat to human health.<sup>1,2</sup> Bacterial RNAP is a multisubunit enzyme responsible for transcription.<sup>3</sup> It is necessary for cell survival allowing efficacy, and structurally distinguished from eukaryotic

counterparts affording therapeutic selectivity.<sup>4</sup> However, the only clinically used drugs targeting RNAP are the rifamycins which are applied to treat *Mycobacterium tuberculosis* infections, and the recently FDA approved Fidaxomicin for *Clostridium difficile* infections.<sup>5</sup> Hence, while proven as a drug target, RNAP is still underexploited. Our mission is to discover and optimize RNAP inhibitors with an alternative binding site compared to rifamycins, and consequently, with low probability of cross resistance. Recently the “switch region”, a binding pocket distinct from the rifamycins binding site, was discovered and proved to be a promising target site for antibacterial drug discovery.<sup>6–8</sup> The RNAP inhibitors myxopyronin B (Myx B), a natural  $\alpha$ -pyrone antibiotic isolated from the myxobacterium *Myxococcus fulvus*,<sup>9</sup> and its synthetic derivative desmethyl myxopyronin B (dMyx B),<sup>10</sup> have been identified to bind to the “switch region”.<sup>6,7</sup> Although the myxopyronins are highly active *in vitro* and show no cross resistance to rifamycins,<sup>6,11,12</sup> their clinical application is hampered by inadequate physicochemical properties.<sup>13</sup>

These facts motivated us and other research groups to develop novel “switch region” inhibitors. McPhillie *et al.* used a structure based *de novo* design based on the crystal structure of the dMyx B binding site. Although the compounds inhibited RNAP, they displayed no antibacterial activity.<sup>14</sup> Buurmann *et al.* applied a high throughput screening, identified RNAP inhibitors and confirmed the switch region as their target site. However, they showed only weak antibacterial activity.<sup>15</sup> Yakushiji *et al.* pursued a hybrid strategy, combining the core  $\alpha$ -pyrone of Myx with holothin. The resulting RNAP inhibitor was active against Gram positive bacteria.<sup>16</sup>

In a previous work of our group, based on a hit candidate discovered by virtual screening, a series of 5-aryl-3-ureidothiophene-2-carboxylic acids (class I) was synthesized and optimized based on SAR studies. Moreover, the binding mode was experimentally validated. The compounds showed good antibacterial activities accompanied by a low resistance frequency (Fig. 1).<sup>17</sup>

In this work, we focused on finding new chemical scaffolds inspired from class I with better or at least retained biological activities. To achieve this goal, we followed an analog design strategy accompanied by SAR exploration (Fig. 1). The study was supported by molecular modeling to gain deeper insights into the structural features necessary for activity.

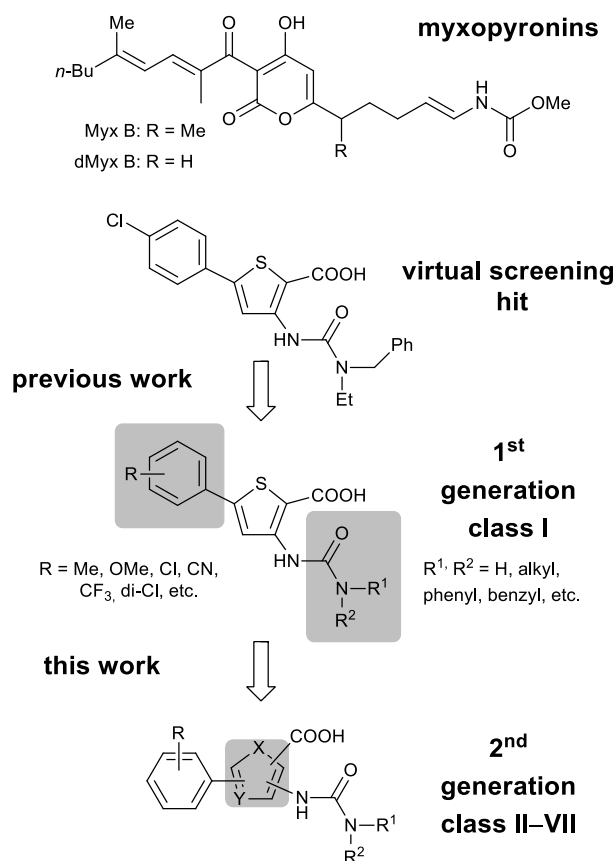


**Figure 1.** Development of second generation bacterial RNAP inhibitors of the ureido-heterocyclic-carboxylic acid type.

## RESULTS & DISCUSSION

### Design Strategy

Analog design was accomplished through two approaches: *via* design of regioisomers of the parent class I, and *via* bioisosteric exchange of the heterocyclic core. By reversing the positions of ureido and carboxyl substituents of class I (class II), shifting the aryl position in class I (class IV), or shifting the aryl position in class II (class III), three classes of regioisomers were initially investigated to identify the optimum configuration of the aryl-ureido-thiophene-carboxylic acids for interaction with the target enzyme (Fig. 2). Based on our previous results,<sup>17</sup> as aryl motif phenyl rings bearing substituents with high  $\pi$  and  $\sigma$  values, namely 4-chlorophenyl and 3,4-dichlorophenyl, were chosen. It was also shown that at the ureido motif hydrophobic and bulky substituents are preferred, therefore *n*-hexyl, benzyl and *N*-ethylbenzyl amine were employed. In the next step, the biological results of classes I–IV were taken into consideration. Based on classes I and II, displaying the highest RNAP inhibitory activity, the classical isosteric ring equivalents –O– for –S– (classes V and VI) or –N= for –CH= (class VII) were investigated (Fig. 2).

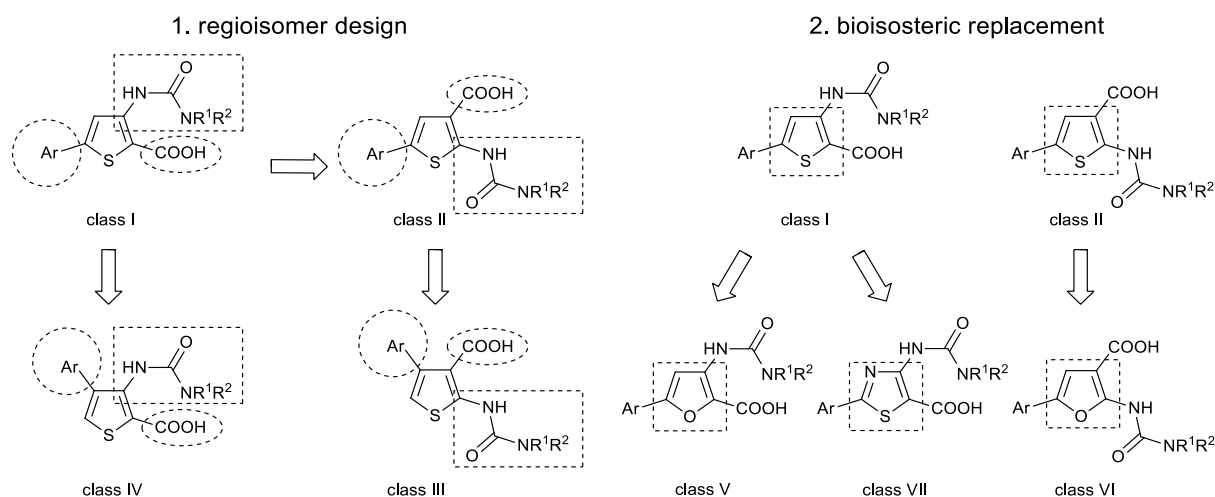
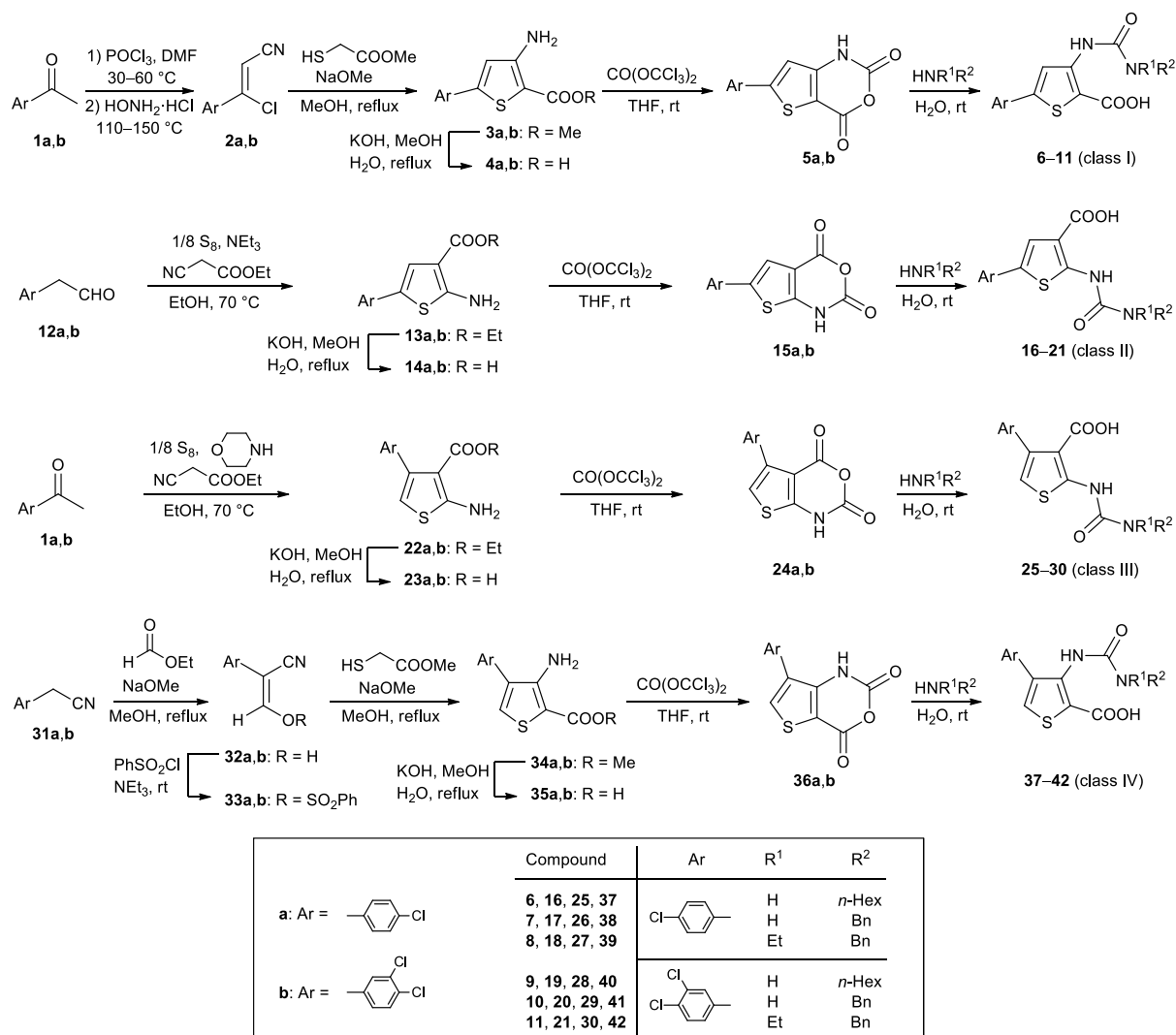


**Figure 2.** Analog design strategies based on the parent class I.

## Chemistry

The synthesis of compounds **6–11** (class I) started by reacting the acetophenones **1a,b** (Scheme 1) with  $\text{POCl}_3$  in DMF followed by  $\text{NH}_2\text{OH}\cdot\text{HCl}$  according to a modified Vilsmeier-Haack-Arnold reaction<sup>18</sup> to give the  $\beta$ -chlorocinnamionitriles **2a,b** which were cyclized using methyl thioglycolate under basic condition (NaOMe) to afford the methyl 5-aryl-3-aminothiophene-2-carboxylates **3a,b**.<sup>17,19</sup> Esters were saponified to the corresponding acids **4a,b** which were treated with triphosgene to form the thiaisatoic anhydrides **5a,b**. The latter reacted with the appropriate amines in water followed by acidic workup to yield the desired 5-aryl-3-ureidothiophene-2-carboxylic acids **6–11**.<sup>17,20,21</sup> The compounds of classes II and III were synthesized by a straightforward procedures *via* Gewald reaction of the arylacetaldehydes **12a,b** or the acetophenones **1a,b** (Scheme 1) with ethyl cyanoacetate and elemental sulfur under basic conditions in a one-pot reaction to afford the ethyl esters **13a,b** and **22a,b**<sup>22,23</sup> respectively. After saponification, synthesis of both the 5- and 4-aryl-2-ureidothiophene-3-carboxylic acids **16–21** and **25–30** *via* the thiaisatoic anhydrides **15a,b** and **24a,b** was also successfully employed as described for the class I derivatives. The synthesis of compounds of class IV was achieved by treating the arylacetonitriles **31a,b** (Scheme 1) with ethyl formate in presence of NaOMe, followed by acidic workup to furnish the 2-aryl-3-hydroxyacrylonitriles **32a,b**.<sup>24–26</sup> Ring closure was accomplished by activation of **32a,b** using benzenesulfonyl chloride to yield the sulfonates **33a,b** which reacted with methyl thioglycolate under basic condition to produce the methyl 3-amino-4-arylthiophene-2-

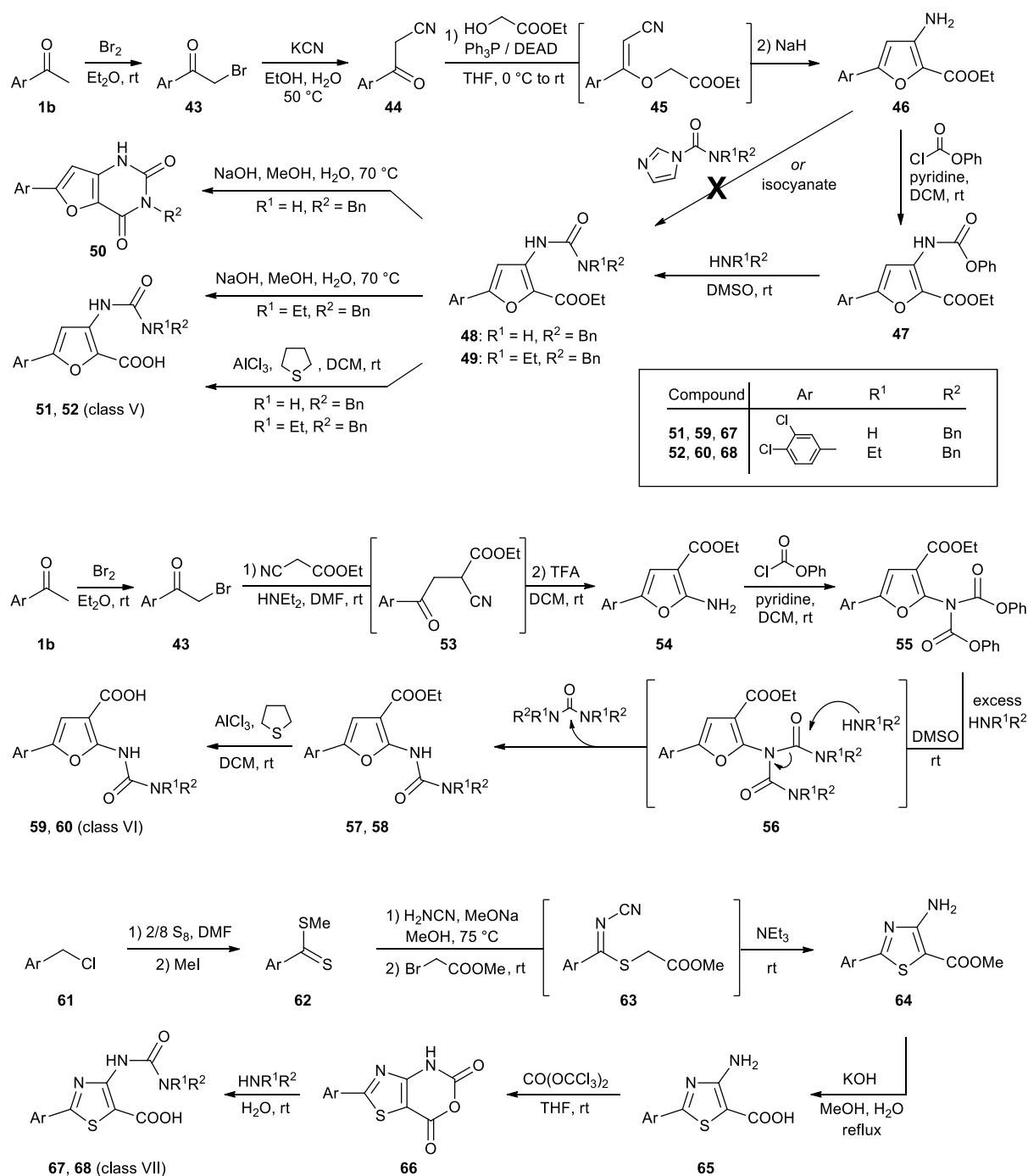
carboxylates **34a,b**.<sup>26</sup> Further synthetic steps *via* the thiaisatoic anhydrides **36a,b** proceeded smoothly to deliver the desired 4-aryl-3-ureidothiophene-2-carboxylic acids **37–42**.



**Scheme 1.** Synthesis of compound classes I–IV.

For the synthesis of compounds **51** and **52** (class V), acetophenone **1b** (Scheme 2) was converted to the  $\beta$ -ketonitrile **44** *via* bromination<sup>27</sup> and subsequent nucleophilic substitution using KCN.<sup>28,29</sup> Compound **44** was further reacted under Mitsunobu conditions<sup>30</sup> with ethyl glycolate to the intermediate vinyl ether **45** that was cyclized under basic condition (NaH) to yield the ethyl 3-aminofuran-2-carboxylate **46**. We initially attempted to adopt the “isatoic anhydride strategy” for the furan class as described for synthesis of the ureidothiophene analogs. Unfortunately, the required 3-aminofuran-2-carboxylic acid could not be obtained. Various conditions for alkaline hydrolysis of the ester **46** led to decomposition of the furan

ring, and a ring opening product was isolated. This observation is attributed to the unusual instability and weak aromatic properties characterizing the aminofurans.<sup>31–33</sup> Therefore, we decided to postpone the hydrolysis to the end of the synthesis as the ureido-furan derivatives are less electron rich and should be less prone to decomposition.<sup>34</sup> To prepare the urea derivatives, compound **46** was treated directly with the carbamoylimidazoles<sup>35</sup> or isocyanate<sup>36</sup> but no conversion was observed. Finally, an alternative route *via* the phenyl carbamate **47** followed by nucleophilic substitution with the appropriate amines<sup>37</sup> gave the desired ureido-furan-carboxylic esters **48** and **49**. The hydrolysis to the free acids proceeded smoothly under basic condition for the *N*-benzyl-*N*-ethylurea derivative **49** to afford **52**, but for the *N*-benzyl derivative **48** cyclization yielding the uracil derivative **50** occurred. Therefore, non-saponificative, mild dealkylation was conducted using AlCl<sub>3</sub> in tetrahydrothiophene (THT)<sup>38</sup> affording the desired carboxylic acid **51**. The synthesis of the regioisomeric furan system class VI proceeded *via* coupling of the phenacyl bromide **43** (Scheme 2) with ethyl cyanoacetate to give the intermediate **53** that was cyclized under acidic condition (TFA) to deliver the 2-aminofuran-carboxylic ester **54**. Interestingly, reaction of **54** with phenyl chloroformate afforded only the diacylated product **55** even when a stoichiometric amount of reagent was used. This is consistent with previous findings regarding the reactivity of 2-aminofurans.<sup>39</sup> The subsequent transformation into the urea derivatives **57** and **58** required an excess of the amine to eliminate the second carbamoyl group from the intermediate **56**. Finally, the acids **59** and **60** were obtained by dealkylation using AlCl<sub>3</sub> in THT. The thiazole class VII was prepared starting from the benzyl chloride **61** (Scheme 2) that was reacted with elemental sulfur and alkylated with methyl iodide to give the carbodithioate **62**. For the ring closure, **62** was first reacted with cyanamide in basic medium (NaOMe) and further *S*-alkylated with methyl bromoacetate to give the intermediate **63** that was cyclized under basic conditions affording the 4-aminothiazole ester **64**. After alkaline hydrolysis, the acid **65** was converted to the thiazoloisatoic anhydride **66**. This intermediate reacted in the same manner as described for the thiophene derivatives to the ureidothiazole carboxylic acids **67** and **68**.



**Scheme 2.** Synthesis of compound classes V–VII.

### *In vitro* RNA polymerase inhibitory activity

Compounds of classes I–VII were tested for their inhibitory activity against *E. coli* RNAP and the results are shown in table 1. Generally compounds with 3,4-dichloro substituents exhibited higher activity than 4-chlorophenyl derivatives in the same class. This finding is in accordance with our previous study of the parent class I.<sup>17</sup> An increase of activity was also observed with substituents having larger hydrophobic volume at the ureido motif with the

general trend benzylethyl  $\sim$  *n*-hexyl > benzyl. Compounds of class II showed RNAP inhibitory activities as good as the parent class I. Interestingly, the 3,4-dichloro derivatives **19–21** (IC<sub>50</sub>: 18, 43, and 21  $\mu$ M respectively) showed identical activities to their analogous compounds **9–11** of class I (IC<sub>50</sub>: 18, 46, and 22  $\mu$ M respectively). The class III analogs **28–30** displayed moderate activities (IC<sub>50</sub>: 75, 84, and 57  $\mu$ M respectively, about 2–4 fold decrease), while class IV derivatives **40–42** possessed weaker activities (IC<sub>50</sub>: 74 to >100  $\mu$ M, >4 fold decrease).

The outstanding role of classes I and II regarding RNAP inhibition can be explained on the basis of molecular similarity, *i.e.* similar molecules exhibit similar activities.<sup>40–42</sup> The similarity of classes I–IV was analyzed *in silico* by using molecular fingerprint method, where a graph 3-point pharmacophore (GpiDAPH3) was applied as 2D fingerprint system. As similarity metric the Tanimoto coefficient (T<sub>C</sub>) was used.<sup>43</sup> Class II showed maximum similarity to I (T<sub>C</sub> = 1.00), followed by III (T<sub>C</sub> = 0.93), while IV exhibited low similarity (T<sub>C</sub> = 0.65). Another similarity assessment *via* flexible alignment of classes I–IV revealed that the aryl, ureido, and carboxyl substituents as well as the thiophene core of I and II are coincided (Figure 3A). Class III also matches except that the carboxyl group is located in the opposite position to that of I and II, whereas neither the ureido nor the carboxyl substituents of IV fit to the configuration of I and II (Figure 3A). Hence class I and II are similar with respect to their configuration in space. Consequently they can assume the same orientation and binding mode, which results in the same inhibitory activities. These results were confirmed by docking of compounds **11**, **21**, and **30** representing classes I–III respectively, in the dMyx B binding site of *T. Thermophilus* RNA polymerase (PDB code 3EQL).<sup>7</sup> Both **11** and **21** bind to the crescent shape pocket in the same manner (Figure 3B, C). The thiophene core is located at the top of the cavity opening, anchored by hydrogen bond or ion pair interaction of the carboxyl group with the  $\beta$ 'Lys610 residue. The 3,4-dichlorophenyl moiety occupies the lower part of the enecarbamate binding pocket of dMyx B. The ureido group carrying the lipophilic benzyl and ethyl substituents is located deeply in the hydrophobic pocket occupied by the dMyx B dienone side chain, and stabilized by CH- $\pi$  interaction with  $\beta$ Leu1088 as well as an intramolecular hydrogen bond with the carboxyl group. On the other hand compound **30** (class III) binds mainly through CH- $\pi$  interaction between the lipophilic substituted ureido moiety and  $\beta$ Leu1088, but lacks the interaction with  $\beta$ 'Lys610, as the carboxyl group is oriented in the opposite direction (Figure 3D). Accordingly, a lower inhibitory activity of **30** (IC<sub>50</sub>: 57  $\mu$ M) in comparison with compounds **11** or **21** (IC<sub>50</sub>: 22  $\mu$ M, 21  $\mu$ M) was observed.

**Table 1** *In vitro* inhibitory activity against *E. coli* RNA polymerase and antibacterial activities.

Compd	Ar	R <sup>1</sup> R <sup>2</sup>	Inhibition of <i>E. coli</i> RNAP <sup>a</sup>
<b>6</b>		H, <i>n</i> -Hex	68 μM
<b>7</b>		H, Bn	31%
<b>8<sup>b</sup></b>		Et, Bn	75 μM
<b>9<sup>b</sup></b>		H, <i>n</i> -Hex	18 μM
<b>10<sup>b</sup></b>		H, Bn	46 μM
<b>11<sup>b</sup></b>		Et, Bn	22 μM
<b>16</b>		H, <i>n</i> -Hex	14%
<b>17</b>		H, Bn	84 μM
<b>18</b>		Et, Bn	54 μM
<b>19</b>		H, <i>n</i> -Hex	18 μM
<b>20</b>		H, Bn	43 μM
<b>21</b>		Et, Bn	21 μM
<b>25</b>		H, <i>n</i> -Hex	11%
<b>26</b>		H, Bn	n.i.
<b>27</b>		Et, Bn	14%
<b>28</b>		H, <i>n</i> -Hex	75 μM
<b>29</b>		H, Bn	84 μM
<b>30</b>		Et, Bn	57 μM
<b>37</b>		H, <i>n</i> -Hex	n.i.
<b>38</b>		H, Bn	n.i.
<b>39</b>		Et, Bn	n.i.
<b>40</b>		H, <i>n</i> -Hex	74 μM
<b>41</b>		H, Bn	8%
<b>42</b>		Et, Bn	100 μM
<b>51</b>		H, Bn	116 μM
<b>52</b>		Et, Bn	61 μM
<b>59</b>		H, Bn	26%
<b>60</b>		Et, Bn	60 μM
<b>67</b>		H, Bn	48 μM
<b>68</b>		Et, Bn	51 μM
Myx B			0.35 μM
Rif			0.03 μM

<sup>a</sup> IC<sub>50</sub> values (μM) or % inhibition at 100 μM of *E. coli* RNAP; n.i. = inhibition ≤5% at 100 μM. <sup>b</sup> previously reported<sup>17</sup>

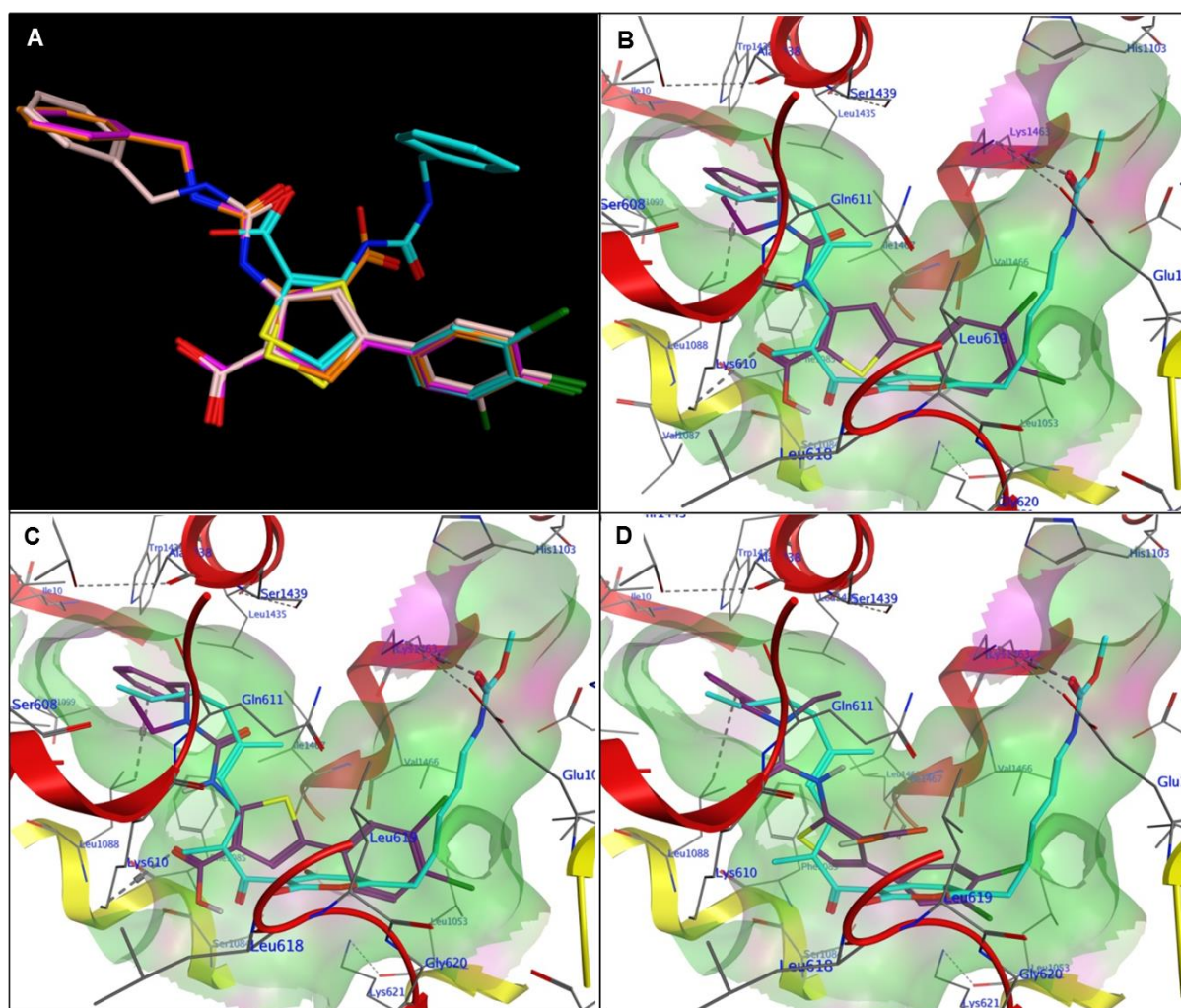


**Figure 3.** (A) Flexible alignment of compounds **10** (white), **20** (magenta), **29** (orange), and **41** (turquoise). (B) Docking pose of compound **11** (violet) in the dMyx B (turquoise) binding site: hydrophobic surface (green), polar surface (pink),  $\beta$  chain (yellow),  $\beta'$  chain (red). (C) Docking pose of **21** (violet). (D) Docking pose of **30** (violet).

The effect of exchanging the heterocyclic core on the RNAP inhibitory activity was studied for compounds of classes V–VII. The results revealed that both of the furan classes V and VI displayed about a threefold decrease in activity compared to the corresponding thiophene analogs (class I and II), whereas the thiazole class VII exhibited only a slightly lowered potency (Table 1). By replacement or introduction of hetero atoms the electronic properties as well as the size of the ring is influenced and both effects can have an impact on the affinity to target. The latter is more likely to be responsible for the observed differences in activity. The ring size influences interatomic distances, bond angles, and determines the overall shape of the ligand.<sup>44</sup> According to the observed activities, thiophene is obviously most appropriate to keep the aryl, ureido, and carboxyl functionalities in the optimal geometry necessary for binding to the target enzyme. This is reflected by the relationship of the angle ( $\alpha$ ) between the

aryl and ureido substituents and RNAP activity ( $pIC_{50}$ ) for classes I–VII (Figure 4). A parabolic curve was obtained, with the optimum range for  $\alpha$  between 150 and 159° (classes I, II, and VII located at the maximum). The observed exception for class III ( $\alpha = 156^\circ$ ) can be explained by the different localization of the carboxyl group leading to a reduced binding affinity as discussed above.

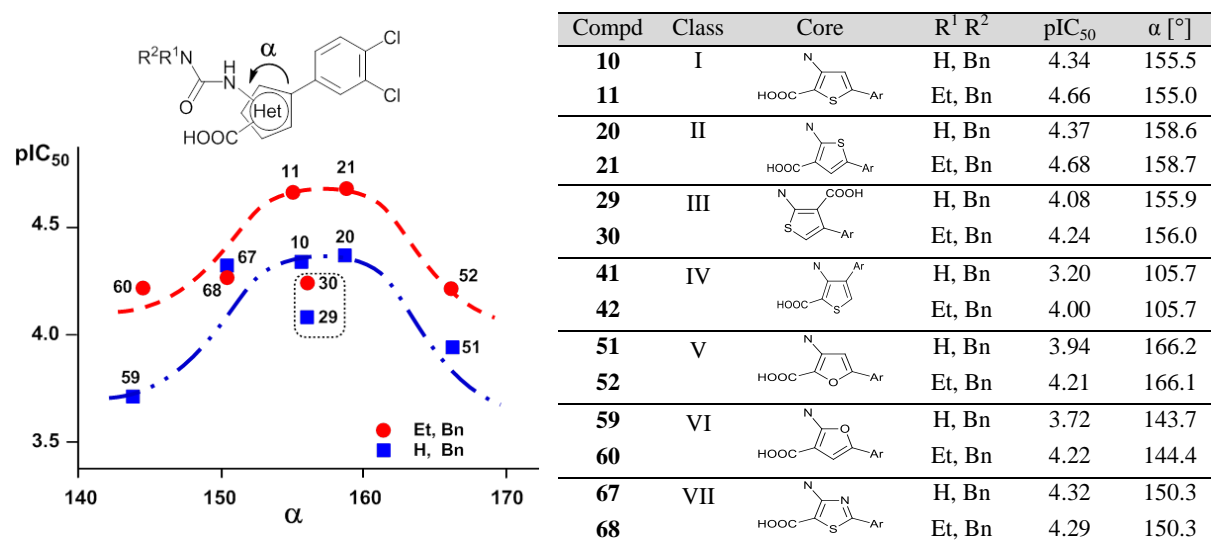


**Figure 4.** Relationship between RNAP inhibitory activity ( $pIC_{50}$ ) and angle  $\alpha$ .

### Antibacterial activity

To explore the antibacterial spectrum of our RNAP inhibitors, eight compounds representing the most active classes were selected. Compounds with *n*-hexyl substituents were excluded due to solubility problems. The antibacterial activities were evaluated in the Gram positive *B. subtilis* and *S. aureus*, as well as in the Gram negative strains *E. coli* K12, *P. aeruginosa*, *E. coli* TolC, a mutant deficient in the AcrAB-TolC efflux system, and two Rif-resistant *E. coli* TolC mutants and are expressed as minimal inhibitory concentrations (MIC) values. As reference compounds Myx B and Rif were used (Table 2). It was found that the compounds possess antibacterial activities against the Gram positive strains. Regarding the Gram negative bacteria with the exception of *E. coli* TolC, compounds were not active similarly to Myx B. It is noteworthy that the antibacterial activity against *S. aureus* is well correlating with the RNAP inhibitory activity, whereas in case of *B. subtilis* and *E. coli* TolC the correlation was less pronounced. Similar discrepancies between RNAP inhibition and MIC values are also observed for Myx B and Rif (Table 2), and have been frequently

reported.<sup>17,45,46</sup> In the experiments with the Rif-resistant strains all of the five tested compounds representing different classes showed no reduction of antibacterial activity compared to the normal *E. coli* TolC strain. This demonstrates that there is no cross resistance with Rif as it has been expected due to the different binding sites.

**Table 2.** Antibacterial activities of selected aryl-ureido-heterocyclic-carboxylic acids.

Compd	IC <sub>50</sub> RNAP ( $\mu$ M)	MIC <sub>95</sub> ( $\mu$ g/mL) <sup>a</sup>						
		<i>S. aureus</i>	<i>B. subtilis</i>	<i>E. coli</i> TolC	<i>E. coli</i> TolC $\beta$ Q513L <sup>b</sup>	<i>E. coli</i> TolC $\beta$ H526Y <sup>b</sup>	<i>E. coli</i> K12	<i>P. aeruginosa</i>
<b>11</b>	22	8	11	14	14	16	>25	>25
<b>18</b>	54	20	5	11	-	-	>25	>25
<b>21</b>	21	10	2	10	7	9	>25	>25
<b>29</b>	84	80	15	10	-	-	>100	>100
<b>30</b>	57	23	6	7	7	7	>100	>100
<b>52</b>	61	33	12	30	25	25	>50	>50
<b>60</b>	60	28	14	>50	-	-	>50	>50
<b>68</b>	51	36	45	47	50	50	>50	>50
Myx B	0.35	0.5	1	1	1	1	>25	>25
Rif	0.03	0.02	5	6	>100	>100	7	13

<sup>a</sup> > MIC determination was limited due to insufficient solubility of the test compound.

<sup>b</sup> Rif-resistant *E. coli* TolC strains with mutations in the *rpoB* gene encoding for the RNAP  $\beta$  subunit.

### Role of cell wall penetration and drug efflux for antibacterial activity in *E. coli* strains

Considering the facts that RNAP is highly conserved in bacteria,<sup>3</sup> and our compounds were active against Gram positive strains as well as *E. coli* TolC, but not against Gram negative bacteria, the most likely conclusion to be drawn is that they are unable to accumulate in the cytoplasm to inhibit RNAP. This could be due to cell wall impermeability, *i.e.* slow diffusion through porins or the outer membrane (OM) lipid bilayer, efflux mechanisms or both. The observed activity in the TolC mutant lacking the OM part of the tripartite efflux machinery gives a strong hint that efflux plays a prominent role for our compounds. To verify this hypothesis and to get a better understanding of their uptake pathway, the antibacterial effect for selected compounds was determined in presence of the OM permeability enhancer polymyxin B nonapeptide (PMBN)<sup>47</sup> or the efflux pumps inhibitor PA $\beta$ N.<sup>48,49</sup> MIC values were determined against *E. coli* TolC, *E. coli* D22 (LPS mutant with increased OM permeability) and *E. coli* K12 (intact cell wall system) and are shown in table 3.

**Table 3.** Effect of PMBN and PA $\beta$ N on antibacterial activities of selected aryl-ureido-heterocyclic-carboxylic acids.

Compd	<i>E. coli</i> TolC			<i>E. coli</i> K12			<i>E. coli</i> D22	
	MIC <sub>95</sub> <sup>a</sup>	MIC <sub>95</sub> + PMBN (1 $\mu$ g/mL)	MIC <sub>95</sub> + PA $\beta$ N (10 $\mu$ g/mL)	MIC <sub>50</sub>	MIC <sub>50</sub> + PMBN (1 $\mu$ g/mL)	MIC <sub>50</sub> + PA $\beta$ N (20 $\mu$ g/mL)	MIC <sub>50</sub>	MIC <sub>50</sub> + PA $\beta$ N (20 $\mu$ g/mL)
<b>11</b>	14	7	1	>25	>25	>25	>50	>25
<b>21</b>	10	4	1	>25	>25	4	>25	12
<b>30</b>	7	5	1	>100	>100	18	40	15
<b>52</b>	30	11	6	>50	>50	>50	>100	49
<b>68</b>	47	22	4	>50	>50	>50	>50	>50

<sup>a</sup> MIC values in  $\mu$ g/mL.

PMBN produced only a slight decrease in *E. coli* TolC MIC values (factors 1.4–2.7) and no effect was observed in the K12 strain. Moreover, the compounds showed no enhanced activity against the *E. coli* D22 strain. It cannot be excluded that an increased membrane permeability may be counteracted by efflux.<sup>50</sup> It is known that PMBN enhances penetration of antibiotics which diffuse across the OM (10–300 fold decrease in MIC values against *E. coli*), but it has only a slight effect when antibiotics traverse through porins.<sup>47</sup> Hence, the uptake pathway of our compounds into Gram negative bacteria appears to be mainly permeation through the porins. On the other hand, PA $\beta$ N increased the susceptibility to the compounds in *E. coli* TolC by factors of 5–14 and by factors  $\geq 3$  in the K12 and D22 strains. These results indicate that both the OM barrier and efflux pumps contribute to the inactivity of our compounds in Gram negative bacteria, however, efflux mechanisms play the major role. Obviously, beside AcrAB-TolC other efflux systems are involved in *E. coli* drug efflux.

### Spontaneous resistance rate

Low propensity of resistance development is a criterion for an effective antibacterial agent. Spontaneous resistance rate towards Myx B in *S. aureus* was found to be 4 to 7  $\times 10^{-8}$ , similar to that of Rif.<sup>12</sup> However, Myx B-resistant mutants possessed higher fitness costs compared to Rif-resistant mutants, giving an advantage to Myx B, and other RNAP “switch region” inhibitors, of having a lower clinical prevalence of resistance than Rif.<sup>12</sup> Determination of *in vitro* resistance rate for **30** in *E. coli* TolC at 2  $\times$  MIC revealed a significant lower rate ( $< 4.2 \times 10^{-11}$ ) compared to Rif ( $8.3 \times 10^{-8}$ ) and Myx B ( $7.1 \times 10^{-8}$ ) as previously observed for the class I derivatives.<sup>17</sup> This observation indicates that the probability of resistance development is reduced with the ureido-thiophene-carboxylic acids compared to MyxB and Rif. An explanation for this finding could be that our compounds occupy only a part of the “switch region” whereas Myx B fills a larger space including the enecarbamate binding

pocket. Mutations in this part, responsible for Myx resistance,<sup>6,12</sup> should not prevent our compounds from binding and inhibiting the enzyme.<sup>17</sup> Another explanation for a reduced resistance rate could be an additional effect on another target.

### Cytotoxicity

The *in vitro* toxicity of selected compounds was evaluated by monitoring the cytotoxicity in HEK 293 cells at different time points using doxorubicin (LD<sub>50</sub>: 0.3 μM) and Rif (LD<sub>50</sub>: 80 μM) as positive and negative controls respectively. After 72 h, the compounds displayed LD<sub>50</sub> values in the range of 25 to >100 μM comparable to Rif (Table 4).

**Table 4.** Cytotoxicity of selected aryl-ureido-heterocyclic-carboxylic acids.

Compd	LD <sub>50</sub> (μM)		
	24 h	48 h	72 h
<b>8</b>	95	78	91
<b>10</b>	>100	>100	>100
<b>11</b>	67	50	46
<b>18</b>	84	82	75
<b>21</b>	61	57	62
<b>30</b>	40	17	25
<b>52</b>	61	61	57
Doxorubicin	5	0.7	0.3
Rif	24% <sup>a</sup>	38% <sup>a</sup>	80

<sup>a</sup> at 100 μM

### CONCLUSION

Following an analog design strategy novel chemical scaffolds as bacterial RNAP inhibitors were developed. Derived from the parent class I, a series of regioisomeric ureido-thiophene-carboxylic acid derivatives and bioisosteric heterocyclic classes were designed and studied. The synthetic route *via* the “isatoic anhydrides” for the thiophene and thiazole derivatives was robust and feasible. For the synthesis of the furan derivatives the established strategy had to be modified due to the instability of the furan system. Thereby, class II possessing the same RNAP inhibitory activity as the parent class I, as well as classes III, and V–VII with only slightly lowered potency were discovered. The detailed investigation of the SAR, including molecular alignment, docking studies and angle analysis contributed to a deeper understanding of the structural requirements for interaction with the protein target. The compounds were active against Gram positive bacteria including the pathogen *S. aureus* but

ineffective against Gram negative bacteria. The non-susceptibility can be attributed to drug efflux. Nevertheless, the observed low mammalian cytotoxicity, the reduced resistance frequency and the activity against Rif-resistant strains make these novel scaffolds promising for further optimization as antibacterial agents against Gram positive pathogens.

## EXPERIMENTAL

### Materials and methods

Starting materials and solvents were purchased from commercial suppliers, and used without further purification. All chemical yields refer to purified compounds, and were not optimized. Reaction progress was monitored using TLC Silica gel 60 F<sub>254</sub> aluminium sheets, and visualization was accomplished by UV at 254 nm. Flash chromatography was performed using silica gel 60 Å (40–63 µm). Preparative RP-HPLC was carried out on a Waters Corporation setup contains a 2767 sample manager, a 2545 binary gradient module, a 2998 PDA detector and a 3100 electron spray mass spectrometer. Purification was performed using a Waters XBridge column (C18, 150 × 19 mm, 5 µm), a binary solvent system A and B (A = water with 0.1% formic acid; B = MeCN with 0.1% formic acid) as eluent, a flow rate of 20 mL/min and a gradient of 60% to 95% B in 8 min were applied. Melting points were determined on a Stuart Scientific melting point apparatus SMP3 (Bibby Sterilin, UK), and are uncorrected. NMR spectra were recorded either on Bruker DRX-500 (<sup>1</sup>H, 500 MHz; <sup>13</sup>C, 126 MHz), or Bruker Fourier 300 (<sup>1</sup>H, 300 MHz; <sup>13</sup>C, 75 MHz) spectrometer at 300 K. Chemical shifts are recorded as δ values in ppm units by reference to the hydrogenated residues of deuterated solvent as internal standard (CDCl<sub>3</sub>: δ = 7.26, 77.02; DMSO-d<sub>6</sub>: δ = 2.50, 39.99). Splitting patterns describe apparent multiplicities and are designated as s (singlet), br s (broad singlet), d (doublet), dd (doublet of doublet), t (triplet), q (quartet), m (multiplet). Coupling constants (*J*) are given in Hertz (Hz). Purity of all compounds used in biological assays was ≥95% as measured by LC/MS Finnigan Surveyor MSQ Plus (Thermo Fisher Scientific, Dreieich, Germany). The system consists of LC pump, autosampler, PDA detector, and single-quadrupole MS detector, as well as the standard software Xcalibur for operation. RP C18 Nucleodur 100-5 (125 × 3 mm) column (Macherey-Nagel GmbH, Düren, Germany) was used as stationary phase, and a binary solvent system A and B (A = water with 0.1% TFA; B = MeCN with 0.1% TFA) was used as mobile phase. In a gradient run the percentage of B was increased from an initial concentration of 0% at 0 min to 100% at 15 min and kept at 100% for 5 min. The injection volume was 10 µL and flow rate was set to 800 µL/min. MS (ESI) analysis was carried out at a spray voltage of 3800 V, a capillary

temperature of 350 °C and a source CID of 10 V. Spectra were acquired in positive mode from 100 to 1000 m/z and at 254 nm for UV tracing.

## Chemistry

Synthesis of 5-(aryl)-3-[3-(substituted)ureido]thiophene-2-carboxylic acids **6–11** was previously described,<sup>17</sup> as well as the experimental data of compounds **8–11**.<sup>17</sup>

**5-(4'-Chlorophenyl)-3-(3-hexylureido)thiophene-2-carboxylic acid 6.**<sup>21</sup> Beige crystals; mp 198–199 °C;  $\delta_{\text{H}}$  (300 MHz, DMSO- $d_6$ ) 0.86 (3 H, t,  $J = 4.8$  Hz, Me), 1.19–1.49 (8 H, m, Me(CH<sub>2</sub>)<sub>4</sub>CH<sub>2</sub>NH), 3.08 (2 H, m, CH<sub>2</sub>CH<sub>2</sub>NH), 7.50 (2 H, d,  $J = 7.8$  Hz, 3',5'-Ar-H), 7.63 (1 H, t,  $J = 4.8$  Hz, NHCH<sub>2</sub>), 7.68 (2 H, d,  $J = 7.8$  Hz, 2',6'-Ar-H), 8.28 (1 H, s, C4-H), 9.33 (1 H, br s, NHCO), 13.13 (1 H, br s, COOH);  $\delta_{\text{C}}$  (75 MHz, DMSO- $d_6$ ) 14.39 (C6''), 22.54 (C5''), 26.56 (C3''), 29.85 (C2''), 31.47 (C4''), 39.78 (C1''), 107.40 (C2), 118.89 (C4), 127.81 (C2', C6'), 129.77 (C3', C5'), 132.23 (C1'), 134.07 (C4'), 145.64 (C5), 146.74 (C3), 154.25 (NHCO), 165.23 (COOH); m/z (ESI+) 381 (17%, (M + H)<sup>+</sup>), 761 (33, 2M + H), 295 (40, M – C<sub>6</sub>H<sub>13</sub>), 236 (100, M – C<sub>6</sub>H<sub>13</sub>, NH, CO<sub>2</sub>);  $t_{\text{R}} = 14.86$  min.

**3-(3-Benzylureido)-5-(4'-chlorophenyl)thiophene-2-carboxylic acid 7.**<sup>21</sup> White crystals; mp 216–217 °C;  $\delta_{\text{H}}$  (300 MHz, DMSO- $d_6$ ) 4.31 (2 H, d,  $J = 5.7$  Hz, CH<sub>2</sub>), 7.21–7.38 (5 H, m, Ph), 7.51 (2 H, d,  $J = 8.6$  Hz, 3',5'-Ar-H), 7.70 (2 H, d,  $J = 8.6$  Hz, 2',6'-Ar-H), 8.22 (1 H, t,  $J = 5.7$  Hz, NHCH<sub>2</sub>), 8.30 (1 H, s, C4-H), 9.43 (1 H, br s, NHCO), 13.15 (1 H, br s, COOH);  $\delta_{\text{C}}$  (75 MHz, DMSO- $d_6$ ) 43.46 (CH<sub>2</sub>), 107.42 (C2), 118.91 (C4), 127.30 (C4''), 127.76 (C2'', C6''), 127.87 (C2', C6'), 128.79 (C3'', C5''), 129.79 (C3', C5'), 132.15 (C1'), 134.15 (C4'), 140.26 (C1''), 145.90 (C5), 146.65 (C3), 154.36 (NHCO), 165.16 (COOH); m/z (ESI+) 387 (19%, (M + H)<sup>+</sup>), 772 (10, 2M), 295 (10, M – C<sub>7</sub>H<sub>7</sub>), 236 (100, M – C<sub>7</sub>H<sub>7</sub>, NH, CO<sub>2</sub>);  $t_{\text{R}} = 13.38$  min.

## General procedures for synthesis of 2-(aryl)acetaldehydes **12a** and **12b**

To a stirred ice-cooled suspension of pyridinium chlorochromate (12.9 g, 60.0 mmol) in anhydrous DCM (80 mL), the appropriate 2-(aryl)ethanol.<sup>51,52</sup> (40.0 mmol) in DCM (10 mL) was added in one portion. The reaction mixture was allowed to warm to rt, and stirred for 2 h, then anhydrous Et<sub>2</sub>O (100 mL) was added, and the supernatant was decanted from the black gum. The insoluble residue was washed thoroughly with anhydrous Et<sub>2</sub>O (2 × 50 mL), the combined organic solution was passed through a short pad of silica, and the solvent was removed by vacuum distillation. The crude product was used directly in the next step without further purification. Purity was determined to be 70–80% as indicated from <sup>1</sup>H-NMR spectra.

**2-(4'-Chlorophenyl)acetaldehyde 12a.**<sup>53</sup> Yellow oil;  $\delta_{\text{H}}$  (300 MHz,  $\text{CDCl}_3$ ) 3.67 (2 H, d,  $J = 1.0$  Hz,  $\text{CH}_2$ ), 7.15 (2 H, d,  $J = 8.1$  Hz, 3',5'Ar-H), 7.33 (2 H, d,  $J = 8.1$  Hz, 2',6'Ar-H), 9.74 (1 H, t,  $J = 1.0$  Hz, CHO).

**2-(3',4'-Dichlorophenyl)acetaldehyde 12b.**<sup>54</sup> Yellow oil;  $\delta_{\text{H}}$  (300 MHz,  $\text{CDCl}_3$ ) 3.68 (2 H, d,  $J = 1.9$  Hz,  $\text{CH}_2$ ), 7.05 (1 H, dd,  $J = 8.0, 2.0$  Hz, 6'Ar-H), 7.32 (1 H, d,  $J = 2.0$  Hz, 2'Ar-H), 7.37 (1 H, d,  $J = 8.0$  Hz, 5'Ar-H), 9.75 (1 H, t,  $J = 1.9$  Hz, CHO).

### General procedures for synthesis of ethyl 2-amino-5-(aryl)thiophene-3-carboxylates 13a and 13b

To a stirred suspension of the appropriate aldehyde **12a** or **12b** (30.0 mmol), ethyl cyanoacetate (3.39 g, 30.0 mmol), and sulfur (0.96 g, 30.0 mmol) in EtOH (30 mL), a solution of  $\text{NEt}_3$  (4.04 g, 30.0 mmol) in EtOH (5 mL) was added slowly. The reaction mixture was stirred at 70 °C for 12 h, then solvent was removed by vacuum distillation. The obtained residue was dissolved in DCM (50 mL) and washed with water ( $2 \times 50$  mL). The organic layer was dried ( $\text{MgSO}_4$ ) and concentrated. The crude material was purified by flash chromatography ( $\text{SiO}_2$ , *n*-hexane/EtOAc = 6:1).

**Ethyl 2-amino-5-(4'-chlorophenyl)thiophene-3-carboxylate 13a (5.49 g, 65%).** Pale yellow solid; mp 100–101 °C;  $\delta_{\text{H}}$  (300 MHz,  $\text{CDCl}_3$ ) 1.36 (3 H, t,  $J = 7.1$  Hz, Me), 4.30 (2 H, q,  $J = 7.1$  Hz,  $\text{CH}_2\text{O}$ ), 6.03 (2 H, br s,  $\text{NH}_2$ ), 7.21 (1 H, s, C4-H), 7.27 (2 H, d,  $J = 8.9$  Hz, 3',5'Ar-H), 7.35 (2 H, d,  $J = 8.9$  Hz, 2',6'Ar-H);  $\delta_{\text{C}}$  (75 MHz,  $\text{CDCl}_3$ ) 14.54 (Me), 59.94 ( $\text{CH}_2$ ), 108.04 (C3), 121.79 (C4), 123.48 (C5), 125.81 (C2', C6'), 128.91 (C3', C5'), 132.16 (C4'), 132.56 (C1'), 162.17 (C2), 165.29 (C=O);  $m/z$  (ESI+) 281 (8%,  $\text{M}^+$ ), 236 (100, M – EtO);  $t_{\text{R}} = 14.05$  min.

**Ethyl 2-amino-5-(3',4'-dichlorophenyl)thiophene-3-carboxylate 13b (6.05 g, 64%).** Pale yellow solid; mp 130–131 °C;  $\delta_{\text{H}}$  (300 MHz,  $\text{CDCl}_3$ ) 1.37 (3 H, t,  $J = 7$  Hz, Me), 4.30 (2 H, q,  $J = 7.0$  Hz,  $\text{CH}_2\text{O}$ ), 6.08 (2 H, br s,  $\text{NH}_2$ ), 7.22 (1 H, dd,  $J = 8.0, 2.0$  Hz, 6'Ar-H), 7.23 (1 H, s, C4-H), 7.36 (1 H, d,  $J = 8.0$  Hz, 5'Ar-H), 7.48 (1 H, d,  $J = 2.0$  Hz, 2'Ar-H);  $\delta_{\text{C}}$  (75 MHz,  $\text{CDCl}_3$ ) 14.53 (Me), 60.03 ( $\text{CH}_2$ ), 108.11 (C3), 121.90 (C4), 122.78 (C6'), 123.74 (C5), 126.11 (C2'), 130.04 (C4'), 130.62 (C5'), 132.91 (C3'), 134.12 (C1'), 162.48 (C2), 165.20 (C=O);  $m/z$  (ESI+) 315 (18%,  $\text{M}^+$ ), 270 (100, M – EtO);  $t_{\text{R}} = 15.14$  min.

### General procedures for synthesis of 2-amino-5-(aryl)thiophene-3-carboxylic acids 14a and 14b

To a stirred solution of the appropriate ester **13a** or **13b** (25.0 mmol) in MeOH (100 mL), KOH (6.17 g, 110 mmol) in water (100 mL) was added. The reaction mixture was stirred at

reflux for 3–5 h (TLC monitoring), then MeOH was evaporated by vacuum distillation. The residue was diluted with water (50 mL) and washed with EtOAc (2 × 50 mL). The aqueous layer was cooled in an ice bath and acidified by KHSO<sub>4</sub> (saturated aqueous solution) to pH 3–4. The precipitated solid was collected by filtration, washed with cold water (2 × 30 mL), *n*-hexane (2 × 30 mL), and dried over CaCl<sub>2</sub> in amber glass vacuum desiccator.

**2-Amino-5-(4'-chlorophenyl)thiophene-3-carboxylic acid 14a (4.11 g, 65%).** Beige solid; mp 195–197 °C;  $\delta_{\text{H}}$  (300 MHz, DMSO-*d*<sub>6</sub>) 7.26 (1 H, s, C4-H), 7.36 (2 H, d, *J* = 8.6 Hz, 3',5'-Ar-H), 7.45 (2 H, d, *J* = 8.6 Hz, 2',6'-Ar-H), 7.47 (2 H, br s, NH<sub>2</sub>), 12.10 (1 H, br s, COOH);  $\delta_{\text{C}}$  (75 MHz, DMSO-*d*<sub>6</sub>) 106.36 (C3), 120.76 (C4), 123.19 (C5), 125.94 (C2', C6'), 129.30 (C3', C5'), 130.69 (C4'), 133.31 (C1'), 163.93 (C2), 166.48 (C=O); *m/z* (ESI+) 253 (72%, M<sup>+</sup>), 255 (28, [M+2]<sup>+</sup>), 236 (100, M – OH), 209 (14, M – CO<sub>2</sub>); *t<sub>R</sub>* = 10.83 min.

**2-Amino-5-(3',4'-dichlorophenyl)thiophene-3-carboxylic acid 14b (5.88 g, 82%).** Beige solid; mp 229–231 °C;  $\delta_{\text{H}}$  (300 MHz, DMSO-*d*<sub>6</sub>) 7.38 (1 H, dd, *J* = 8.0, 2.0 Hz, 6'-Ar-H), 7.39 (1 H, s, C4-H), 7.52 (1 H, d, *J* = 8.0 Hz, 5'-Ar-H), 7.55 (2 H, br s, NH<sub>2</sub>), 7.69 (1 H, d, *J* = 2.0 Hz, 2'-Ar-H), 12.15 (1 H, br s, COOH);  $\delta_{\text{C}}$  (75 MHz, DMSO-*d*<sub>6</sub>) 106.57 (C3), 119.11 (C4), 124.37 (C6'), 124.77 (C5), 125.60 (C2'), 128.26 (C4'), 131.33 (C5'), 132.16 (C3'), 135.18 (C1'), 164.37 (C2), 166.43 (C=O); *m/z* (ESI+) 287 (88%, M<sup>+</sup>), 289 (56, [M+2]<sup>+</sup>), 270 (100, M – OH), 243 (8, M – CO<sub>2</sub>), 227 (25, M – CO<sub>2</sub>, NH<sub>2</sub>); *t<sub>R</sub>* = 11.87 min.

### General procedures for synthesis of 6-(aryl)-1*H*-thieno[2,3-*d*][1,3]oxazine-2,4-diones 15a and 15b

To a stirred solution of the appropriate acid **14a** or **14b** (6.00 mmol) in THF (60 mL), triphosgene (1.29 g, 4.36 mmol) was added portionwise over 30 min. The reaction mixture was stirred at rt for 2 h, then NaHCO<sub>3</sub> (saturated aqueous solution, 30 mL) was added cautiously, and the resulting mixture was extracted with EtOAc/THF (1:1, 2 × 50 mL). The combined organic layer was washed with brine (50 mL), dried (MgSO<sub>4</sub>), and the solvent was removed by vacuum distillation. The obtained crude material was suspended in *n*-hexane/EtOAc (4:1, 50 mL), stirred in a water bath at 40 °C for 10 min, cooled, and collected by filtration.

**6-(4'-Chlorophenyl)-1*H*-thieno[2,3-*d*][1,3]oxazine-2,4-dione 15a (1.2 g, 74%).** Beige solid; mp 254–256 °C;  $\delta_{\text{H}}$  (300 MHz, DMSO-*d*<sub>6</sub>) 7.40 (2 H, d, *J* = 8.7 Hz, 3',5'-Ar-H), 7.48 (1 H, s, C5-H), 7.60 (2 H, d, *J* = 8.7 Hz, 2',6'-Ar-H), 11.73 (1 H, br s, NH);  $\delta_{\text{C}}$  (75 MHz, DMSO-*d*<sub>6</sub>) 109.70 (C4a), 119.10 (C5), 126.74 (C2', C6'), 128.28 (C6), 129.39 (C3', C5'), 131.75 (C4'), 133.00 (C1'), 150.22 (C7a), 152.83 (C2), 159.67 (C4); *m/z* (ESI+) 279 (20%, M<sup>+</sup>), 235 (100, M – CO<sub>2</sub>); *t<sub>R</sub>* = 10.40 min.

**6-(3',4'-Dichlorophenyl)-1*H*-thieno[2,3-*d*][1,3]oxazine-2,4-dione 15b (1.5 g, 81%).** Beige solid; mp >300 °C;  $\delta_{\text{H}}$  (300 MHz, DMSO- $d_6$ ) 7.61 (2 H, m, 5',6'Ar-H), 7.79 (1 H, s, C5-H), 7.96 (1 H, s, 2'Ar-H), 12.76 (1 H, br s, NH);  $\delta_{\text{C}}$  (75 MHz, DMSO- $d_6$ ) 111.46 (C4a), 120.60 (C5), 125.72 (C6'), 127.17 (C2'), 130.87 (C4'), 131.57 (C5'), 131.83 (C6), 132.50 (C3'), 133.21 (C1'), 147.81 (C7a), 155.32 (C2), 155.82 (C4); m/z (ESI+) 313 (14%,  $M^+$ ), 355 (100,  $M + H$ , MeCN), 627 (28,  $2M + H$ ), 296 (35,  $M - OH$ );  $t_{\text{R}} = 11.44$  min.

### General procedures for synthesis of 5-(aryl)-2-[3-(substituted)ureido]thiophene-3-carboxylic acids 16–21

To a stirred suspension of thiaisatoic anhydride **15a** or **15b** (0.64 mmol) in water (8 mL), the appropriate amine (1.40 mmol) was added. The reaction mixture was stirred at rt for 2 h, then poured on ice-cooled 2M HCl (40 mL), and extracted with EtOAc/THF (1:1, 40 mL). The organic layer was washed with 2M HCl (40 mL), brine (40 mL), dried ( $\text{MgSO}_4$ ), and concentrated in vacuo. The obtained crude material was suspended in *n*-hexane/EtOAc (4:1, 50 mL), stirred in a water bath at 40 °C for 10 min, cooled, and collected by filtration.

#### **5-(4'-Chlorophenyl)-2-(3-hexylureido)thiophene-3-carboxylic acid 16 (132 mg, 54%).**

Pale brown crystals; mp 230–232 °C;  $\delta_{\text{H}}$  (300 MHz, DMSO- $d_6$ ) 0.87 (3 H, t,  $J = 6.8$  Hz, Me), 1.03–1.57 (8 H, m,  $\text{Me}(\text{CH}_2)_4\text{CH}_2\text{NH}$ ), 3.11 (2 H, m,  $\text{CH}_2\text{CH}_2\text{NH}$ ), 7.40 (2 H, d,  $J = 8.6$  Hz, 3',5'Ar-H), 7.43 (1 H, s, C4-H), 7.59 (2 H, d,  $J = 8.6$  Hz, 2',6'Ar-H), 7.94 (1 H, t,  $J = 4.2$  Hz,  $\text{NHCH}_2$ ), 10.24 (1 H, br s, NHCO), 12.82 (1 H, br s, COOH);  $\delta_{\text{C}}$  (75 MHz, DMSO- $d_6$ ) 14.39 (C6''), 22.54 (C5''), 26.50 (C3''), 29.71 (C2''), 31.43 (C4''), 39.86 (C1''), 111.55 (C3), 121.27 (C4), 126.63 (C2', C6'), 128.77 (C5), 129.45 (C3', C5'), 131.62 (C4'), 133.17 (C1'), 151.41 (C2), 153.88 (NHCO), 166.35 (COOH); m/z (ESI+) 380 (33%,  $M^+$ ), 761 (100,  $2M + H$ ), 295 (18,  $M - \text{C}_6\text{H}_{13}$ );  $t_{\text{R}} = 14.38$  min.

#### **2-(3-Benzylureido)-5-(4'-chlorophenyl)thiophene-3-carboxylic acid 17 (136 mg, 55%).**

Pale brown crystals; mp 250–252 °C;  $\delta_{\text{H}}$  (300 MHz, DMSO- $d_6$ ) 4.34 (2 H, d,  $J = 5.6$  Hz,  $\text{CH}_2$ ), 7.15–7.39 (5 H, m, Ph), 7.41 (2 H, d,  $J = 8.6$  Hz, 3',5'Ar-H), 7.45 (1 H, s, C4-H), 7.59 (2 H, d,  $J = 8.6$  Hz, 2',6'Ar-H), 8.49 (1 H, t,  $J = 5.3$  Hz,  $\text{NHCH}_2$ ), 10.35 (1 H, br s, NHCO), 12.87 (1 H, br s, COOH);  $\delta_{\text{C}}$  (75 MHz, DMSO- $d_6$ ) 43.67 ( $\text{CH}_2$ ), 111.79 (C3), 121.29 (C4), 126.68 (C2', C6'), 127.45 (C4''), 127.81 (C2'', C6''), 128.86 (C3'', C5''), 129.02 (C5), 129.46 (C3', C5'), 131.70 (C4'), 133.09 (C1'), 139.75 (C1''), 151.20 (C2), 154.01 (NHCO), 166.29 (COOH); m/z (ESI+) 387 (30%,  $(M + H)^+$ ), 773 (22,  $2M + H$ ), 295 (26,  $M - \text{C}_7\text{H}_7$ ), 170 (100);  $t_{\text{R}} = 13.18$  min.

**2-(3-Benzyl-3-ethylureido)-5-(4'-chlorophenyl)thiophene-3-carboxylic acid 18 (136 mg, 51%).** Pale brown crystals; mp 215–216 °C;  $\delta_{\text{H}}$  (300 MHz, DMSO- $d_6$ ) 1.16 (3 H, t,

$J = 7.1$  Hz, Me), 3.42 (2 H, q,  $J = 7.1$  Hz, MeCH<sub>2</sub>N), 4.60 (2 H, s, PhCH<sub>2</sub>N), 7.24–7.39 (5 H, m, Ph), 7.41 (2 H, d,  $J = 8.6$  Hz, 3',5'-Ar-H), 7.48 (1 H, s, C4-H), 7.62 (2 H, d,  $J = 8.6$  Hz, 2',6'-Ar-H), 10.96 (1 H, br s, NHCO), 13.15 (1 H, br s, COOH);  $\delta_C$  (75 MHz, DMSO-d<sub>6</sub>) 13.52 (Me), 42.42 (MeCH<sub>2</sub>N), 49.96 (PhCH<sub>2</sub>N), 112.30 (C3), 120.98 (C4), 126.79 (C2', C6'), 127.64 (C4''), 127.75 (C2'', C6''), 129.04 (C3'', C5''), 129.48 (C3', C5'), 129.68 (C5), 131.87 (C4'), 132.97 (C1'), 138.06 (C1''), 151.67 (C2), 153.10 (NHCO), 167.43 (COOH);  $m/z$  (ESI+) 415 (100%, (M + H)<sup>+</sup>), 829 (90, 2M + H);  $t_R = 14.08$  min.

**5-(3',4'-Dichlorophenyl)-2-(3-hexylureido)thiophene-3-carboxylic acid 19 (165 mg, 62%).** Beige crystals; mp 245–247 °C;  $\delta_H$  (300 MHz, DMSO-d<sub>6</sub>) 0.86 (3 H, t,  $J = 6.8$  Hz, Me), 1.16–1.56 (8 H, m, Me(CH<sub>2</sub>)<sub>4</sub>CH<sub>2</sub>NH), 3.11 (2 H, m, CH<sub>2</sub>CH<sub>2</sub>NH), 7.53 (1 H, dd,  $J = 8.0, 2.0$  Hz, 6'-Ar-H), 7.56 (1 H, s, C4-H), 7.59 (1 H, d,  $J = 8.0$  Hz, 5'-Ar-H), 7.83 (1 H, d,  $J = 2.0$  Hz, 2'-Ar-H), 7.97 (1 H, t,  $J = 4.7$  Hz, NHCH<sub>2</sub>), 10.26 (1 H, br s, NHCO), 12.89 (1 H, br s, COOH);  $\delta_C$  (75 MHz, DMSO-d<sub>6</sub>) 14.39 (C6''), 22.53 (C5''), 26.49 (C3''), 29.69 (C2''), 31.43 (C4''), 39.85 (C1''), 111.65 (C3), 122.63 (C4), 125.03 (C6'), 126.41 (C2'), 127.27 (C5), 129.29 (C4'), 131.51 (C5'), 132.28 (C3'), 135.00 (C1'), 151.88 (C2), 153.85 (NHCO), 166.27 (COOH);  $m/z$  (ESI+) 414 (100%, M<sup>+</sup>), 416 (69, [M+2]<sup>+</sup>), 829 (67, 2M + H), 329 (42, M – C<sub>6</sub>H<sub>13</sub>);  $t_R = 15.40$  min.

**2-(3-Benzylureido)-5-(3',4'-dichlorophenyl)thiophene-3-carboxylic acid 20 (194 mg, 72%).** White crystals; mp 256–258 °C;  $\delta_H$  (300 MHz, DMSO-d<sub>6</sub>) 4.34 (2 H, d,  $J = 5.6$  Hz, CH<sub>2</sub>), 7.22–7.39 (5 H, m, Ph), 7.53 (1 H, dd,  $J = 8.0, 2.0$  Hz, 6'-Ar-H), 7.58 (1 H, s, C4-H), 7.60 (1 H, d,  $J = 8.0$  Hz, 5'-Ar-H), 7.84 (1 H, d,  $J = 2.0$  Hz, 2'-Ar-H), 8.51 (1 H, t,  $J = 5.6$  Hz, NHCH<sub>2</sub>), 10.38 (1 H, br s, NHCO), 12.93 (1 H, br s, COOH);  $\delta_C$  (75 MHz, DMSO-d<sub>6</sub>) 43.68 (CH<sub>2</sub>), 111.97 (C3), 122.68 (C4), 125.08 (C6'), 126.47 (C2'), 127.46 (C4''), 127.49 (C5), 127.82 (C2'', C6''), 128.86 (C3'', C5''), 129.37 (C4'), 131.52 (C5'), 132.30 (C3'), 134.94 (C1'), 139.71 (C1''), 151.63 (C2), 153.99 (NHCO), 166.24 (COOH);  $m/z$  (ESI+) 421 (47%, (M + H)<sup>+</sup>), 843 (100, 2M + 3H), 329 (11, M – C<sub>7</sub>H<sub>7</sub>);  $t_R = 13.94$  min.

**2-(3-Benzyl-3-ethylureido)-5-(3',4'-dichlorophenyl)thiophene-3-carboxylic acid 21 (210 mg, 73%).** Beige crystals; mp 228–230 °C;  $\delta_H$  (300 MHz, DMSO-d<sub>6</sub>) 1.16 (3 H, t,  $J = 7.1$  Hz, Me), 3.42 (2 H, q,  $J = 7.1$  Hz, MeCH<sub>2</sub>N), 4.60 (2 H, s, PhCH<sub>2</sub>N), 7.24–7.40 (5 H, m, Ph), 7.55 (1 H, dd,  $J = 8.0, 2.0$  Hz, 6'-Ar-H), 7.59 (1 H, d,  $J = 8.0$  Hz, 5'-Ar-H), 7.60 (1 H, s, C4-H), 7.86 (1 H, d,  $J = 2.0$  Hz, 2'-Ar-H), 10.98 (1 H, br s, NHCO), 13.22 (1 H, br s, COOH);  $\delta_C$  (75 MHz, DMSO-d<sub>6</sub>) 13.52 (Me), 42.47 (MeCH<sub>2</sub>N), 49.99 (PhCH<sub>2</sub>N), 112.45 (C3), 122.35 (C4), 125.17 (C6'), 126.58 (C2'), 127.66 (C4''), 127.76 (C5), 128.15 (C2'', C6''), 129.04 (C3'', C5''),

129.54 (C4'), 131.53 (C5'), 132.33 (C3'), 134.80 (C1'), 138.03 (C1''), 152.11 (C2), 153.07 (NHCO), 167.38 (COOH); m/z (ESI+) 448 (100%, M<sup>+</sup>); t<sub>R</sub> = 14.99 min.

Synthesis and characterization of ethyl 2-amino-4-(aryl)thiophene-3-carboxylates **22a**<sup>22</sup> and **22b**<sup>23</sup> were previously described.

Synthesis of 2-amino-4-(aryl)thiophene-3-carboxylic acids **23a** and **23b** were performed as described for **14a** and **14b**.

**2-Amino-4-(4'-chlorophenyl)thiophene-3-carboxylic acid 23a (3.48 g, 55%).** Pale brown solid; mp 137–139 °C; δ<sub>H</sub> (300 MHz, DMSO-d<sub>6</sub>) 6.17 (1 H, s, C5-H), 7.26 (2 H, d, *J* = 8.6 Hz, 3',5'Ar-H), 7.34 (2 H, d, *J* = 8.6 Hz, 2',6'Ar-H), 7.40 (2 H, br s, NH<sub>2</sub>), 11.76 (1 H, br s, COOH); δ<sub>C</sub> (75 MHz, DMSO-d<sub>6</sub>) 103.60 (C3), 105.90 (C5), 127.63 (C2', C6'), 130.87 (C3', C5'), 131.61 (C4'), 137.69 (C4), 139.95 (C1'), 165.71 (C2), 166.66 (C=O); m/z (ESI+) 254 (48%, (M + H)<sup>+</sup>), 507 (4, 2M + H), 236 (100, M – OH); t<sub>R</sub> = 10.16 min.

**2-Amino-4-(3',4'-dichlorophenyl)thiophene-3-carboxylic acid 23b (3.59 g, 50%).** Pale brown solid; mp 142–144 °C; δ<sub>H</sub> (300 MHz, DMSO-d<sub>6</sub>) 6.27 (1 H, s, C5-H), 7.24 (1 H, dd, *J* = 8.0, 2.0 Hz, 6'Ar-H), 7.41 (2 H, br s, NH<sub>2</sub>), 7.47 (1 H, d, *J* = 2.0 Hz, 2'Ar-H), 7.53 (1 H, d, *J* = 8.0 Hz, 5'Ar-H), 11.96 (1 H, br s, COOH); δ<sub>C</sub> (75 MHz, DMSO-d<sub>6</sub>) 103.37 (C3), 106.79 (C5), 129.53 (C6'), 129.75 (C5'), 130.25 (C4'), 130.32 (C2'), 130.86 (C3'), 138.52 (C4), 139.41 (C1'), 165.78 (C2), 166.44 (C=O); m/z (ESI+) 288 (100%, (M + H)<sup>+</sup>), 575 (19, 2M + H), 270 (77, M – OH); t<sub>R</sub> = 11.04 min.

Synthesis of 5-(aryl)-1*H*-thieno[2,3-*d*][1,3]oxazine-2,4-diones **24a** and **24b** were performed as described for preparation of **15a** and **15b**.

**5-(4'-Chlorophenyl)-1*H*-thieno[2,3-*d*][1,3]oxazine-2,4-dione 24a (1.2 g, 71%).** Pale grey solid; mp 235–237 °C; δ<sub>H</sub> (300 MHz, DMSO-d<sub>6</sub>) 7.16 (1 H, s, C6-H), 7.46 (2 H, d, *J* = 8.9 Hz, 3',5'Ar-H), 7.51 (2 H, d, *J* = 8.9 Hz, 2',6'Ar-H), 12.68 (1 H, br s, NH); δ<sub>C</sub> (75 MHz, DMSO-d<sub>6</sub>) 107.59 (C4a), 116.09 (C6), 128.36 (C2', C6'), 131.12 (C3', C5'), 131.35 (C4'), 133.21 (C5), 137.56 (C1'), 147.93 (C7a), 154.98 (C2), 157.82 (C4); m/z (ESI+) 279 (100%, M<sup>+</sup>), 559 (6, 2M + H); t<sub>R</sub> = 10.23 min.

**5-(3',4'-Dichlorophenyl)-1*H*-thieno[2,3-*d*][1,3]oxazine-2,4-dione 24b (1.5 g, 80%).** Beige solid; mp 236–238 °C; δ<sub>H</sub> (300 MHz, DMSO-d<sub>6</sub>) 7.27 (1 H, s, C6-H), 7.48 (1 H, dd, *J* = 8.0, 2.0 Hz, 6'Ar-H), 7.68 (1 H, d, *J* = 8.0 Hz, 5'Ar-H), 7.75 (1 H, d, *J* = 2.0 Hz, 2'Ar-H), 12.70 (1 H, br s, NH); δ<sub>C</sub> (75 MHz, DMSO-d<sub>6</sub>) 107.58 (C4a), 117.07 (C6), 129.59 (C6'), 130.51 (C5'), 131.01 (C4'), 131.13 (C2'), 131.15 (C3'), 134.83 (C5), 136.08 (C1'), 147.87 (C7a), 155.07 (C2), 157.85 (C4); m/z (ESI+) 313 (8%, M<sup>+</sup>), 355 (100, M + H, MeCN), 626 (12, 2M), 296 (20, M – OH); t<sub>R</sub> = 10.77 min.

Synthesis of 4-(aryl)-2-[3-(substituted)ureido]thiophene-3-carboxylic acids **25–30** were performed as described for preparation of **16–21**.

**4-(4'-Chlorophenyl)-2-(3-hexylureido)thiophene-3-carboxylic acid 25 (180 mg, 74%).**

Pale grey crystals; mp 191–193 °C;  $\delta_{\text{H}}$  (300 MHz, DMSO- $d_6$ ) 0.87 (3 H, t,  $J = 6.7$  Hz, Me), 1.21–1.51 (8 H, m, Me(CH $_2$ ) $_4$ CH $_2$ NH), 3.10 (2 H, m, CH $_2$ CH $_2$ NH), 6.63 (1 H, s, C5-H), 7.29 (2 H, d,  $J = 8.6$  Hz, 3',5'-Ar-H), 7.36 (2 H, d,  $J = 8.6$  Hz, 2',6'-Ar-H), 7.87 (1 H, t,  $J = 5.1$  Hz, NHCH $_2$ ), 10.39 (1 H, br s, NHCO), 12.50 (1 H, br s, COOH);  $\delta_{\text{C}}$  (75 MHz, DMSO- $d_6$ ) 14.39 (C6''), 22.55 (C5''), 26.52 (C3''), 29.78 (C2''), 31.45 (C4''), 39.84 (C1''), 108.92 (C3), 114.32 (C5), 127.73 (C2', C6'), 131.06 (C3', C5'), 131.79 (C4'), 137.31 (C4), 138.31 (C1'), 153.29 (C2), 154.16 (NHCO), 166.76 (COOH); m/z (ESI+) 381 (100%, (M + H) $^+$ ), 761 (51, 2M + H), 295 (77, M – C $_6$ H $_{13}$ ), 236 (58, M – C $_6$ H $_{13}$ , NH, CO $_2$ );  $t_{\text{R}} = 13.37$  min.

**2-(3-Benzylureido)-4-(4'-chlorophenyl)thiophene-3-carboxylic acid 26 (200 mg, 81%).**

Pale brown crystals; mp 197–199 °C;  $\delta_{\text{H}}$  (300 MHz, DMSO- $d_6$ ) 4.33 (2 H, d,  $J = 5.7$  Hz, CH $_2$ ), 6.66 (1 H, s, C5-H), 7.24–7.37 (9 H, m, 4'-ClC $_6$ H $_4$ , Ph), 8.40 (1 H, t,  $J = 4.8$  Hz, NHCH $_2$ ), 10.60 (1 H, br s, NHCO), 12.56 (1 H, br s, COOH);  $\delta_{\text{C}}$  (75 MHz, DMSO- $d_6$ ) 43.57 (CH $_2$ ), 109.64 (C3), 114.39 (C5), 127.39 (C4''), 127.74 (C2'', C6''), 127.75 (C2', C6'), 128.84 (C3'', C5''), 131.08 (C3', C5'), 131.78 (C4'), 137.30 (C4), 138.44 (C1'), 139.96 (C1''), 152.79 (C2), 154.30 (NHCO), 166.85 (COOH); m/z (ESI+) 387 (100%, (M + H) $^+$ ), 773 (37, 2M + H), 295 (44, M – C $_7$ H $_7$ ), 236 (50, M – C $_7$ H $_7$ , NH, CO $_2$ );  $t_{\text{R}} = 12.21$  min.

**2-(3-Benzyl-3-ethylureido)-4-(4'-chlorophenyl)thiophene-3-carboxylic acid 27 (240 mg, 90%).**

Pale grey crystals; mp 175–177 °C;  $\delta_{\text{H}}$  (300 MHz, DMSO- $d_6$ ) 1.15 (3 H, t,  $J = 6.2$  Hz, Me), 3.41 (2 H, q,  $J = 6.2$  Hz, MeCH $_2$ N), 4.60 (2 H, s, PhCH $_2$ N), 6.71 (1 H, s, C5-H), 7.22–7.50 (9 H, m, 4'-ClC $_6$ H $_4$ , Ph), 11.38 (1 H, br s, NHCO), 12.84 (1 H, br s, COOH);  $\delta_{\text{C}}$  (75 MHz, DMSO- $d_6$ ) 13.54 (Me), 42.28 (MeCH $_2$ N), 49.84 (PhCH $_2$ N), 109.67 (C3), 114.80 (C5), 127.58 (C4''), 127.69 (C2'', C6''), 127.74 (C2', C6'), 129.03 (C3'', C5''), 131.22 (C3', C5'), 131.97 (C4'), 137.03 (C4), 138.22 (C1'), 138.46 (C1''), 153.45 (C2), 153.80 (NHCO), 167.93 (COOH); m/z (ESI+) 415 (100%, (M + H) $^+$ ), 829 (6, 2M + H), 236 (12, M – C $_7$ H $_7$ , EtN, CO $_2$ );  $t_{\text{R}} = 13.18$  min.

**4-(3',4'-Dichlorophenyl)-2-(3-hexylureido)thiophene-3-carboxylic acid 28 (172 mg, 65%).**

Pale brown crystals; mp 178–180 °C;  $\delta_{\text{H}}$  (300 MHz, DMSO- $d_6$ ) 0.87 (3 H, t,  $J = 6.8$  Hz, Me), 1.21–1.50 (8 H, m, Me(CH $_2$ ) $_4$ CH $_2$ NH), 3.10 (2 H, m, CH $_2$ CH $_2$ NH), 6.72 (1 H, s, C5-H), 7.27 (1 H, dd,  $J = 8.0, 2.0$  Hz, 6'-Ar-H), 7.53 (1 H, d,  $J = 2.0$  Hz, 2'-Ar-H), 7.56 (1 H, d,  $J = 8.0$  Hz, 5'-Ar-H), 7.86 (1 H, t,  $J = 5.0$  Hz, NHCH $_2$ ), 10.49 (1 H, br s, NHCO), 12.62 (1 H, br s, COOH);  $\delta_{\text{C}}$  (75 MHz, DMSO- $d_6$ ) 14.40 (C6''), 22.54 (C5''), 26.51 (C3''),

29.77 (C2''), 31.44 (C4''), 39.82 (C1''), 109.21 (C3), 115.00 (C5), 129.67 (C6'), 129.74 (C5'), 129.82 (C4'), 130.33 (C2'), 131.10 (C3'), 136.99 (C4), 139.16 (C1'), 153.12 (C2), 154.16 (NHCO), 166.70 (COOH); *m/z* (ESI+) 415 (100%, (M + H)<sup>+</sup>), 829 (30, 2M + H), 329 (92, M - C<sub>6</sub>H<sub>13</sub>); *t<sub>R</sub>* = 14.26 min.

**2-(3-Benzylureido)-4-(3',4'-dichlorophenyl)thiophene-3-carboxylic acid 29 (210 mg, 78%).** Beige crystals; mp 188–190 °C;  $\delta_{\text{H}}$  (300 MHz, DMSO-d<sub>6</sub>) 4.34 (2 H, d, *J* = 5.6 Hz, CH<sub>2</sub>), 6.77 (1 H, s, C5-H), 7.24–7.39 (6 H, m, 6'Ar-H, Ph), 7.53 (1 H, d, *J* = 2.0 Hz, 2'Ar-H), 7.56 (1 H, d, *J* = 8.0 Hz, 5'Ar-H), 8.45 (1 H, t, *J* = 5.0 Hz, NHCH<sub>2</sub>), 10.51 (1 H, br s, NHCO), 12.69 (1 H, br s, COOH);  $\delta_{\text{C}}$  (75 MHz, DMSO-d<sub>6</sub>) 43.59 (CH<sub>2</sub>), 109.06 (C3), 115.30 (C5), 127.42 (C4''), 127.76 (C2'', C6''), 128.85 (C3'', C5''), 129.75 (C6'), 129.78 (C5'), 129.86 (C4'), 130.38 (C2'), 131.11 (C3'), 136.97 (C4), 139.01 (C1'), 139.88 (C1''), 153.19 (C2), 154.28 (NHCO), 166.48 (COOH); *m/z* (ESI+) 421 (100%, (M + H)<sup>+</sup>), 841 (23, 2M + H), 329 (25, M - C<sub>7</sub>H<sub>7</sub>); *t<sub>R</sub>* = 12.98 min.

**2-(3-Benzyl-3-ethylureido)-4-(3',4'-dichlorophenyl)thiophene-3-carboxylic acid 30 (172 mg, 60%).** Beige crystals; mp 193–195 °C;  $\delta_{\text{H}}$  (300 MHz, DMSO-d<sub>6</sub>) 1.15 (3 H, t, *J* = 7.0 Hz, Me), 3.41 (2 H, q, *J* = 7.0 Hz, MeCH<sub>2</sub>N), 4.60 (2 H, s, PhCH<sub>2</sub>N), 6.80 (1 H, s, C5-H), 7.24–7.39 (6 H, m, 6'Ar-H, Ph), 7.55 (1 H, d, *J* = 2.0 Hz, 2'Ar-H), 7.56 (1 H, d, *J* = 8.0 Hz, 5'Ar-H), 11.43 (1 H, br s, NHCO), 12.92 (1 H, br s, COOH);  $\delta_{\text{C}}$  (75 MHz, DMSO-d<sub>6</sub>) 13.54 (Me), 42.27 (MeCH<sub>2</sub>N), 49.82 (PhCH<sub>2</sub>N), 109.72 (C3), 115.50 (C5), 127.59 (C4''), 127.70 (C2'', C6''), 129.03 (C3'', C5''), 129.84 (C6'), 129.88 (C4', C5'), 130.35 (C2'), 131.26 (C3'), 137.08 (C4), 138.23 (C1'), 138.83 (C1''), 153.46 (C2), 153.78 (NHCO), 167.77 (COOH); *m/z* (ESI+) 449 (100%, (M + H)<sup>+</sup>), 897 (7, 2M + H), 270 (13, M - C<sub>7</sub>H<sub>7</sub>, EtN, CO<sub>2</sub>); *t<sub>R</sub>* = 14.00 min.

Synthesis of methyl 3-amino-4-(aryl)thiophene-2-carboxylates **34a**<sup>26</sup> and **34b** were performed according to reported procedures.<sup>26</sup>

**Methyl 3-amino-4-(4'-chlorophenyl)thiophene-2-carboxylate 34a.**<sup>26</sup> Beige solid; mp 104–105 °C (lit.,<sup>26</sup> 106 °C);  $\delta_{\text{H}}$  (300 MHz, CDCl<sub>3</sub>) 3.86 (3 H, s, OMe), 5.57 (2 H, br s, NH<sub>2</sub>), 7.23 (1 H, s, C5-H), 7.37 (2 H, d, *J* = 8.7 Hz, 3',5'Ar-H), 7.43 (2 H, d, *J* = 8.7 Hz, 2',6'Ar-H);  $\delta_{\text{C}}$  (75 MHz, CDCl<sub>3</sub>) 51.39 (Me), 101.69 (C2), 128.88 (C5), 129.39 (C2', C6'), 129.44 (C3', C5'), 132.08 (C4), 132.82 (C1'), 134.00 (C4'), 151.27 (C3), 165.03 (C=O); *m/z* (ESI+) 268 (16%, (M + H)<sup>+</sup>), 236 (100, M - MeO); *t<sub>R</sub>* = 13.20 min.

**Methyl 3-amino-4-(3',4'-dichlorophenyl)thiophene-2-carboxylate 34b.** White solid; mp 135–137 °C;  $\delta_{\text{H}}$  (300 MHz, DMSO-d<sub>6</sub>) 3.76 (3 H, s, OMe), 6.38 (2 H, br s, NH<sub>2</sub>), 7.45 (1 H, dd, *J* = 8.0, 2.0 Hz, 6'Ar-H), 7.69 (1 H, d, *J* = 2.0 Hz, 2'Ar-H), 7.71 (1 H, d, *J* = 8.0 Hz,

5'Ar-H), 7.78 (1 H, s, C5-H);  $\delta_C$  (75 MHz, DMSO- $d_6$ ) 51.65 (Me), 99.91 (C2), 128.75 (C6'), 130.31 (C2'), 130.73 (C4'), 130.77 (C5), 131.39 (C4), 131.60 (C5'), 131.99 (C3'), 135.08 (C1'), 152.58 (C3), 164.64 (C=O);  $m/z$  (ESI+) 302 (12%, (M + H)<sup>+</sup>), 270 (100, M – MeO);  $t_R$  = 12.79 min.

Synthesis of 3-amino-4-(aryl)thiophene-2-carboxylic acids **35a** and **35b** were performed as described for preparation of **14a** and **14b**.

**3-Amino-4-(4'-chlorophenyl)thiophene-2-carboxylic acid 35a (reported as reaction intermediate and not isolated)** <sup>20,55</sup> (5.38 g, 85%). White solid; mp 160–162 °C;  $\delta_H$  (300 MHz, DMSO- $d_6$ ) 6.45 (2 H, br s, NH<sub>2</sub>), 7.49–7.56 (4 H, m, 4'-ClC<sub>6</sub>H<sub>4</sub>), 7.64 (1 H, s, C5-H), 11.86 (1 H, br s, COOH);  $\delta_C$  (75 MHz, DMSO- $d_6$ ) 101.28 (C2), 129.32 (C2', C6'), 130.00 (C5), 130.15 (C3', C5'), 132.08 (C4), 132.68 (C1'), 133.62 (C4'), 152.19 (C3), 166.00 (C=O);  $m/z$  (ESI+) 254 (18%, (M + H)<sup>+</sup>), 236 (100, M – OH);  $t_R$  = 10.69 min.

**3-Amino-4-(3',4'-dichlorophenyl)thiophene-2-carboxylic acid 35b (5.52 g, 77%)**. Beige solid; mp 127–129 °C;  $\delta_H$  (300 MHz, DMSO- $d_6$ ) 7.46 (1 H, dd,  $J$  = 8.0, 2.0 Hz, 6'Ar-H), 7.70 (1 H, d,  $J$  = 8.0 Hz, 5'Ar-H), 7.70 (1 H, d,  $J$  = 2.0 Hz, 2'Ar-H), 7.73 (1 H, s, C5-H), 7.74 (2 H, br s, NH<sub>2</sub>), 12.49 (1 H, br s, COOH);  $\delta_C$  (75 MHz, DMSO- $d_6$ ) 101.46 (C2), 128.67 (C6'), 130.21 (C2'), 130.59 (C4'), 130.79 (C5), 130.81 (C5'), 131.36 (C4), 131.96 (C3'), 135.35 (C1'), 152.16 (C3), 165.94 (C=O);  $m/z$  (ESI+) 287 (12%, M<sup>+</sup>), 270 (100, M – OH);  $t_R$  = 11.53 min.

Synthesis of 7-(aryl)-1*H*-thieno[3,2-*d*][1,3]oxazine-2,4-diones **36a** and **36b** were performed as described for preparation of **15a** and **15b**.

**7-(4'-Chlorophenyl)-1*H*-thieno[3,2-*d*][1,3]oxazine-2,4-dione 36a** <sup>20,55</sup> (1.23 g, 73%). White solid; mp 214–216 °C (lit., <sup>20</sup> 245 °C, lit., <sup>55</sup> >260 °C);  $\delta_H$  (300 MHz, DMSO- $d_6$ ) 7.49 (2 H, d,  $J$  = 8.8 Hz, 3',5'Ar-H), 7.54 (2 H, d,  $J$  = 8.8 Hz, 2',6'Ar-H), 8.25 (1 H, s, C6-H), 11.86 (1 H, br s, NH);  $\delta_C$  (75 MHz, DMSO- $d_6$ ) 107.66 (C4a), 129.20 (C2', C6'), 129.35 (C7), 130.97 (C3', C5'), 131.03 (C1'), 133.66 (C4'), 136.87 (C6), 147.24 (C7a), 149.41 (C2), 156.06 (C4);  $m/z$  (ESI+) 279 (24%, M<sup>+</sup>), 251 (100, M – CO);  $t_R$  = 10.18 min.

**7-(3',4'-Dichlorophenyl)-1*H*-thieno[3,2-*d*][1,3]oxazine-2,4-dione 36b (1.36 g, 72%)**. Beige solid; mp 249–251 °C;  $\delta_H$  (300 MHz, DMSO- $d_6$ ) 7.43 (1 H, dd,  $J$  = 8.0, 2.0 Hz, 6'Ar-H), 7.70 (1 H, d,  $J$  = 2.0 Hz, 2'Ar-H), 7.73 (1 H, d,  $J$  = 8.0 Hz, 5'Ar-H), 8.32 (1 H, s, C6-H), 11.96 (1 H, br s, NH);  $\delta_C$  (75 MHz, DMSO- $d_6$ ) 107.73 (C4a), 129.58 (C6'), 129.64 (C7), 131.25 (C2'), 131.27 (C5'), 131.71 (C4'), 131.82 (C3'), 132.50 (C1'), 137.70 (C6), 146.70 (C7a), 149.24 (C2), 155.77 (C4);  $m/z$  (ESI+) 313 (13%, M<sup>+</sup>), 627 (13, 2M + H), 285 (100, M – CO);  $t_R$  = 11.14 min.

Synthesis of 4-(aryl)-3-[3-(substituted)ureido]thiophene-2-carboxylic acids **37–42** were performed as described for preparation of **16–21**

**4-(4'-Chlorophenyl)-3-(3-hexylureido)thiophene-2-carboxylic acid 37<sup>21</sup> (195 mg, 80%).**

White crystals; mp 176–178 °C;  $\delta_{\text{H}}$  (300 MHz, DMSO- $d_6$ ) 0.86 (3 H, t,  $J = 6.4$  Hz, Me), 1.12–1.30 (8 H, m, Me(CH $_2$ ) $_4$ CH $_2$ NH), 2.84 (2 H, m, CH $_2$ CH $_2$ NH), 6.88 (1 H, t,  $J = 5.9$  Hz, NHCH $_2$ ), 7.37 (2 H, d,  $J = 7.8$  Hz, 3',5'Ar-H), 7.42 (2 H, d,  $J = 7.8$  Hz, 2',6'Ar-H), 7.79 (1 H, s, C5-H), 8.34 (1 H, br s, NHCO), 13.15 (1 H, br s, COOH);  $\delta_{\text{C}}$  (75 MHz, DMSO- $d_6$ ) 14.42 (C6''), 22.51 (C5''), 26.31 (C3''), 30.08 (C2''), 31.49 (C4''), 39.47 (C1''), 118.68 (C2), 128.59 (C2', C6'), 128.70 (C3', C5'), 129.01 (C5), 131.83 (C4'), 135.76 (C1'), 138.35 (C4), 142.42 (C3), 154.72 (NHCO), 164.24 (COOH); m/z (ESI+) 381 (25%, (M + H) $^+$ ), 761 (17, 2M + H), 295 (53, M – C $_6$ H $_{13}$ ), 236 (100, M – C $_6$ H $_{13}$ , NH, CO $_2$ );  $t_{\text{R}} = 12.71$  min.

**3-(3-Benzylureido)-4-(4'-chlorophenyl)thiophene-2-carboxylic acid 38<sup>21</sup> (225 mg, 91%).**

White crystals; mp 196–198 °C (lit.,<sup>21</sup> 216 °C);  $\delta_{\text{H}}$  (300 MHz, DMSO- $d_6$ ) 4.10 (2 H, d,  $J = 5.9$  Hz, CH $_2$ ), 7.06–7.32 (5 H, m, Ph), 7.38–7.46 (5H, m, 4'-ClC $_6$ H $_4$ , NHCH $_2$ ), 7.82 (1 H, s, C5-H), 8.49 (1 H, br s, NHCO), 13.23 (1 H, br s, COOH);  $\delta_{\text{C}}$  (75 MHz, DMSO- $d_6$ ) 43.06 (CH $_2$ ), 119.38 (C2), 127.05 (C4''), 127.32 (C2'', C6''), 128.54 (C3'', C5''), 128.75 (C2', C6'), 128.88 (C3', C5'), 129.09 (C5), 131.92 (C4'), 135.68 (C1'), 138.63 (C4), 140.70 (C1''), 142.13 (C3), 155.03 (NHCO), 164.17 (COOH); m/z (ESI+) 387 (40%, (M + H) $^+$ ), 773 (36, 2M + H), 295 (51, M – C $_7$ H $_7$ ), 236 (100, M – C $_7$ H $_7$ , NH, CO $_2$ );  $t_{\text{R}} = 10.41$  min.

**3-(3-Benzyl-3-ethylureido)-4-(4'-chlorophenyl)thiophene-2-carboxylic acid 39<sup>21</sup> (212 mg, 80%).**

White crystals; mp 157–159 °C;  $\delta_{\text{H}}$  (500 MHz, DMSO- $d_6$ ) 1.09 (3 H, t,  $J = 6.3$  Hz, Me), 3.24 (2 H, q,  $J = 6.6$  Hz, MeCH $_2$ N), 4.37 (2 H, s, PhCH $_2$ N), 7.02–7.32 (5 H, m, Ph), 7.43 (2 H, d,  $J = 8.8$  Hz, 3',5'Ar-H), 7.46 (2 H, d,  $J = 8.8$  Hz, 2',6'Ar-H), 7.83 (1 H, s, C5-H), 8.52 (1 H, br s, NHCO), 13.23 (1 H, br s, COOH);  $\delta_{\text{C}}$  (126 MHz, DMSO- $d_6$ ) 13.04 (Me), 40.77 (MeCH $_2$ N), 48.40 (PhCH $_2$ N), 119.87 (C2), 126.85 (C4''), 127.18 (C2'', C6''), 128.14 (C3'', C5''), 128.27 (C2', C6'), 128.28 (C5), 128.66 (C3', C5'), 131.56 (C4'), 134.97 (C1'), 138.44 (C4), 138.48 (C1''), 142.51 (C3), 154.37 (NHCO), 163.87 (COOH); m/z (ESI+) 415 (100%, (M + H) $^+$ ), 829 (21, 2M + H), 236 (37, M – C $_7$ H $_7$ , EtN, CO $_2$ );  $t_{\text{R}} = 12.74$  min.

**4-(3',4'-Dichlorophenyl)-3-(3-hexylureido)thiophene-2-carboxylic acid 40 (220 mg, 83%).**

White crystals; mp 189–191 °C;  $\delta_{\text{H}}$  (300 MHz, DMSO- $d_6$ ) 0.85 (3 H, t,  $J = 7$  Hz, Me), 1.02–1.39 (8 H, m, Me(CH $_2$ ) $_4$ CH $_2$ NH), 2.85 (2 H, m, CH $_2$ CH $_2$ NH), 7.01 (1 H, t,  $J = 5.5$  Hz, NHCH $_2$ ), 7.38 (1 H, dd,  $J = 8.0, 2.0$  Hz, 6'Ar-H), 7.57 (1 H, d,  $J = 8.0$  Hz, 5'Ar-H), 7.62 (1 H, d,  $J = 2.0$  Hz, 2'Ar-H), 7.89 (1 H, s, C5-H), 8.42 (1 H, br s, NHCO), 13.19 (1 H, br s, COOH);  $\delta_{\text{C}}$  (75 MHz, DMSO- $d_6$ ) 14.42 (C6''), 22.48 (C5''), 26.29 (C3''), 30.14 (C2''), 31.47

(C4''), 39.53 (C1''), 118.34 (C2), 127.16 (C6'), 128.59 (C2'), 129.67 (C5), 129.82 (C4'), 130.72 (C5'), 131.31 (C3'), 136.81 (C4), 137.56 (C1'), 142.41 (C3), 154.63 (NHCO), 164.21 (COOH); *m/z* (ESI+) 415 (76%, (M + H)<sup>+</sup>), 829 (37, 2M + H), 329 (100, M – C<sub>6</sub>H<sub>13</sub>), 270 (96, M – C<sub>6</sub>H<sub>13</sub>, NH, CO<sub>2</sub>); *t<sub>R</sub>* = 12.65 min.

**3-(3-Benzylureido)-4-(3',4'-dichlorophenyl)thiophene-2-carboxylic acid 41 (221 mg, 82%).** Off white crystals; mp 182–184 °C;  $\delta_{\text{H}}$  (300 MHz, DMSO-d<sub>6</sub>) 4.12 (2 H, d, *J* = 5.9 Hz, CH<sub>2</sub>), 7.03–7.35 (5 H, m, Ph), 7.40 (1 H, dd, *J* = 8.0, 2.0 Hz, 6'Ar-H), 7.51 (1 H, t, *J* = 5.9 Hz, NHCH<sub>2</sub>), 7.59 (1 H, d, *J* = 8.0 Hz, 5'Ar-H), 7.67 (1 H, d, *J* = 2.0 Hz, 2'Ar-H), 7.91 (1 H, s, C5-H), 8.54 (1 H, br s, NHCO), 12.69 (1 H, br s, COOH);  $\delta_{\text{C}}$  (75 MHz, DMSO-d<sub>6</sub>) 43.09 (CH<sub>2</sub>), 119.18 (C2), 127.04 (C4''), 127.19 (C2'', C6''), 127.36 (C6'), 128.58 (C3'', C5''), 128.80 (C2'), 129.80 (C5), 129.83 (C4'), 130.90 (C5'), 131.42 (C3'), 137.15 (C4), 137.52 (C1'), 140.57 (C1''), 142.09 (C3), 154.98 (NHCO), 164.12 (COOH); *m/z* (ESI+) 421 (58%, (M + H)<sup>+</sup>), 841 (24, 2M + H), 329 (83, M – C<sub>7</sub>H<sub>7</sub>), 270 (100, M – C<sub>7</sub>H<sub>7</sub>, NH, CO<sub>2</sub>); *t<sub>R</sub>* = 9.60 min.

**3-(3-Benzyl-3-ethylureido)-4-(3',4'-dichlorophenyl)thiophene-2-carboxylic acid 42 (236 mg, 82%).** Off white crystals; mp 171–173 °C;  $\delta_{\text{H}}$  (300 MHz, DMSO-d<sub>6</sub>) 1.09 (3 H, t, *J* = 6.8 Hz, Me), 3.25 (2 H, q, *J* = 6.8 Hz, MeCH<sub>2</sub>N), 4.40 (2 H, s, PhCH<sub>2</sub>N), 6.91–7.37 (5 H, m, Ph), 7.43 (1 H, dd, *J* = 8.0, 2.0 Hz, 6'Ar-H), 7.63 (1 H, d, *J* = 8.0 Hz, 5'Ar-H), 7.70 (1 H, d, *J* = 2.0 Hz, 2'Ar-H), 7.94 (1 H, s, C5-H), 8.55 (1 H, br s, NHCO), 13.36 (1 H, br s, COOH);  $\delta_{\text{C}}$  (75 MHz, DMSO-d<sub>6</sub>) 13.48 (Me), 41.32 (MeCH<sub>2</sub>N), 49.00 (PhCH<sub>2</sub>N), 120.31 (C2), 127.35 (C4''), 127.51 (C2'', C6''), 127.70 (C6'), 128.70 (C3'', C5''), 129.01 (C2'), 129.54 (C5), 129.97 (C4'), 130.98 (C5'), 131.50 (C3'), 137.17 (C4), 137.44 (C1'), 138.86 (C1''), 142.85 (C3), 154.80 (NHCO), 164.28 (COOH); *m/z* (ESI+) 449 (100%, (M + H)<sup>+</sup>), 897 (9, 2M + H), 270 (10, M – C<sub>7</sub>H<sub>7</sub>, EtN, CO<sub>2</sub>); *t<sub>R</sub>* = 13.02 min.

**Ethyl 3-amino-5-(3',4'-dichlorophenyl)furan-2-carboxylate 46.** To a stirred ice-cooled solution of triphenylphosphine (5.12 g, 19.5 mmol) in anhydrous THF (70 mL), diethyl azodicarboxylate (3.40 g, 19.5 mmol) was added dropwise. After 10 min, ethyl glycolate (2.03 g, 19.5 mmol) was added dropwise, then **44**<sup>28</sup> (3.21 g, 15.0 mmol) was added portionwise. The reaction mixture was allowed to warm to rt, and stirred for 15 h. Sodium hydride (55–65% in mineral oil, 1.80 g, 42.0 mmol) was added, and the reaction was further stirred for 6 h. The reaction mixture was treated with water (10 mL), and the solvent was removed by vacuum distillation. The obtained residue was dissolved in EtOAc (70 mL), washed with water (50 mL), dried (MgSO<sub>4</sub>), and concentrated. The crude material was purified by flash chromatography (SiO<sub>2</sub>, *n*-hexane/EtOAc = 3:1). (3.90 g, 87%); white solid;

mp 153–155 °C;  $\delta_{\text{H}}$  (300 MHz,  $\text{CDCl}_3$ ) 1.42 (3 H, t,  $J = 7.1$  Hz, Me), 4.40 (2 H, q,  $J = 7.1$  Hz,  $\text{CH}_2\text{O}$ ), 4.64 (2 H, br s,  $\text{NH}_2$ ), 6.39 (1 H, s, C4-H), 7.47 (1 H, d,  $J = 8.0$  Hz, 5'Ar-H), 7.55 (1 H, dd,  $J = 8.0, 2.0$  Hz, 6'Ar-H), 7.81 (1 H, d,  $J = 2.0$  Hz, 2'Ar-H);  $\delta_{\text{C}}$  (75 MHz,  $\text{CDCl}_3$ ) 14.65 (Me), 60.13 ( $\text{CH}_2$ ), 100.98 (C4), 124.03 (C6'), 126.16 (C3), 126.62 (C2'), 129.38 (C1'), 130.76 (C5'), 132.98 (C4'), 133.16 (C3'), 144.74 (C2), 153.45 (C5), 160.37 (C=O);  $m/z$  (ESI+) 300 (83%,  $(\text{M} + \text{H})^+$ ), 599 (6,  $2\text{M} + \text{H}$ ), 254 (100,  $\text{M} - \text{EtO}$ );  $t_{\text{R}} = 13.72$  min.

**Ethyl 5-(3',4'-dichlorophenyl)-3-(phenoxy-carbonylamino)furan-2-carboxylate 47.** To a stirred ice-cooled solution of **46** (1.00 g, 3.33 mmol), and pyridine (264 mg, 3.33 mmol) in anhydrous DCM (20 mL), phenyl chloroformate (525 mg, 3.33 mmol) was added dropwise. The reaction mixture was stirred at rt for 12 h. The solvent was evaporated under vacuum, and the residue was dissolved in EtOAc (50 mL), washed with 1M HCl ( $2 \times 25$  mL), brine (25 mL), dried ( $\text{MgSO}_4$ ), and the solvent was removed by vacuum distillation. The obtained material was triturated with *n*-hexane (20 mL), collected by filtration and dried. (1.20 g, 86%); pale yellow solid; mp 120–121 °C;  $\delta_{\text{H}}$  (300 MHz,  $\text{CDCl}_3$ ) 1.46 (3 H, t,  $J = 7.1$  Hz, Me), 4.46 (2 H, q,  $J = 7.1$  Hz,  $\text{CH}_2\text{O}$ ), 7.18–7.45 (5 H, m, Ph), 7.48 (1 H, d,  $J = 8.0$  Hz, 5'Ar-H), 7.51 (1 H, s, C4-H), 7.57 (1 H, dd,  $J = 8.0, 2.0$  Hz, 6'Ar-H), 7.85 (1 H, d,  $J = 2.0$  Hz, 2'Ar-H), 8.76 (1 H, br s,  $\text{NHCO}$ );  $\delta_{\text{C}}$  (75 MHz,  $\text{CDCl}_3$ ) 14.51 (Me), 61.19 ( $\text{CH}_2$ ), 102.14 (C4), 121.43 (C2'', C6''), 124.09 (C6'), 126.04 (C4''), 126.68 (C2'), 128.48 (C3), 129.01 (C1'), 129.50 (C3'', C5''), 130.93 (C5'), 133.36 (C4'), 133.42 (C3'), 136.53 (C2), 150.40 (C1''), 151.38 ( $\text{NHCO}$ ), 153.68 (C5), 160.12 (C=O);  $m/z$  (ESI+) 420 (100%,  $(\text{M} + \text{H})^+$ ), 374 (7,  $\text{M} - \text{EtO}$ );  $t_{\text{R}} = 17.56$  min.

#### General procedures for synthesis of ethyl 3-[3-(substituted)ureido]-5-(3',4'-dichlorophenyl)furan-2-carboxylate 48 and 49

To a stirred solution of **47** (300 mg, 0.71 mmol) in anhydrous DMSO (10 mL) under a nitrogen atmosphere, the appropriate amine (0.75 mmol) was added dropwise. The reaction mixture was stirred at rt for 2 h, then EtOAc (50 mL) was added. The organic layer was washed with 2M HCl ( $2 \times 30$  mL), 1M NaOH ( $2 \times 30$  mL), brine (30 mL), dried ( $\text{MgSO}_4$ ), and the solvent was removed by vacuum distillation. The obtained residues were purified by flash chromatography ( $\text{SiO}_2$ , *n*-hexane/EtOAc = 1:1).

**Ethyl 3-(3-benzylureido)-5-(3',4'-dichlorophenyl)furan-2-carboxylate 48 (283 mg, 92%,).** White solid; mp 211–213 °C;  $\delta_{\text{H}}$  (300 MHz,  $\text{DMSO-d}_6$ ) 1.33 (3 H, t,  $J = 7.1$  Hz, Me), 4.33 (2 H, d,  $J = 4.7$  Hz,  $\text{PhCH}_2\text{NH}$ ), 4.35 (2 H, q,  $J = 7.1$  Hz,  $\text{CH}_2\text{O}$ ), 7.23–7.38 (5 H, m, Ph), 7.71 (1 H, d,  $J = 8.0$  Hz, 5'Ar-H), 7.76 (1 H, dd,  $J = 8.0, 2.0$  Hz, 6'Ar-H), 7.87 (1 H, s, C4-H), 8.02 (1 H, d,  $J = 2.0$  Hz, 2'Ar-H), 8.06 (1 H, t,  $J = 5.8$  Hz,  $\text{NHCH}_2$ ), 8.66 (1 H, br s,  $\text{NHCO}$ );  $\delta_{\text{C}}$

(75 MHz, DMSO- $d_6$ ) 14.88 (Me), 43.43 (PhCH<sub>2</sub>NH), 60.70 (CH<sub>2</sub>O), 104.25 (C4), 125.12 (C6'), 126.71 (C2'), 127.36 (C4''), 127.75 (C2'', C6''), 128.58 (C3), 128.83 (C3'', C5''), 129.77 (C1'), 131.81 (C5'), 132.17 (C4'), 132.51 (C3'), 138.53 (C2), 140.12 (C1''), 152.57 (C5), 154.45 (NHCO), 159.57 (C=O); m/z (ESI+) 433 (100%, (M + H)<sup>+</sup>), 865 (27, 2M + H), 341 (8, M - C<sub>7</sub>H<sub>7</sub>), 254 (59, M - C<sub>7</sub>H<sub>7</sub>, NCO, EtO); t<sub>R</sub> = 15.99 min.

**Ethyl 3-(3-benzyl-3-ethylureido)-5-(3',4'-dichlorophenyl)furan-2-carboxylate 49 (278 mg, 85%).** Reddish liquid;  $\delta_H$  (500 MHz, CDCl<sub>3</sub>) 1.25 (3 H, t,  $J = 7.3$  Hz, MeCH<sub>2</sub>N), 1.36 (3 H, t,  $J = 7.3$  Hz, MeCH<sub>2</sub>O), 3.42 (2 H, q,  $J = 7.3$  Hz, MeCH<sub>2</sub>N), 4.36 (2 H, q,  $J = 7.3$  Hz, CH<sub>2</sub>O), 4.62 (2 H, s, PhCH<sub>2</sub>N), 7.25–7.36 (5 H, m, Ph), 7.48 (1 H, d,  $J = 8.0$  Hz, 5'Ar-H), 7.60 (1 H, dd,  $J = 8.0, 2.0$  Hz, 6'Ar-H), 7.71 (1 H, s, C4-H), 7.89 (1 H, d,  $J = 2.0$  Hz, 2'Ar-H), 8.84 (1 H, br s, NHCO);  $\delta_C$  (126 MHz, CDCl<sub>3</sub>) 13.16 (MeCH<sub>2</sub>N), 14.51 (MeCH<sub>2</sub>O), 42.03 (MeCH<sub>2</sub>N), 50.02 (PhCH<sub>2</sub>N), 60.80 (CH<sub>2</sub>O), 102.98 (C4), 124.12 (C6'), 126.73 (C2'), 127.49 (C4''), 127.58 (C2'', C6''), 127.76 (C3), 128.76 (C3'', C5''), 129.44 (C1'), 130.87 (C5'), 133.11 (C4'), 133.28 (C3'), 137.42 (C2), 137.70 (C1''), 152.94 (C5), 154.11 (NHCO), 159.64 (C=O); m/z (ESI+) 461 (100%, (M + H)<sup>+</sup>), 921 (8, 2M + H); t<sub>R</sub> = 17.00 min.

**3-Benzyl-6-(3',4'-dichlorophenyl)furo[3,2-*d*]pyrimidine-2,4(1*H*,3*H*)-dione 50.** To a stirred solution of **48** (130 mg, 0.3 mmol) in MeOH (10 mL), NaOH (20 mg, 0.5 mmol) in water (10 mL) was added. The reaction mixture was stirred at 70 °C for 3 h. The mixture was concentrated in vacuo. The residue was diluted with water (10 mL), and washed with EtOAc (20 mL). The aqueous layer was cooled in ice bath and acidified with KHSO<sub>4</sub> (saturated aqueous solution) to pH 3–4. The precipitated solid was collected by filtration, washed with cold water (20 mL), and *n*-hexane (20 mL).

(93 mg, 80%); white solid; mp 281–283 °C dec;  $\delta_H$  (500 MHz, DMSO- $d_6$ ) 5.04 (2 H, s, CH<sub>2</sub>), 7.23–7.32 (6 H, m, C7-H, Ph), 7.76 (1 H, d,  $J = 8.0$  Hz, 5'Ar-H), 7.88 (1 H, dd,  $J = 8.0, 2.0$  Hz, 6'Ar-H), 8.20 (1 H, d,  $J = 2.0$  Hz, 2'Ar-H), 11.87 (1 H, br s, NH);  $\delta_C$  (126 MHz, DMSO- $d_6$ ) 43.13 (CH<sub>2</sub>), 98.87 (C7), 125.03 (C6'), 126.89 (C2'), 127.04 (C4''), 127.37 (C2'', C6''), 128.27 (C3'', C5''), 128.81 (C7a), 129.83 (C1'), 131.39 (C5'), 132.12 (C4'), 132.45 (C3'), 137.35 (C1''), 137.79 (C4a), 150.88 (C4), 153.00 (C2), 156.43 (C6); m/z (ESI+) 387 (68%, (M + H)<sup>+</sup>), 773 (29, 2M + H), 186 (100); t<sub>R</sub> = 13.16 min.

### General procedures for synthesis of 3-[3-(substituted)ureido]-5-(3',4'-dichlorophenyl)furan-2-carboxylic acid **51** and **52**

To a stirred ice-cooled solution of the appropriate ester **48** or **49** (1.00 mmol), and THT (5 mL) in anhydrous DCM (5 mL), AlCl<sub>3</sub> (1.33 g, 10.0 mmol) was added portionwise. The reaction mixture was stirred at rt for 72 h (TLC monitoring, TLC samples were diluted with

MeOH). The reaction mixture was concentrated under vacuum, then cold water (10 mL) was added followed by 1M HCl to pH 4–5. The mixture was extracted with EtOAc (3 × 25 mL). The combined organic layers were dried (MgSO<sub>4</sub>), and the solvent was removed by vacuum distillation. The crude material was purified using preparative RP-HPLC.

**3-(3-Benzylureido)-5-(3',4'-dichlorophenyl)furan-2-carboxylic acid 51 (100 mg, 25%).**

White crystals; mp 195–197 °C dec;  $\delta_{\text{H}}$  (500 MHz, DMSO-d<sub>6</sub>) 4.31 (2 H, d,  $J = 5.7$  Hz, CH<sub>2</sub>), 7.23–7.37 (5 H, m, Ph), 7.71 (1 H, d,  $J = 8.0$  Hz, 5'Ar-H), 7.77 (1 H, dd,  $J = 8.0, 2.0$  Hz, 6'Ar-H), 7.84 (1 H, s, C4-H), 8.03 (1 H, d,  $J = 2.0$  Hz, 2'Ar-H), 8.06 (1 H, t,  $J = 5.7$  Hz, NHCH<sub>2</sub>), 8.65 (1 H, br s, NHCO), 13.23 (1 H, br s, COOH);  $\delta_{\text{C}}$  (125 MHz, DMSO-d<sub>6</sub>) 42.92 (CH<sub>2</sub>), 103.73 (C4), 124.55 (C6'), 126.11 (C2'), 126.83 (C4''), 127.24 (C2'', C6''), 127.51 (C3), 128.32 (C3'', C5''), 129.51 (C1'), 131.30 (C5'), 131.44 (C4'), 131.99 (C3'), 137.28 (C2), 139.72 (C1''), 151.55 (C5), 154.05 (NHCO), 160.57 (COOH);  $m/z$  (ESI+) 405 (90%, (M + H)<sup>+</sup>), 809 (14, 2M + H), 313 (93, M – C<sub>7</sub>H<sub>7</sub>), 254 (100, M – C<sub>7</sub>H<sub>7</sub>, NH, CO<sub>2</sub>);  $t_{\text{R}} = 13.60$  min.

**3-(3-Benzyl-3-ethylureido)-5-(3',4'-dichlorophenyl)furan-2-carboxylic acid 52 (120 mg, 28%).**

Pale yellow crystals; mp 160–162 °C dec;  $\delta_{\text{H}}$  (500 MHz, DMSO-d<sub>6</sub>) 1.15 (3 H, t,  $J = 7.2$  Hz, Me), 3.38 (2 H, q,  $J = 6.9$  Hz, MeCH<sub>2</sub>N), 4.56 (2 H, s, PhCH<sub>2</sub>N), 7.25–7.37 (5 H, m, Ph), 7.72 (1 H, d,  $J = 8.0$  Hz, 5'Ar-H), 7.79 (1 H, dd,  $J = 8.0, 2.0$  Hz, 6'Ar-H), 7.82 (1 H, s, C4-H), 8.06 (1 H, d,  $J = 2.0$  Hz, 2'Ar-H), 8.79 (1 H, br s, NHCO), 13.46 (1 H, br s, COOH);  $\delta_{\text{C}}$  (125 MHz, DMSO-d<sub>6</sub>) 13.11 (Me), 41.82 (MeCH<sub>2</sub>N), 49.39 (PhCH<sub>2</sub>N), 103.45 (C4), 124.62 (C6'), 126.23 (C2'), 126.92 (C4''), 127.16 (C2'', C6''), 127.94 (C3), 128.50 (C3'', C5''), 129.39 (C1'), 131.31 (C5'), 131.60 (C4'), 132.02 (C3'), 137.95 (C2), 137.99 (C1''), 151.99 (C5), 153.06 (NHCO), 161.20 (COOH);  $m/z$  (ESI+) 433 (66%, (M + H)<sup>+</sup>), 865 (8, 2M + H), 389 (100, [M+H] – CO<sub>2</sub>);  $t_{\text{R}} = 13.64$  min.

**Ethyl 2-amino-5-(3',4'-dichlorophenyl)furan-3-carboxylate 54.** To a stirred ice-cooled solution of **43**<sup>27</sup> (4.83 g, 18.0 mmol) in anhydrous DMF (13 mL) under a nitrogen atmosphere, ethyl cyanoacetate (2.05 g, 18.0 mmol), and diethylamine (3.95 g, 54.0 mmol) were added slowly. The reaction mixture was allowed to warm to rt, and stirred for 2 h. The mixture was diluted with DCM (100 mL), washed with 2M HCl (2 × 50 mL), dried (MgSO<sub>4</sub>), and concentrated under vacuum till half of the volume. Trifluoroacetic acid (50 mL) was added in one portion to the solution. The reaction was stirred at rt for 40 h. The solvent was removed by vacuum distillation. The residue was dissolved in DCM (50 mL), cautiously washed with NaHCO<sub>3</sub> (saturated aqueous solution, 50 mL), the organic layer was dried (MgSO<sub>4</sub>), and concentrated. The crude material was purified by flash chromatography (SiO<sub>2</sub>, *n*-hexane/EtOAc = 6:1). (2.15 g, 40%); white solid; mp 110–111 °C;  $\delta_{\text{H}}$  (300 MHz, CDCl<sub>3</sub>)

1.36 (3 H, t,  $J = 7.1$  Hz, Me), 4.29 (2 H, q,  $J = 7.1$  Hz, CH<sub>2</sub>O), 5.62 (2 H, br s, NH<sub>2</sub>), 6.78 (1 H, s, C4-H), 7.29 (1 H, dd,  $J = 8.0, 2.0$  Hz, 6'Ar-H), 7.38 (1 H, d,  $J = 8.0$  Hz, 5'Ar-H), 7.57 (1 H, d,  $J = 2.0$  Hz, 2'Ar-H);  $\delta_C$  (75 MHz, CDCl<sub>3</sub>) 14.54 (Me), 59.84 (CH<sub>2</sub>), 91.80 (C3), 106.46 (C4), 121.60 (C6'), 124.09 (C2'), 129.87 (C4'), 130.10 (C1'), 130.61 (C5'), 132.90 (C3'), 141.30 (C5), 161.55 (C2), 164.83 (C=O);  $m/z$  (ESI+) 300 (100%, (M + H)<sup>+</sup>), 599 (79, 2M + H), 254 (91, M – EtO);  $t_R = 15.98$  min.

**Ethyl 2-[bis(phenoxy carbonyl)amino]-5-(3',4'-dichlorophenyl)furan-3-carboxylate 55.**

To a stirred ice-cooled solution of **54** (1.00 g, 3.33 mmol), and pyridine (528 mg, 6.66 mmol) in anhydrous DCM (30 mL), phenyl chloroformate (1.05 g, 6.66 mmol) was added dropwise, and the reaction mixture was stirred at rt for 12 h. The solvent was evaporated under vacuum. The residue was dissolved in EtOAc (60 mL), washed with 1M HCl (2 × 30 mL), brine (30 mL), dried (MgSO<sub>4</sub>), and the solvent was removed by vacuum distillation. The crude material was triturated with *n*-hexane (30 mL), collected by filtration and dried. (1.48 g, 82%); white solid; mp 166–168 °C;  $\delta_H$  (300 MHz, CDCl<sub>3</sub>) 1.29 (3 H, t,  $J = 7.1$  Hz, Me), 4.32 (2 H, q,  $J = 7.1$  Hz, CH<sub>2</sub>O), 7.02 (1 H, s, C4-H), 7.08–7.34 (10 H, m, 2 Ph), 7.42 (1 H, d,  $J = 8.0$  Hz, 5'Ar-H), 7.46 (1 H, dd,  $J = 8.0, 2.0$  Hz, 6'Ar-H), 7.72 (1 H, d,  $J = 2.0$  Hz, 2'Ar-H);  $\delta_C$  (75 MHz, CDCl<sub>3</sub>) 14.31 (Me), 61.37 (CH<sub>2</sub>), 107.34 (C4), 114.59 (C3), 121.10 (C2'', C6'', C2''', C6'''), 123.24 (C6'), 125.91 (C2'), 126.59 (C4'', C4'''), 128.97 (C4'), 129.57 (C3'', C5'', C3''', C5'''), 130.98 (C5'), 132.67 (C1'), 133.40 (C3'), 145.63 (C5), 149.04 (N(C=O)<sub>2</sub>), 149.64 (C2), 150.24 (C1'', C1'''), 161.41 (C=O);  $m/z$  (ESI+) 540 (100%, (M + H)<sup>+</sup>), 494 (13, M – EtO);  $t_R = 16.97$  min.

**General procedures for synthesis of ethyl 2-[3-(substituted)ureido]-5-(3',4'-dichlorophenyl)furan-3-carboxylate 57 and 58**

To a stirred solution of **55** (300 mg, 0.55 mmol) in anhydrous DMSO (10 mL) under a nitrogen atmosphere, the appropriate amine (2.20 mmol) was added dropwise. The reaction mixture was stirred at rt for 2 h, then EtOAc (50 mL) was added. The organic layer was washed with 2M HCl (2 × 30 mL), 1M NaOH (2 × 30 mL), brine (30 mL), dried (MgSO<sub>4</sub>), and the solvent was removed by vacuum distillation. The product was purified from the *sym*-urea side product using flash chromatography (SiO<sub>2</sub>, EtOAc/THF = 4:1).

**Ethyl 2-(3-benzylureido)-5-(3',4'-dichlorophenyl)furan-3-carboxylate 57 (203 mg, 85%).**

White solid; mp 223–225 °C dec;  $\delta_H$  (500 MHz, DMSO-d<sub>6</sub>) 1.28 (3 H, t,  $J = 7.0$  Hz, Me), 4.25 (2 H, q,  $J = 7.0$  Hz, CH<sub>2</sub>O), 4.33 (2 H, d,  $J = 5.8$  Hz, PhCH<sub>2</sub>NH), 7.26–7.38 (6 H, m, C4-H, Ph), 7.63 (1 H, dd,  $J = 8.0, 2.0$  Hz, 6'Ar-H), 7.66 (1 H, d,  $J = 8.0$  Hz, 5'Ar-H), 7.89 (2 H, m, 2'Ar-H, NHCH<sub>2</sub>), 9.27 (1 H, br s, NHCO);  $\delta_C$  (125 MHz, DMSO-d<sub>6</sub>) 14.28 (Me), 43.00

(PhCH<sub>2</sub>NH), 59.95 (CH<sub>2</sub>O), 99.11 (C3), 107.18 (C4), 122.86 (C6'), 124.32 (C2'), 126.93 (C4''), 127.27 (C2'', C6''), 128.37 (C3'', C5''), 129.29 (C4'), 129.96 (C1'), 131.04 (C5'), 131.78 (C3'), 139.39 (C1''), 143.37 (C5), 152.04 (NHCO), 153.33 (C2), 162.92 (C=O); m/z (ESI+) 433 (100%, (M + H)<sup>+</sup>), 865 (60, 2M + H), 341 (15, M - C<sub>7</sub>H<sub>7</sub>), 254 (30, M - C<sub>7</sub>H<sub>7</sub>, NCO, EtO); t<sub>R</sub> = 15.31 min.

**Ethyl 2-(3-benzyl-3-ethylureido)-5-(3',4'-dichlorophenyl)furan-3-carboxylate 58 (208 mg, 82%).** Reddish liquid; δ<sub>H</sub> (500 MHz, CDCl<sub>3</sub>) 1.26 (3 H, t, *J* = 7.0 Hz, MeCH<sub>2</sub>N), 1.33 (3 H, t, *J* = 7.0 Hz, MeCH<sub>2</sub>O), 3.41 (2 H, q, *J* = 7.0 Hz, MeCH<sub>2</sub>N), 4.27 (2 H, q, *J* = 7.0 Hz, CH<sub>2</sub>O), 4.64 (2 H, s, PhCH<sub>2</sub>N), 6.82 (1 H, s, C4-H), 7.28–7.37 (5 H, m, Ph), 7.40 (1 H, d, *J* = 8.0 Hz, 5'Ar-H), 7.49 (1 H, dd, *J* = 8.0, 2.0 Hz, 6'Ar-H), 7.72 (1 H, d, *J* = 2.0 Hz, 2'Ar-H), 9.34 (1 H, br s, NHCO); δ<sub>C</sub> (126 MHz, CDCl<sub>3</sub>) 13.15 (MeCH<sub>2</sub>N), 14.39 (MeCH<sub>2</sub>O), 42.24 (MeCH<sub>2</sub>N), 50.11 (PhCH<sub>2</sub>N), 60.56 (CH<sub>2</sub>O), 97.53 (C3), 104.74 (C4), 122.60 (C6'), 124.92 (C2'), 127.29 (C4''), 127.56 (C2'', C6''), 128.65 (C3'', C5''), 129.71 (C4'), 130.68 (C5'), 130.89 (C1'), 133.01 (C3'), 136.96 (C1''), 144.79 (C5), 151.77 (NHCO), 155.08 (C2), 165.16 (C=O); m/z (ESI+) 461 (100%, (M + H)<sup>+</sup>), 921 (25, 2M + H); t<sub>R</sub> = 16.94 min.

Synthesis of 2-[3-(substituted)ureido]-5-(3',4'-dichlorophenyl)furan-3-carboxylic acid **59** and **60** were performed as described for preparation of **51** and **52**

**2-(3-Benzylureido)-5-(3',4'-dichlorophenyl)furan-3-carboxylic acid 59 (73 mg, 18%).** White crystals; mp 200–202 °C dec; δ<sub>H</sub> (500 MHz, DMSO-d<sub>6</sub>) 4.32 (2 H, d, *J* = 6.0 Hz, CH<sub>2</sub>), 7.25–7.38 (6 H, m, C4-H, Ph), 7.61 (1 H, dd, *J* = 8.0, 2.0 Hz, 6'Ar-H), 7.66 (1 H, d, *J* = 8.0 Hz, 5'Ar-H), 7.86 (1 H, d, *J* = 2.0 Hz, 2'Ar-H), 7.95 (1 H, t, *J* = 5.7 Hz, NHCH<sub>2</sub>), 9.29 (1 H, br s, NHCO), 12.68 (1 H, br s, COOH); δ<sub>C</sub> (125 MHz, DMSO-d<sub>6</sub>) 42.95 (CH<sub>2</sub>), 99.52 (C3), 107.73 (C4), 122.74 (C6'), 124.10 (C2'), 126.91 (C4''), 127.25 (C2'', C6''), 128.36 (C3'', C5''), 128.97 (C4'), 130.15 (C1'), 131.10 (C5'), 131.72 (C3'), 139.42 (C1''), 142.85 (C5), 151.98 (NHCO), 153.27 (C2), 164.63 (COOH); m/z (ESI+) 405 (100%, (M + H)<sup>+</sup>), 809 (54, 2M + H), 313 (71, M - C<sub>7</sub>H<sub>7</sub>), 295 (24, M - C<sub>7</sub>H<sub>7</sub>, H<sub>2</sub>O), 254 (16, M - C<sub>7</sub>H<sub>7</sub>, NH, CO<sub>2</sub>); t<sub>R</sub> = 12.54 min.

**2-(3-Benzyl-3-ethylureido)-5-(3',4'-dichlorophenyl)furan-3-carboxylic acid 60 (95 mg, 22%).** White crystals; mp 175–177 °C dec; δ<sub>H</sub> (500 MHz, DMSO-d<sub>6</sub>) 1.11 (3 H, t, *J* = 7.2 Hz, Me), 3.34 (2 H, q, *J* = 7.2 Hz, MeCH<sub>2</sub>N), 4.56 (2 H, s, PhCH<sub>2</sub>N), 7.26–7.38 (6 H, m, C4-H, Ph), 7.65 (1 H, dd, *J* = 8.0, 2.0 Hz, 6'Ar-H), 7.67 (1 H, d, *J* = 8.0 Hz, 5'Ar-H), 7.91 (1 H, d, *J* = 2.0 Hz, 2'Ar-H), 9.25 (1 H, br s, NHCO), 12.77 (1 H, br s, COOH); δ<sub>C</sub> (125 MHz, DMSO-d<sub>6</sub>) 13.10 (Me), 41.35 (MeCH<sub>2</sub>N), 49.11 (PhCH<sub>2</sub>N), 104.55 (C3), 107.98 (C4), 123.00 (C6'), 124.45 (C2'), 127.09 (C4''), 127.29 (C2'', C6''), 128.44 (C3'', C5''), 129.47 (C4'), 130.00

(C1'), 131.16 (C5'), 131.81 (C3'), 138.04 (C1''), 144.24 (C5), 152.81 (NHCO), 152.87 (C2), 164.54 (COOH);  $m/z$  (ESI+) 433 (100%, (M + H)<sup>+</sup>), 865 (16, 2M + H), 254 (5, M - C<sub>7</sub>H<sub>7</sub>, EtN, CO<sub>2</sub>);  $t_R$  = 13.71 min.

**Methyl 3,4-dichlorobenzenecarbodithioate 62.** To a stirred mixture of sulfur (3.52 g, 110 mmol), and Net<sub>3</sub> (15.2 g, 150 mmol) in DMF (25 mL), 3,4-dichlorobenzyl chloride **61** (9.77 g, 50.0 mmol) was added dropwise. The reaction mixture was stirred at 60 °C for 6 h then cooled in an ice bath. Iodomethane (7.81 g, 55.0 mmol) was added slowly maintaining the temperature below 10 °C. The reaction was further stirred for 1 h then filtered. The filtrate was poured into stirred ice-cooled water (100 mL). The precipitated bright red crystals were collected by filtration, washed with water, and dried. (10.4 g, 88%); red solid; mp 60–62 °C;  $\delta_H$  (500 MHz, CDCl<sub>3</sub>) 2.78 (3 H, s, Sme), 7.46 (1 H, d,  $J$  = 8.0 Hz, C5-H), 7.83 (1 H, dd,  $J$  = 8.0, 2.0 Hz, C6-H), 8.10 (1 H, d,  $J$  = 2.0 Hz, C2-H);  $\delta_C$  (126 MHz, CDCl<sub>3</sub>) 20.77 (Me), 125.68 (C6), 128.58 (C2), 130.22 (C5), 132.83 (C4), 136.62 (C3), 144.03 (C1), 225.21 (C=S);  $m/z$  (ESI+) 236 (22%, M<sup>+</sup>), 187 (100, M - CH<sub>2</sub>, Cl);  $t_R$  = 16.53 min.

**Methyl 4-amino-2-(3',4'-dichlorophenyl)-1,3-thiazole-5-carboxylate 64.** To a stirred ice-cooled solution of sodium (0.81 g, 35.0 mmol), and cyanamide (1.27 g, 30.0 mmol) in anhydrous MeOH (50 mL) under a nitrogen atmosphere, compound **62** (7.11 g, 30 mmol) was added portionwise, and the reaction mixture was stirred at 75 °C for 3 h. The solvent was removed under vacuum, and the residue was triturated with ether, and filtered. The intermediate **63** was dissolved in MeOH (50 mL) and methyl bromoacetate (6.88 g, 45.0 mmol) was added dropwise. The reaction mixture was stirred at rt for 2 h then NEt<sub>3</sub> (12.5 mL, 90.0 mmol) was added, and the reaction was further stirred for 12 h. The solvent was removed by vacuum distillation, and the crude material was purified by flash chromatography (SiO<sub>2</sub>, *n*-hexane/EtOAc = 3:1). (3.18 g, 35%); yellow solid; mp 156–158 °C;  $\delta_H$  (500 MHz, CDCl<sub>3</sub>) 3.83 (3 H, s, OMe), 5.88 (2 H, br s, NH<sub>2</sub>), 7.48 (1 H, d,  $J$  = 8.0 Hz, 5'Ar-H), 7.69 (1 H, dd,  $J$  = 8.0, 2.0 Hz, 6'Ar-H), 8.00 (1 H, d,  $J$  = 2.0 Hz, 2'Ar-H);  $\delta_C$  (126 MHz, CDCl<sub>3</sub>) 51.70 (Me), 94.46 (C5), 125.56 (C6'), 128.22 (C2'), 130.98 (C5'), 132.68 (C4'), 133.50 (C3'), 135.32 (C1'), 163.12 (C4), 164.33 (C=O), 167.46 (C2);  $m/z$  (ESI+) 303 (17%, (M + H)<sup>+</sup>), 344 (100, M + H, MeCN), 271 (6, M - MeO);  $t_R$  = 14.39 min.

**4-Amino-2-(3',4'-dichlorophenyl)-1,3-thiazole-5-carboxylic acid 65.** To a stirred solution of **64** (3.03 g, 10.0 mmol) in MeOH (30 mL), KOH (2.24 g, 40.0 mmol) in water (30 mL) was added. The reaction mixture was stirred at reflux for 2 h then the MeOH was evaporated by vacuum distillation. The residue was diluted with water (10 mL), and washed with EtOAc (20 mL). The aqueous layer was cooled in an ice bath and acidified by KHSO<sub>4</sub> (saturated

aqueous solution) to pH 3–4. The precipitate was collected by filtration, washed with cold water (20 mL), *n*-hexane (20 mL), and dried over CaCl<sub>2</sub> in amber glass vacuum desiccator. (1.91 g, 66%); yellow solid; mp 131–133 °C dec;  $\delta_{\text{H}}$  (500 MHz, DMSO-*d*<sub>6</sub>) 6.98 (2 H, br s, NH<sub>2</sub>), 7.77 (1 H, d, *J* = 8.0 Hz, 5'Ar-H), 7.87 (1 H, dd, *J* = 8.0, 2.0 Hz, 6'Ar-H), 8.09 (1 H, d, *J* = 2.0 Hz, 2'Ar-H), 12.92 (1 H, br s, COOH);  $\delta_{\text{C}}$  (126 MHz, DMSO-*d*<sub>6</sub>) 93.37 (C5), 126.27 (C6'), 127.48 (C2'), 131.53(C5'), 132.09 (C4'), 132.76 (C3'), 133.65 (C1'), 163.25 (C4), 164.65 (C=O), 165.42 (C2); *m/z* (ESI+) 289 (20%, (M + H)<sup>+</sup>), 330 (100, M + H, MeCN), 271 (11, M – OH); *t<sub>R</sub>* = 12.12 min.

**2-(3',4'-Dichlorophenyl)-4*H*-[1,3]thiazolo[4,5-*d*][1,3]oxazine-5,7-dione 66.** The compound was prepared as described for preparation of **15a** and **15b**. (1.32 g, 70%); yellow solid; mp 219–221 °C dec;  $\delta_{\text{H}}$  (500 MHz, DMSO-*d*<sub>6</sub>) 7.77 (1 H, d, *J* = 8.0 Hz, 5'Ar-H), 8.15 (1 H, dd, *J* = 8.0, 2.0 Hz, 6'Ar-H), 8.37 (1 H, d, *J* = 2.0 Hz, 2'Ar-H), 11.11 (1 H, br s, NH);  $\delta_{\text{C}}$  (126 MHz, DMSO-*d*<sub>6</sub>) 95.81 (C7a), 128.16 (C6'), 129.87 (C2'), 130.72 (C5'), 131.21 (C4'), 131.99 (C3'), 133.07 (C1'), 153.29 (C5), 153.56 (C3a), 164.45 (C7), 165.28 (C2); *m/z* (ESI+) 314 (100%, M<sup>+</sup>), 355 (94, M + MeCN), 629 (18, 2M + H); *t<sub>R</sub>* = 11.75 min.

Synthesis of 2-(3',4'-dichlorophenyl)-4-[3-(substituted)ureido]-1,3-thiazole-5-carboxylic acids **67** and **68** were performed as described for preparation of **16–21**.

**4-(3-Benzylureido)-2-(3',4'-dichlorophenyl)-1,3-thiazole-5-carboxylic acid 67 (65 mg, 24%).** Yellow crystals; mp 213–215 °C;  $\delta_{\text{H}}$  (500 MHz, DMSO-*d*<sub>6</sub>) 4.48 (2 H, d, *J* = 5.4 Hz, CH<sub>2</sub>), 7.27–7.40 (5 H, m, Ph), 7.75 (1 H, d, *J* = 8.0 Hz, 5'Ar-H), 7.92 (1 H, dd, *J* = 8.0, 2.0 Hz, 6'Ar-H), 8.18 (1 H, d, *J* = 2.0 Hz, 2'Ar-H), 8.53 (1 H, t, *J* = 5.7 Hz, NHCH<sub>2</sub>), 9.04 (1 H, br s, NHCO), 13.80 (1 H, br s, COOH);  $\delta_{\text{C}}$  (125 MHz, DMSO-*d*<sub>6</sub>) 43.38 (CH<sub>2</sub>), 102.27 (C5), 126.64 (C6'), 126.99 (C4''), 127.13 (C2'', C6''), 127.93 (C2'), 128.48 (C3'', C5''), 131.45 (C5'), 131.79 (C4'), 132.30 (C3'), 134.40 (C1'), 139.30 (C1''), 152.25 (NHCO), 154.44 (C4), 164.02 (COOH), 165.77 (C2); *m/z* (ESI+) 422 (100%, (M + H)<sup>+</sup>), 843 (11, 2M + H), 330 (23, M – C<sub>7</sub>H<sub>7</sub>), 271 (24, M – C<sub>7</sub>H<sub>7</sub>, NH, CO<sub>2</sub>); *t<sub>R</sub>* = 14.98 min.

**4-(3-Benzyl-3-ethylureido)-2-(3',4'-dichlorophenyl)-1,3-thiazole-5-carboxylic acid 68 (63 mg, 22%).** Yellow crystals; mp 191–193 °C;  $\delta_{\text{H}}$  (500 MHz, DMSO-*d*<sub>6</sub>) 1.14 (3 H, t, *J* = 6.9 Hz, Me), 3.37 (2 H, q, *J* = 6.9 Hz, MeCH<sub>2</sub>N), 4.58 (2 H, s, PhCH<sub>2</sub>N), 7.26–7.38 (5 H, m, Ph), 7.81 (1 H, d, *J* = 8.0 Hz, 5'Ar-H), 7.95 (1 H, dd, *J* = 8.0, 2.0 Hz, 6'Ar-H), 8.18 (1 H, d, *J* = 2.0 Hz, 2'Ar-H), 9.64 (1 H, br s, NHCO), 13.57 (1 H, br s, COOH);  $\delta_{\text{C}}$  (125 MHz, DMSO-*d*<sub>6</sub>) 13.16 (Me), 41.44 (MeCH<sub>2</sub>N), 49.12 (PhCH<sub>2</sub>N), 102.30 (C5), 126.41 (C6'), 127.05 (C4''), 127.27 (C2'', C6''), 127.61 (C2'), 128.43 (C3'', C5''), 131.59 (C5'), 132.15 (C4'), 132.74 (C3'), 133.76 (C1'), 138.24 (C1''), 152.83 (NHCO), 154.86 (C4), 163.98

(COOH), 164.25 (C2);  $m/z$  (ESI+) 450 (100%, (M + H)<sup>+</sup>), 899 (4, 2M + H), 271 (4, M – C<sub>7</sub>H<sub>7</sub>, EtN, CO<sub>2</sub>);  $t_R$  = 13.14 min.

## Biology

**Transcription Assay.** The assay was performed as described previously<sup>56</sup> with slight modifications. *E. coli* RNA polymerase holoenzyme was purchased from Epicentre Biotechnologies (Madison, WI). Final concentrations in a total volume of 30  $\mu$ L were one unit of RNA polymerase (0.5  $\mu$ g) which was used along with 60 nCi of [5,6-<sup>3</sup>H]-UTP, 400  $\mu$ M of ATP, CTP and GTP as well as 100  $\mu$ M of UTP, 20 units of RNase inhibitor (RiboLock, Fermentas), 10 mM DTT, 40 mM Tris-HCl (pH 7.5), 150 mM KCl, 10 mM MgCl<sub>2</sub> and 0.1% CHAPS. As a DNA template 3500 ng of religated pcDNA3.1/V5-His-TOPO were used per reaction. Prior to starting the experiment, the compounds were dissolved in DMSO (final concentration during experiment: 2%). Dilution series of the compounds were prepared using a liquid handling system (Janus, PerkinElmer, Waltham, MA). The components described above (including the compounds) were preincubated in absence of NTPs and DNA for 10 min at 25 °C. Transcription reaction was started by the addition of a mixture containing DNA template and NTPs and incubated for 10 min at 37 °C. The reaction was stopped by the addition of 10% TCA, followed by a transfer of this mixture to a 96-well Multiscreen GFB plate (Millipore, Billerica, MA) and incubation for 45 min at 4 °C. The plate underwent several centrifugation and washing steps with 10% TCA and 95% EtOH to remove residual unincorporated <sup>3</sup>H-UTP. After that the plate was dried for 30 min at 50 °C and 30  $\mu$ L of scintillation fluid (Optiphase Supermix, PerkinElmer) was added to each well. After 10 min the wells were assayed for presence of <sup>3</sup>H-RNA by counting using Wallac MicroBeta TriLux system (Perkin Elmer). To obtain inhibition values for each sample, their counts were related to DMSO control.

**Determination of IC<sub>50</sub> values.** Three different concentrations of the compound were chosen (two samples for each concentration) in the linear range of the log dose response curve (20–80% inhibition) including concentrations above and below the IC<sub>50</sub> value. Values of percent inhibition were plotted versus the inhibitor molar concentrations on a semi-log plot. IC<sub>50</sub> values were calculated as the molar concentration causing 50% inhibition of RNAP activity. At least three independent determinations were performed for each compound (standard deviation <20%).

**Minimal inhibitory concentration determinations.** MIC values were determined in 96-well plates (Sarstedt, Nümbrecht, Germany) against *Staphylococcus aureus subsp. aureus* (Newman strain), *Bacillus subtilis subsp. subtilis*, *Pseudomonas aeruginosa* PAO1, *E. coli* K12, *E. coli* TolC, and the Rif-resistant *E. coli* TolC mutants: *E. coli* TolC  $\beta$  Q513L and *E. coli* TolC  $\beta$  H526Y. As bacteria start OD<sub>600</sub> 0.03 was used in a total volume of 200  $\mu$ L in lysogeny broth (LB) medium containing the compounds dissolved in DMSO (maximal DMSO concentration in the experiment: 1%). Final compound concentrations (in duplicates) were prepared by serial dilution ranging from 0.02–100  $\mu$ g/mL depending on their antibacterial activity and solubility in growth medium. The ODs were measured using a POLARstar Omega (BMG labtech, Offenburg, Germany) after inoculation and after incubation for 18 h at 37 °C with 50 rpm (200 rpm for *P. aeruginosa* PAO1). Given MIC values are means of two independent determinations (three if MIC <10  $\mu$ g/mL) and defined as the lowest concentration of compound that reduced OD<sub>600</sub> by  $\geq$ 95%.

**Selection of Rif-resistant *E. coli* TolC spontaneous mutants.** An *E. coli* TolC culture with an OD<sub>600</sub> 0.70 in LB was subcultured to fresh medium containing 3-fold the MIC of Rif every 24h with a dilution factor of 1:5. The cultures were incubated at 37 °C for 24 h with shaking. After 4 cycles the bacteria were transferred on LB agar plates containing 3-fold the MIC of Rif. The plates were incubated at 37 °C for 24 h. Single colonies were picked and transferred to liquid culture in the presence of 3-fold the MIC of Rif. Rif-resistant mutants were characterized by sequencing of RNAP rpoB.

**MIC determinations in presence of polymyxin B nonapeptide (PMBN) or phenyl-arginine- $\beta$ -naphthylamide (PA $\beta$ N).** The same procedures followed as mentioned above with minor modifications: Before inoculation, bacteria were cultured in LB medium containing PMBN (1  $\mu$ g/mL) or PA $\beta$ N (20  $\mu$ g/mL) (10  $\mu$ g/mL in case of *E. coli* TolC) for 2 h and subsequently diluted with the same medium to OD<sub>600</sub> 0.06. Inocula of 100  $\mu$ L were added to the wells containing 100  $\mu$ L of the specific concentrations of the compounds in PMBN/PA $\beta$ N containing medium. MIC<sub>50</sub> values were determined for *E. coli* K12, and *E. coli* D22.

**Determination of resistance rate.** Procedures were performed according to a described method<sup>12</sup> with modifications. Defined numbers of *E. coli* TolC cells ( $10^4$ – $10^{12}$ ) were incubated in LB in presence of the 2 $\times$  MIC of Rif, Myx B or compound **30** in parallel (16 h, 37 °C, 50 rpm, 0.5% DMSO). On each of the three following days, a fraction of each sample was supplemented with fresh compound containing LB followed by recultivation (conditions as before). The final cultures were plated on LB agar to determine the bacterial start

concentration which was needed to yield at least one colony on the plates. This threshold was determined to be the resistance rate.

**Cytotoxicity.** HEK 293 cells, a Human Embryonic Kidney 293 cell line, ( $2 \times 10^5$  cells per well) were seeded in 24-well, flat-bottomed plates. Culturing of cells, incubations and OD measurements were performed as described previously<sup>57</sup> with slight modifications. 24 h after seeding the cells, the incubation was started by the addition of compounds in a final DMSO concentration of 1%. The living cell mass was determined after 24, 48 and 72 h followed by the calculation of LD<sub>50</sub> values.

### Computational chemistry

All computational work was performed using Molecular Operating Environment (MOE) version 2010.10, Chemical Computing Group Inc., 1010 Sherbrooke St. West, Suite 910, Montreal, Quebec, H3A 2R7, Canada.

**Similarity analysis.** A database containing the compounds **11**, **21**, **30**, and **42** was created and 2D fingerprint GpiDAPH3 (graph pi-donor-acceptor-polar-hydrophobe-3 point pharmacophore) was calculated for all entries. Compound **11** was selected as reference structure and sent to MOE window. In the database viewer window, similarity search was performed by setting the fingerprint system to GpiDAPH3, and using the similarity metric Tanimoto coefficient ( $T_C$ ) to measure similarity between molecules.  $T_C$  values range from 0 (no similarity) to 1 (complete similarity).

**Flexible alignment.** Four ligands (**10**, **20**, **29**, and **41** representing classes I–IV respectively) were sketched using molecular builder of MOE, and each structure was subjected to energy minimization up to a gradient 0.05 Kcal/mol Å using the MMFF94x force field. The compounds were aligned using the flexible alignment mode of MOE with stochastic conformational search option was turned on, and configuration limit was set to 200 and iteration limit was set to 1000. Alignment had the best similarity score was retained and refined by MOE.

**Preparation of protein structure for docking.** X-ray crystal structure of the *T. Thermophilus* RNA polymerase holoenzyme in complex with dMyx B (Protein Data Bank (PDB) code 3EQL)<sup>7</sup> was used to perform the molecular docking study. In the sequence editor panel of MOE, chains C and D (corresponding to  $\beta$  and  $\beta'$  subunits respectively) were

selected, and all other chains were deleted. Hydrogen atoms were added to the receptor atoms, and the potential of protein was fixed.

**Ligand-receptor docking.** The binding site was set to dummy atoms which were identified by the site finder mode, and the amino acid residues were chosen where dMyx B binds in the switch region. Docking placement was triangle matcher with rotate bonds option was turned on, the 1<sup>st</sup> rescoring was ASE with force field refinement, and the 2<sup>nd</sup> rescoring was alpha HB.

**Calculation of angle.** Each structure was loaded from a previously prepared database of the target compounds into the MOE window, then it was subjected to energy minimization up to gradient 0.05 Kcal/mol Å using the MMFF94x force field. Angle between the aryl group and the ureido side chain was determined by activating the measure button and choosing angles option, then selecting carbon atom no. 1 of the aryl group, the corresponding carbon atom on the heterocyclic ring, and nitrogen atom no. 1 of the ureido group respectively.

## ACKNOWLEDGEMENT

The authors thank Jeannine Jung and Jannine Ludwig for technical assistance, and Dr. Dagmar Kail and Dr. Carsten Börger for performing the RP-HPLC purification. Furthermore we are grateful to Prof. Rolf Müller, Department of Microbial Natural Products at HIPS for kindly providing Myx B. Walid A. M. Elgaher gratefully acknowledges a scholarship from the German Academic Exchange Service (DAAD).

**REFERENCES**

- 1 A. R. M. Coates, G. Halls and Y. Hu, *Br. J. Pharmacol.*, 2011, **163**, 184.
- 2 K. Bush, P. Courvalin, G. Dantas, J. Davies, B. Eisenstein, P. Huovinen, G. A. Jacoby, R. Kishony, B. N. Kreiswirth, E. Kutter, S. A. Lerner, S. Levy, K. Lewis, O. Lomovskaya, J. H. Miller, S. Mobashery, L. J. V. Piddock, S. Projan, C. M. Thomas, A. Tomasz, P. M. Tulkens, T. R. Walsh, J. D. Watson, J. Witkowski, W. Witte, G. Wright, P. Yeh and H. I. Zgurskaya, *Nat. Rev. Microbiol.*, 2011, **9**, 894.
- 3 I. Chopra, *Curr. Opin. Investig. Drugs*, 2007, **8**, 600.
- 4 M. X. Ho, B. P. Hudson, K. Das, E. Arnold and R. H. Ebright, *Curr. Opin. Struct. Biol.*, 2009, **19**, 715.
- 5 K. Traynor, *Am. J. Health Syst. Pharm.*, 2011, **68**, 1276.
- 6 J. Mukhopadhyay, K. Das, S. Ismail, D. Koppstein, M. Jang, B. Hudson, S. Sarafianos, S. Tuske, J. Patel, R. Jansen, H. Irschik, E. Arnold and R. H. Ebright, *Cell*, 2008, **135**, 295.
- 7 G. A. Belogurov, M. N. Vassilyeva, A. Sevostyanova, J. R. Appleman, A. X. Xiang, R. Lira, S. E. Webber, S. Klyuyev, E. Nudler, I. Artsimovitch and D. G. Vassilyev, *Nature*, 2009, **457**, 332.
- 8 A. Srivastava, M. Talaue, S. Liu, D. Degen, R. Y. Ebright, E. Sineva, A. Chakraborty, S. Y. Druzhinin, S. Chatterjee, J. Mukhopadhyay, Y. W. Ebright, A. Zozula, J. Shen, S. Sengupta, R. R. Niedfeldt, C. Xin, T. Kaneko, H. Irschik, R. Jansen, S. Donadio, N. Connell and R. H. Ebright, *Curr. Opin. Microbiol.*, 2011, **14**, 532.
- 9 H. Irschik, K. Gerth, G. Höfle, W. Kohl and H. Reichenbach, *J. Antibiotics*, 1983, **36**, 1651.
- 10 T. Doundoulakis, A. X. Xiang, R. Lira, K. A. Agrios, S. E. Webber, W. Sisson, R. M. Aust, A. M. Shah, R. E. Showalter, J. R. Appleman and K. B. Simonsen, *Bioorg. Med. Chem. Lett.*, 2004, **14**, 5667.
- 11 T. I. Moy, A. Daniel, C. Hardy, A. Jackson, O. Rehrauer, Y. S. Hwang, D. Zou, K. Nguyen, J. A. Silverman, Q. Li and C. Murphy, *FEMS Microbiol. Lett.*, 2011, **319**, 176.
- 12 A. Srivastava, D. Degen, Y. W. Ebright and R. H. Ebright, *Antimicrob. Agents Chemother.*, 2012, **56**, 6250.
- 13 D. Haebich and F. von Nussbaum, *Angew. Chem. Int. Ed.*, 2009, **48**, 3397.
- 14 M. J. McPhillie, R. Trowbridge, K. R. Mariner, A. J. O'Neill, A. P. Johnson, I. Chopra and C. W. G. Fishwick, *ACS Med. Chem. Lett.*, 2011, **2**, 729.
- 15 E. T. Buurman, M. A. Foulk, N. Gao, V. A. Laganas, D. C. McKinney, D. T. Moustakas, J. A. Rose, A. B. Shapiro and P. R. Fleming, *J. Bacteriol.*, 2012, **194**, 5504.

- 16 F. Yakushiji, Y. Miyamoto, Y. Kunoh, R. Okamoto, H. Nakaminami, Y. Yamazaki, N. Noguchi and Y. Hayashi, *ACS Med. Chem. Lett.*, 2013, **4**, 220.
- 17 J. H. Sahner, M. Groh, M. Negri, J. Hauptenthal and R. W. Hartmann, *Eur. J. Med. Chem.*, 2013, **65**, 223.
- 18 J. Liebscher, B. Neumann and H. Hartmann, *J. Prakt. Chem.*, 1983, **325**, 915.
- 19 H. Hartmann and J. Liebscher, *Synthesis*, 1984, **3**, 275.
- 20 F.-X. L. Foulon, E. Braud, F. Fabis, J.-C. Lancelot and S. Rault, *Tetrahedron*, 2003, **59**, 10051.
- 21 F.-X. L. Foulon, E. Braud, F. Fabis, J.-C. Lancelot and S. Rault, *J. Comb. Chem.*, 2005, **7**, 253.
- 22 V. M. Tormyshev, D. V. Trukhin, O. Yu. Rogozhnikova, T. V. Mikhailina, T. I. Troitskaya and A. Flinn, *Synlett*, 2006, 2559.
- 23 *PCT Int. Appl.*, WO 2002083083 A2, 2002.
- 24 E. L. Anderson, J. E. Jr. Casey, L. C. Greene, J. J. Lafferty and H. E. Reiff, *J. Med. Chem.*, 1964, **7**, 259.
- 25 G. Kirsch, M. D. Cagniant and P. Cagniant, *J. Heterocyclic Chem.*, 1982, **19**, 443.
- 26 F. Jourdan, D. Ladurée and M. Robba, *J. Heterocyclic Chem.*, 1994, **31**, 305.
- 27 *Eur. Pat. Appl.*, EP 508527 A1, 1992.
- 28 R. S. Long, *J. Am. Chem. Soc.*, 1947, **69**, 990.
- 29 H. K. Gakhar, G. S. Gill and J. S. Multani, *J. Ind. Chem. Soc.*, 1971, **48**, 953.
- 30 A. M. Redman, J. Dumas and W. J. Scott, *Org. Lett.*, 2000, **2**, 2061.
- 31 H. B. Stevenson and J. R. Johnson, *J. Am. Chem. Soc.*, 1937, **59**, 2525.
- 32 G. M. Klein, J. P. Heotis and J. A. Buzard, *J. Biol. Chem.*, 1963, **238**, 1625.
- 33 J. F. Blount, D. L. Coffen and D. A. Katonak, *J. Org. Chem.*, 1978, **43**, 3821.
- 34 C. Hansch, A. Leo and R. W. Taft, *Chem. Rev.*, 1991, **91**, 165.
- 35 T. Rawling, A. M. McDonagh, B. Tattam and M. Murray, *Tetrahedron*, 2012, **68**, 6065.
- 36 J. Valgeirsson, E. Ø. Nielsen, D. Peters, T. Varming, C. Mathiesen, A. S. Kristensen and U. Madsen, *J. Med. Chem.*, 2003, **46**, 5834.
- 37 B. Thavonekham, *Synthesis*, 1997, **1997**, 1189.
- 38 M. Node, K. Nishide, M. Sai, K. Fuji and E. Fujita, *J. Org. Chem.*, 1981, **46**, 1991.
- 39 M. E. Sitzmann, *J. Heterocyclic Chem.*, 1979, **16**, 477.
- 40 M. A. Johnson and G. M. Maggiora, in *Concepts and Applications of Molecular Similarity*, John Wiley & Sons, New York, 1990.
- 41 Y. C. Martin, J. L. Kofron and L. M. Traphagen, *J. Med. Chem.*, 2002, **45**, 4350.

- 42 A. Bender and R. C. Glen, *Org. Biomol. Chem.*, 2004, **2**, 3204.
- 43 P. Willett, *Drug Discovery Today*, 2006, **11**, 1046.
- 44 C. W. Thornber, *Chem. Soc. Rev.*, 1979, **8**, 563.
- 45 P. Villain-Guillot, M. Gualtieri, L. Bastide, F. Roquet, J. Martinez, M. Amblard, M. Pugnieri and J.-P. Leonetti, *J. Med. Chem.*, 2007, **50**, 4195.
- 46 F. Arhin, O. Bélanger, S. Ciblat, M. Dehbi, D. Delorme, E. Dietrich, D. Dixit, Y. Lafontaine, D. Lehoux, J. Liu, G. A. McKay, G. Moeck, R. Reddy, Y. Rose, R. Srikumar, K. S. E. Tanaka, D. M. Williams, P. Gros, J. Pelletier, T. R. Parr and A. R. Far, *Bioorg. Med. Chem.*, 2006, **14**, 5812.
- 47 M. Vaara, *Microbiol. Rev.*, 1992, **56**, 395.
- 48 O. Lomovskaya, M. S. Warren, A. Lee, J. Galazzo, R. Fronko, M. Lee, J. Blais, D. Cho, S. Chamberland, T. Renau, R. Leger, S. Hecker, W. Watkins, K. Hoshino, H. Ishida and V. J. Lee, *Antimicrob. Agents Chemother.*, 2001, **45**, 105.
- 49 R. Chollet, J. Chevalier, A. Bryskier and J.-M. Pagès, *Antimicrob. Agents Chemother.*, 2004, **48**, 3621.
- 50 H. Nikaido, *Microbiol. Mol. Biol. Rev.*, 2003, **67**, 593.
- 51 G. Dong, P. Teo, Z. K. Wickens and R. H. Grubbs, *Science*, 2011, **333**, 1609.
- 52 C. A. Mosley, S. J. Myers, E. E. Murray, R. Santangelo, Y. A. Tahirovic, N. Kurtkaya, P. Mullasseril, H. Yuan, P. Lyuboslavsky, P. Le, L. J. Wilson, M. Yepes, R. Dingledine, S. F. Traynelis and D. C. Liotta, *Bioorg. Med. Chem.*, 2009, **17**, 6463.
- 53 N. Chernyak and S. L. Buchwald, *J. Am. Chem. Soc.*, 2012, **134**, 12466.
- 54 A. Rosowsky, H. Chen, H. Fu and S. F. Queener, *Bioorg. Med. Chem.*, 2003, **11**, 59.
- 55 V. Lisowski, F. Fabis, A. Pierré, D.-H. Caignard, P. Renard and S. Rault, *J. Enzyme Inhib. Med. Chem.*, 2002, **17**, 403.
- 56 J. Hauptenthal, K. Hüsecken, M. Negri, C. K. Maurer and R. W. Hartmann, *Antimicrob. Agents Chemother.*, 2012, **56**, 4536.
- 57 J. Hauptenthal, C. Baehr, S. Zeuzem and A. Piiper, *Int. J. Cancer*, 2007, **121**, 206.

### 3.3 Discovery of the first small molecule CsrA-RNA interaction inhibitors using biophysical screening technologies

Christine K. Maurer<sup>‡</sup>, Martina Fruth<sup>‡</sup>, Martin Empting, Olga Avrutina, Jörn Hoßmann, Suvd Nadmid, Jan Gorges, Jennifer Herrmann, Uli Kazmaier, Petra Dersch, Rolf Müller, and Rolf W. Hartmann

<sup>‡</sup> These authors contributed equally to this work.

Full text article and supporting information in *Future Med. Chem.*, 2016, **8**, 931-947.

doi:10.4155/fmc-2016-0033

**Publication C**

## 4 Final discussion

This thesis aimed at the establishment of suitable test systems, which enable the identification and characterization of novel anti-infective agents targeting the RNAP ‘switch region’ or CsrA and thereby providing useful information for rational drug design. The developed test systems were tailored to the specific protein targets and included biophysical and biochemical techniques as well as *in vitro* and *in cellulo* assays. In the following sections, the different assays as well as their outcome for drug discovery efforts targeting RNAP ‘switch region’ and CsrA will be discussed.

For reasons of clarity, the designation of the compounds discussed in chapter 4 is composed of the letter of the corresponding manuscript and the Arabic compound number (e.g., A2 refers to compound 2 from Publication A).

### 4.1 Characterization of RNAP ‘switch region’ inhibitors

#### 4.1.1 Aryl-ureido-heterocyclic-carboxylic acids as novel RNAP inhibitors

The 5-aryl-3-ureidothiophene-2-carboxylic acids were discovered in a virtual screening approach based on a pharmacophore model, which included both protein features from the RNAP ‘switch region’ as well as ligand features from Myx (Sahner et al., 2013b). Chemical optimization guided by SAR studies resulted in a series of potent RNAP inhibitors with IC<sub>50</sub> values in the single-digit micromolar range (Sahner et al., 2013b). This provided the basis for an analog design strategy to explore novel chemical scaffolds as RNAP inhibitors, which is described in Publication B. Starting from the 5-phenyl-3-ureidothiophene-2-carboxylic acids, further subclasses of the aryl-ureido-heterocyclic-carboxylic acids were developed and studied including regioisomeric thiophene as well as bioisosteric furan and thiazole scaffolds. Nonetheless, the *in vitro* activity could not be increased compared to the parent class.

A prerequisite for the development of potent antibiotics is that the *in vitro* effects need to be converted into the desired effects *in cellulo*. The aryl-ureido-heterocyclic-carboxylic acids described in reference (Sahner et al., 2013b) and in Publications A and B possessed potent antibacterial activity against Gram-positive bacteria such as *Bacillus subtilis* and *S. aureus*. The best inhibitors displayed minimal inhibitory concentration (MIC) values in the range of 2 µg/mL. However, these compounds lacked activity against the Gram-negative strains *P. aeruginosa* and *E. coli* K12. Strikingly, their activity was rescued in the strain *E. coli* TolC,

which is deficient in the AcrAB-TolC multidrug efflux system. This indicated that the limited effectiveness in Gram-negative bacteria was mediated by an efficient efflux of the compounds. This hypothesis was further supported by the fact that the efflux pump inhibitor phenylalanine-arginine  $\beta$ -naphthylamide (PA $\beta$ N) increased the susceptibility of the *E. coli* strains K12 (wild type), D22 (lipopolysaccharide mutant with increased outer membrane permeability), and even TolC to the compounds along with a decrease of MIC values by a factor of 2–14. These results suggested that other efflux pumps beside the AcrAB-TolC system are also involved in the efflux of this compound class in *E. coli*. Notably, since Pa $\beta$ N is also described to permeabilize the outer membranes in *E. coli*, the observed effect may not solely arise from efflux pump inhibition (Lamers et al., 2013). However, addition of another outer membrane permeability enhancer, polymyxin B nonapeptide, had no substantial effect on the susceptibility of the tested *E. coli* strains to the tested RNAP inhibitors (Publication B). In order to gain mechanistic insights into the compounds' mode of action, a high performance liquid chromatography (HPLC)-based abortive transcription assay was performed with compounds A1 and A6 as described in Publication A. The results proved that the tested aryl-ureidothiophene-2-carboxylic acids inhibit the bacterial transcription during the initiation phase, likewise other 'switch region' inhibitors. Nonetheless, this is not a clear evidence that RNAP inhibition is mediated exclusively through binding to the 'switch region' since inhibitors of the  $\sigma^{70}$ :core assembly or nucleotide addition would exhibit the same behavior. A previous study indeed reported that the aryl-ureidothiophene-2-carboxylic acid class interferes with the  $\sigma^{70}$ :core assembly in an ELISA-based competition assay (Hüsecken et al., 2014). Due to the fact that these inhibitors retain their activity in  $\sigma$ -independent transcription assay (unpublished data), only using core RNAP, it can be concluded that the mechanism of action is not solely based on interrupting the  $\sigma^{70}$ :core interaction.

To enable further optimization of this structural class, it was essential to validate the switch region as a binding site and to gain detailed information about the ligands' binding mode.

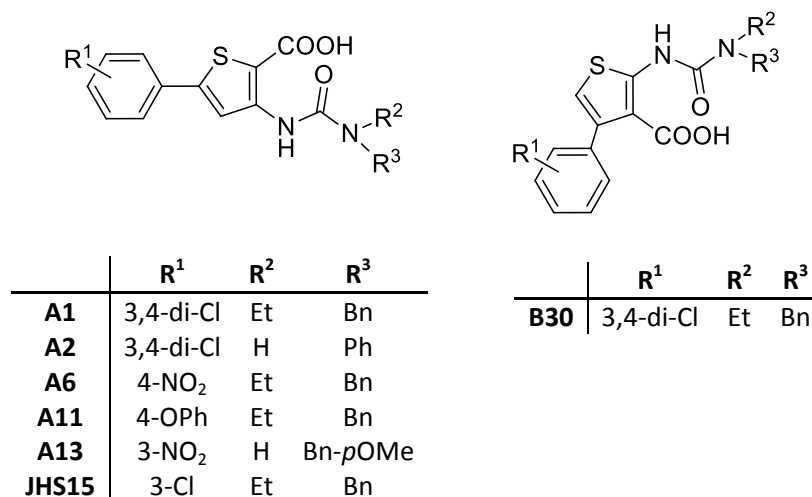


**Figure 11.** Structures of selected aryl-ureidothiophene-carboxylic acids.

#### 4.1.2 Binding site elucidation

In rational drug discovery, knowledge of a ligand's exact binding mode is of great importance. Detailed information about the molecular interactions between a ligand and its macromolecular receptor protein enables optimization towards ligands with enhanced binding affinity and target selectivity (Greer et al., 1994). Therefore, site-directed mutagenesis, ligand-based NMR techniques, and molecular docking were implemented to reveal the compounds' binding site and to further narrow down the protein domains essential for ligand binding (Publication A).

In a first attempt to confirm that the aryl-ureidothiophene-2-carboxylic acids bind to the 'switch region' as proposed from docking studies (Sahner et al., 2013b) single amino acids in the supposed binding site were mutated via site-directed mutagenesis. Subsequently, the effect of the inserted mutations on the RNAP transcription inhibition by the compounds and their antibacterial activity were studied. As an outcome of this experiment it was expected that mutations of amino acids significantly involved in the inhibitor-receptor interaction would result in reduced biological activity. Surprisingly, none of the selected mutations in the 'switch region' had a significant influence neither on the *in vitro* RNAP inhibitory activity nor on the *in cellulo* antibacterial activity of the inhibitors. This might be attributed to the conformational flexibility of this binding site. It has been shown that, during transcription as well as upon binding of dMyx, the 'switch region' undergoes substantial conformational changes (Belogurov et al., 2009; Srivastava et al., 2011; Wiesler et al., 2012). In addition, molecular docking studies suggested that binding of the aryl-ureidothiophene-2-carboxylic

acids in the ‘switch region’ is predominantly based on hydrophobic contacts, CH- $\pi$  and Van der Waals interactions rather than on specific hydrogen bond interactions (Sahner et al., 2013b). It might therefore be hypothesized that the effects of the inserted mutations could be tolerated and/or compensated owing to the overall hydrophobic character of the ‘switch region’ as well as its conformational flexibility. Nevertheless, it cannot be excluded that the mutation experiments missed amino acids critical for ligand binding. More exhaustive mutation experiments would be needed covering the whole interaction area within the supposed binding site.

In a next step, we exploited biophysical techniques to further investigate if the aryl-ureidothiophene-2-carboxylic acids are true ‘switch region’ binders as intended from the inhibitor design concept. To this end, STD NMR competition studies with known ‘switch region’ binders (Myx, Cor, and Rip) and compound A6 were performed. Since STD NMR uses large excess of ligand, A6 was chosen as test compound because of its favourable water solubility compared to that of other congeners of this class. The STD NMR experiments demonstrated that addition of increasing concentrations of compound A6 to an RNAP/Myx mixture results in a total displacement of STD signals belonging to Myx, thereby indicating that compound A6 and Myx compete for the same binding site on RNAP. Moreover, STD signals belonging to Cor and Rip were also significantly diminished upon addition of compound A6, further affirming that A6 is a ‘switch region’ binder.

Conversely, titrating Myx to an RNAP/A6 mixture did not lead to a significant decrease of STD signals belonging to compound A6. This provided indication of the existence of a second binding site for the aryl-ureidothiophene-2-carboxylic acids on RNAP. Tryptophan fluorescence quenching studies with RNAP and compound A6 further corroborated this hypothesis. Monitoring the intrinsic fluorescence quenching of a protein upon titration of its ligand can be applied to determine the binding affinity as well as the binding stoichiometry of the ligand (Epps et al., 1999; Hansen et al., 2002). Dose-response experiments with compound A6 exhibited a biphasic saturation curve, suggesting the existence of more than one binding site for the tested compound (Elalaoui et al., 1994). In addition, previous findings showed that the ureidothiophene carboxylic acids interrupt the  $\sigma^{70}$ :core assembly and therefore might also bind to the  $\sigma^{70}$ :core interface of RNAP (Hüsecken et al., 2014). Existence of a second binding site might also explain the results from the mutagenesis studies. However, it remains to be elucidated whether the compounds’ RNAP inhibitory activity is solely

mediated through binding to the RNAP ‘switch region’ or also arises from binding to other target sites within RNAP.

To rule out an allosteric effect for the displacement of Myx in the STD NMR studies and to obtain detailed information on the binding orientation of the compounds in the binding pocket we implemented INPHARMA NMR experiments. This technique is based on monitoring and evaluating intermolecular protein-mediated NOE signals between two competitively binding ligands. Provided that a structural model of the receptor in complex with the reference ligand is available, as it is the case for *Thermus thermophilus* RNAP in complex with Myx (Mukhopadhyay et al., 2008), the obtained information can be exploited to determine the relative binding mode of a ligand competing with the reference for the same binding site.

INPHARMA experiments were conducted with compound A6 or A13 together with *E. coli* core RNAP and Myx. Thereby, a set of INPHARMA correlations between A6 and Myx as well as between A13 and Myx could be observed, confirming that both members of this inhibitor class compete with Myx. Furthermore, the INPHARMA results revealed that both compounds A6 and A13 interact with the Myx western chain binding site and only minimally extend to the Myx eastern chain binding site. Interestingly, strong INPHARMA cross peaks were detected between methyl -24 of the Myx western chain and protons of both aromatic ring systems of A6 and A13. Therefore, the results propose that compounds A6 and A13 bind to the RNAP ‘switch region’ in two different poses with inverted orientations.

The structural information derived from the INPHARMA NOEs was exploited to evaluate the different binding poses predicted by molecular docking and to select the compounds’ correct binding mode. Noteworthy, binding modes with similar docking scores but inverted orientations were obtained from docking studies for compound A6 as well as for compound A13. Consecutively, the binding mode found by INPHARMA was supported by a co-crystal structure of compound A11 in complex with *E. coli* core RNAP (Murakami, unpublished results). Clear electron density in the Myx western chain binding site indicated the presence of compound A11 as predicted by INPHARMA. Nevertheless, the resolution attained for the complex was not sufficient to detect the binding orientation of this compound in the co-crystal.

In conclusion, the mutagenesis studies led to ambiguous results concerning the interaction profile of the investigated RNAP ‘switch region’ inhibitors. In contrast, the ligand-based NMR techniques implemented in this work have proven to be powerful tools for providing

detailed insights into ligand-protein interactions for this target site. Using a combination of STD NMR, INPHARMA, and molecular docking we were able to unambiguously prove that two representatives of the aryl-ureidothiophene-2-carboxylic acids and Myx bind competitively to the same target site. In addition, the binding mode of the aryl-ureidothiophene-2-carboxylic acids in the RNAP ‘switch region’ could be determined providing a basis for structure-based optimization. However, the applicability of STD NMR and INPHARMA methods are generally limited to low affinity ligands usually present during early stages of drug development. In addition, for INPHARMA studies, a structural model of the reference ligand bound to its receptor is required, which is not always available. Moreover, it should be noted that STD NMR and INPHARMA results need to be treated with care since aggregation or off-target binding events such as unspecific binding to protein surfaces contribute to the NMR signals and might cause artifacts (Lepre et al., 2004; Barile and Pellecchia, 2014). However, a major advantage of NMR spectroscopy methods compared to X-ray crystallography is that structural information can be obtained in solution. This is especially favourable for flexible proteins that can exhibit significantly different conformations in the crystal state from those in solution (Danley, 2006).

Within the scope of our drug development efforts, verification of the RNAP ‘switch region’ as a specific binding site of the aryl-ureidothiophene-2-carboxylic acids was considerably important given the background that this structural class does not only bind to two binding sites on RNAP but also inhibits PqsD, an enzyme involved in the *P. aeruginosa* quorum sensing system. The established binding mode can be used as a basis for structural optimization of the ‘switch region’ inhibitors towards an improved selectivity profile. Previous work demonstrated that it is possible to develop ureidothiophene-2-carboxylic acids, which act selectively on RNAP or PqsD displaying different SARs for the two targets (Sahner et al., 2013a).

#### **4.1.3 Potential of defeating antibiotic resistance**

Our anti-infective drug discovery efforts were focussed on addressing underexploited target sites in order to circumvent antibiotic resistances. In pursuing this strategy, RNAP inhibitors targeting the ‘switch region’ (Sahner et al., 2013b; Publication A; Publication B) have been developed. The aryl-ureido-heterocyclic-carboxylic acid inhibitors exhibit a significantly lower tendency of spontaneous resistance development than Myx or the clinically applied antibiotic Rif. Accordingly, the resistance frequency of this structural class, exemplarily

shown for B30 ( $< 4.2 \times 10^{-11}$ ) and JHS15 ( $< 4.2 \times 10^{-11}$ ) (Figure 11), is reduced by a factor of  $> 1000$  compared to Myx ( $7.1 \times 10^{-8}$ ) and Rif ( $8.3 \times 10^{-8}$ ) (Sahner et al., 2013b; Publication B). This might be attributed to the existence of a second target site aside from the RNAP 'switch region'. In addition, the aryl-ureidothiophene-2-carboxylic acid inhibitors only occupy the area of the Myx western chain binding site and are therefore not affected by single amino acid mutations in the eastern part of the Myx binding site, which confer high level resistance to Myx (Mukhopadhyay et al., 2008).

In order to investigate the inhibitors' ability to overcome existing antibiotic resistances, a subset of compounds was tested for antibacterial activity against Rif-resistant *E. coli* TolC as well as against a set of methicillin-resistant *S. aureus* (MRSA) strains exhibiting different antimicrobial resistance patterns (Publications A and B). As presumed from the compounds' distinct binding site to that of Rif, the inhibitors exhibited no cross-resistance with Rif. Furthermore, the tested aryl-ureidothiophene-2-carboxylic acids were highly potent against the tested MRSA isolates with compound A2 displaying a MIC value of 2  $\mu\text{g}/\text{mL}$ , which is similar to that of Myx.

To summarize, in view of the lower propensity of spontaneous resistance development combined with their potent antibacterial activity against Rif-resistant *E. coli* TolC and clinically relevant MRSA strains, the aryl-ureido-heterocyclic-carboxylic acids can be considered as promising scaffolds for antibacterial drug development.

#### **4.1.4 Evaluation of the RNAP 'switch region' as target for anti-infective drug development**

The RNAP 'switch region' represents a validated antibacterial drug target. A great benefit of this target site is that 'switch region' binders share no cross-resistance with the rifamycins. Additionally, it is highly conserved in bacterial RNAP, which intrinsically qualifies the RNAP 'switch region' as target for broad-spectrum therapy. However, even though several 'switch region' binders have already been identified with potent *in vitro* RNAP inhibitory activity, their antibacterial spectrum is mainly limited to Gram-positive bacteria (Häbich and Nussbaum, 2009). This may be attributed to the generally high lipophilicity of these inhibitors (O'Shea and Moser, 2008; Brown et al., 2014). However, considering the overall hydrophobic character of the 'switch region', chemical modifications leading to more hydrophilic compounds are supposed to result in a loss of activity, which was exemplarily shown in

Publication A. Besides, clinical use of the potent natural product ‘switch region’ RNAP inhibitors Myx, Cor, and Rip is hampered by their inappropriate physicochemical profiles including high molecular weight, insufficient stability, high serum protein binding (Häbich and Nussbaum, 2009). Studies aiming at the development of Myx analogs have shown that even subtle structural changes were not tolerated and led to a loss of biological activity except in the case of dMyx. The only approved ‘switch region’ RNAP inhibitor, fidaxomicin, possesses also a narrow spectrum of antibacterial activity and its application is restricted to *C. difficile*-associated diarrhea. Its high molecular weight and low solubility contribute to its very poor oral bioavailability. All these facts indicate that these natural product inhibitors might not represent optimal chemical lead structures for the development of broad-spectrum antibiotics. Small molecule ‘switch region’ inhibitors including the described classes of the squaramides, the pyridyl-benzamides, or the aryl-ureido-heterocyclic-carboxylic acids have the advantage of being easily synthetically accessible. However, they lack antibacterial activity against Gram-negative pathogens (McPhillie et al., 2011; Buurman et al., 2012; Sahner et al., 2013b).

In conclusion, developing inhibitors with high affinity to the ‘switch region’ combined with desirable ‘drug-like’ properties and broad-spectrum antibacterial activity seems to be a challenging task for this target site.

#### 4.1.5 Outlook

The objective of this work was the *in vitro* characterization of the aryl-ureido-heterocyclic-carboxylic acids with respect to their binding mode, mechanism of action and antibacterial profile. In a next step, the inhibitors should be evaluated in relevant *in vivo* disease models. Due to the inhibitors’ promising *in cellulo* anti-MRSA activity they will be tested in an *in vivo* murine wound model of *S. aureus* infection. The compounds’ insufficient physicochemical properties (high lipophilicity, poor water solubility) could be overcome by the use of a prodrug approach or advanced drug delivery technologies aiming at an improved pharmacokinetic profile. This might include coupling the inhibitors to a carrier system such as liposomes or nanoparticles (Graef et al., 2016).

Furthermore, the established ligand-based NMR methods could be used for the identification of novel molecular scaffolds that bind to the Myx binding site as starting points for medicinal chemistry optimization.

## 4.2 Discovery of inhibitors of the CsrA-RNA interaction

### 4.2.1 Hit identification and *in vitro* activity

In the second part of this thesis, the focus was set on CsrA as a potential novel target for anti-infective drug discovery. Thereby, the main objective was the discovery of inhibitors of the CsrA-RNA interaction, which was pursued by a screening and a ligand-based strategy. Initially, as described in Publication C, a suitable test system enabling the identification and characterization of such inhibitors was established that was based on SPR and fluorescence polarization (FP) techniques.

SPR spectroscopy was selected as method of choice for detecting CsrA-binding molecules because it provides high sensitivity, fast sample throughput, and low protein consumption. Site-directed immobilization of the target protein ensured a homogeneous sensor surface and a better comparability of results obtained with different protein immobilizations. Therefore, CsrA was fused with the AviTag<sup>TM</sup> on the C-terminus of CsrA distal from the CsrA-RNA interaction site to allow site-specific *in vivo* biotinylation using the *E. coli* biotin ligase BirA (Kay et al., 2009). Exploiting the strong interaction between the biomolecules biotin and streptavidin, the purified labeled protein was then captured on streptavidin-coated chips. The functional activity of the immobilized protein was verified by binding experiments using two RNA sequences (RNA\_A and RNA\_B) derived from known RNA targets with proven affinity for CsrA. The obtained dissociation constants were in accordance with those determined by ITC and FP as well as with the ones reported in literature indicating the protein's integrity and assay compatibility.

The screening approach was composed of a primary SPR screen to identify specific CsrA-binders and a secondary FP screen to assess the initial hit compounds' ability to interfere with the CsrA-RNA interaction. Overall, the screening library consisted of around 1,000 structurally diverse small molecules of natural or synthetic origin. Thereof, the class of myxobacterial metabolites (259 compounds) were directly tested in the functional FP assay for reasons of poor availability.

To ensure even the detection of fragment-sized molecules with low binding affinity in the primary SPR screen, a screening concentration of 100  $\mu$ M and relatively high protein immobilization levels (6,000–10,000 RU) were chosen (Shepherd et al, 2014, Gianetti, 2011). One obstacle in establishing the SPR screening set-up was the lack of a known small

molecule CsrA binder, which could be used as a reference in the screening. The CsrA target RNAs were not suitable as a control in the screening set up because of their slow dissociation from the binding site and high molecular weight. Therefore, a library component with reproducible binding to CsrA had to be chosen as a reference to guarantee an accurate ranking of the screened compounds across several runs. Nevertheless, since the reference was not a validated CsrA-RNA inhibitor, an immediate affinity assessment of the screened compounds was not possible and further complicated the choice of a reasonable cut-off value for the screening. The threshold for hit selection was set to a low affinity level to detect CsrA binders covering a broad structural diversity. Furthermore, false positives were ought to be eliminated in the downstream FP screening. The SPR screening of 708 small molecules resulted in the identification of 72 dose-dependent CsrA binders, which is reflected in a hit rate of 10.2%. In the follow-up screen using an FP-based competition assay, 3 out of the 72 initial hits proved to significantly inhibit the CsrA-RNA interaction. The high number of initial hits exhibiting no or only weak inhibition is presumably attributed to the fact that these compounds possess binding sites on CsrA distant to the RNA binding interface or do not interfere with RNA binding. Together with 4 additional hits identified in the FP screen of 259 myxobacterial metabolites, the screening approach resulted in 7 structurally diverse small molecule hits exhibiting  $IC_{50}$  values in the range from 4–106  $\mu$ M in the *in vitro* FP competition assay. Noticeably, none of the seven hits was able to fully displace the RNA molecules from their interaction site on CsrA in the test setting, achieving a maximal inhibition of the interaction of 80%. Possible explanations for this finding could be that the hit compounds might bind to adjacent or partially overlapping sites relative to the RNA binding interface or to an allosteric site, thereby impairing RNA binding (Roehrl et al., 2004). Furthermore, all hit compounds showed reversible and dose-dependent binding to CsrA but not to RNA\_B in SPR experiments. This indicated that inhibition of the CsrA-RNA interaction was derived solely from protein binding as intended by our screening concept and not from interaction with the RNA molecule.

In addition to the screening strategy, we implemented a rational ligand-based approach for the discovery of CsrA-RNA interaction inhibitors. Starting from the conserved core binding sequence ANGGA(N), RNA oligomers of varying length and backbone structure were derived. It turned out that the GGA motif with RNA backbone ( $GGA_{RNA}$ ) was able to fully inhibit the CsrA-RNA interaction displaying an  $IC_{50}$  value of 113  $\mu$ M, whereas the respective shortened GG or GA motifs totally lacked activity. The efforts made to increase the hydrolytic stability and/or permeability by modifications of the backbone of the GGA motif have not

been successful. Both elimination and methylation of the 2'OH groups present in the RNA backbone as well as substitution of the sugar-phosphate backbone with a peptide nucleic acid (PNA) backbone resulted in reduced inhibitory activity compared to  $GGA_{RNA}$ . This is in accordance with modelling studies (Publication C) indicating that the 2'OH groups of the  $GGA_{RNA}$  backbone are involved in inter- and intramolecular H-bonds and therefore critical for activity. Compared to the best small molecule inhibitors identified in the screening approach, the ligand-based  $GGA_{RNA}$  inhibitor exhibits a rather low *in vitro* activity as well as poor ligand efficiency (LE 0.09). Nevertheless, this ligand-based inhibitor bears the advantages of a complete inhibition of the CsrA-RNA interaction and of a known binding site, which enables structure-based optimization. In addition,  $GGA_{RNA}$  could be used as a tool in competition experiments to identify novel inhibitors of the CsrA-GGA interaction hot spot.

In conclusion, both strategies resulted in the discovery of CsrA-RNA interaction inhibitors. Noteworthy, the screening approach showed that the CsrA-RNA interaction, despite its extensive interaction interface, could be inhibited even with fragment-sized molecules such as NAT31–454537 (MW of 229 Da). Therefore, the established screening assays represent tools to identify small molecule inhibitors that might be more drug-like regarding stability or cell permeability.

Opposed to the screening strategy, in the ligand-based approach CsrA-RNA inhibitors with a known binding site were discovered. The most potent inhibitor turned out to be  $GGA_{RNA}$ . Taking into account that shortening or backbone modifications of  $GGA_{RNA}$  were not tolerated concerning activity, further optimization will not be a trivial task. Nonetheless, the ligand-based approach generated valuable information on structural functionalities crucial for binding to the RNA interaction sites of CsrA.

#### 4.2.2 Outlook

CsrA represents a potential target for broad-spectrum anti-infective therapy since it is essential for full virulence of various pathogens and is highly conserved among bacteria. So far, no small molecule inhibitors of CsrA have been available and first target validation efforts were based on bacterial mutant studies (Barnard et al., 2004; Mulcahy et al., 2008). Accordingly, the proof of concept (PoC) is still pending demonstrating that modulation of CsrA activity by small molecule inhibitors results in the desired pharmacological effect *in cellulo* and *in vivo*. In this respect, the identified small molecule CsrA-RNA interaction

inhibitors can serve as tool compounds to study the cellular effects of CsrA-RNA interaction inhibition on bacterial virulence towards a target validation. Therefore, in a next step, co-crystallization trials should be undertaken for binding site elucidation to enable structure-based optimization of the screening hits to highly affine inhibitors, which can be applied for provision of *in vivo* PoC. In this context, fragment-linking strategies could also be considered for hit optimization depending on the inhibitors' binding modes

## 5 References

- Aertsen A., Michiels C. W. (2004) Stress and how bacteria cope with death and survival. *Critical Reviews in Microbiology* 30, 263-273.
- Alekshun M. N., Levy S. B. (2007) Molecular Mechanisms of Antibacterial Multidrug Resistance. *Cell* 128, 1037-1050.
- Altier C., Suyemoto M., Lawhon S. D. (2000) Regulation of *Salmonella enterica* Serovar Typhimurium Invasion Genes by *csrA*. *Infection and Immunity* 68, 6790-6797.
- Artsimovitch I., Seddon J., Sears P. (2012) Fidaxomicin is an inhibitor of the initiation of bacterial RNA synthesis. *Clinical Infectious Diseases : An Official Publication of the Infectious Diseases Society of America* 55 Suppl 2, S127-31.
- Artsimovitch I., Vassylyev D. G. (2006) Is It Easy to Stop RNA Polymerase? *Cell Cycle* 5, 399-404.
- Babitzke P., Romeo T. (2007) CsrB sRNA family: sequestration of RNA-binding regulatory proteins. *Current Opinion in Microbiology* 10, 156-163.
- Baker C. S., Morozov I., Suzuki K., Romeo T., Babitzke P. (2002) CsrA regulates glycogen biosynthesis by preventing translation of *glgC* in *Escherichia coli*. *Molecular Microbiology* 44, 1599-1610.
- Barile E., Pellecchia M. (2014) NMR-based approaches for the identification and optimization of inhibitors of protein-protein interactions. *Chemical Reviews* 114, 4749-4763.
- Barnard F. M., Loughlin M. F., Fainberg H. P., Messenger M. P., Ussery D. W., Williams P., Jenks P. J. (2004) Global regulation of virulence and the stress response by CsrA in the highly adapted human gastric pathogen *Helicobacter pylori*. *Molecular Microbiology* 51, 15-32.
- Bartoschek S., Klabunde T., Defossa E., Dietrich V., Stengelin S., Griesinger C., Carlomagno T., Focken I., Wendt K. U. (2010) Drug design for G-protein-coupled receptors by a ligand-based NMR method. *Angewandte Chemie International Edition* 49, 1426-1429.
- Belogurov G. A., Vassylyeva M. N., Sevostyanova A., Appleman J. R., Xiang A. X., Lira R., Webber S. E., Klyuyev S., Nudler E., Artsimovitch I., Vassylyev D. G. (2009) Transcription inactivation through local refolding of the RNA polymerase structure. *Nature* 457, 332-335.
- Bentley R. (2009) Different roads to discovery; Prontosil (hence sulfa drugs) and penicillin (hence beta-lactams). *Journal of Industrial Microbiology & Biotechnology* 36, 775-786.
- Bhatt S., Edwards A. N., Nguyen H. T. T., Merlin D., Romeo T., Kalman D. (2009) The RNA binding protein CsrA is a pleiotropic regulator of the locus of enterocyte effacement pathogenicity island of enteropathogenic *Escherichia coli*. *Infection and Immunity* 77, 3552-3568.

- Black M. T., Hodgson J. (2005) Novel target sites in bacteria for overcoming antibiotic resistance. *Advanced Drug Delivery Reviews* 57, 1528-1538.
- Boucher H. W., Talbot G. H., Bradley J. S., Edwards J. E., Gilbert D., Rice L. B., Scheld M., Spellberg B., Bartlett J. (2009) Bad Bugs, No Drugs. No ESKAPE! An Update from the Infectious Diseases Society of America. *Clin Infect Dis* 48, 1-12.
- Brown D. G., May-Dracka T. L., Gagnon M. M., Tommasi R. (2014) Trends and exceptions of physical properties on antibacterial activity for Gram-positive and Gram-negative pathogens. *Journal of Medicinal Chemistry* 57, 10144-10161.
- Buurman E. T., Foulk M. A., Gao N., Laganas V. A., McKinney D. C., Moustakas D. T., Rose J. A., Shapiro A. B., Fleming P. R. (2012) Novel rapidly diversifiable antimicrobial RNA polymerase switch region inhibitors with confirmed mode of action in *Haemophilus influenzae*. *Journal of Bacteriology* 194, 5504-5512.
- Cala O., Guillière F., Krimm I. (2014) NMR-based analysis of protein-ligand interactions. *Analytical and Bioanalytical Chemistry* 406, 943-956.
- Campbell, C.T. Surface Plasmon Resonance (SPR) Biosensor Development. <https://depts.washington.edu/campbelc/projects/plasmon.pdf>. 16.03.2016.
- Campbell E. A., Korzheva N., Mustaev A., Murakami K., Nair S., Goldfarb A., Darst S. A. (2001) Structural Mechanism for Rifampicin Inhibition of Bacterial RNA Polymerase. *Cell* 104, 901-912.
- Carlomagno T. (2012) NMR in natural products: understanding conformation, configuration and receptor interactions. *Natural Product Reports* 29, 536-554.
- Chakraborty A., Wang D., Ebright Y. W., Korlann Y., Kortkhonjia E., Kim T., Chowdhury S., Wigneshweraraj S., Irschik H., Jansen R., Nixon B. T., Knight J., Weiss S., Ebright R. H. (2012) Opening and closing of the bacterial RNA polymerase clamp. *Science (New York, N.Y.)* 337, 591-595.
- Chamberlin M. J. (1974) The selectivity of transcription. *Annual Review of Biochemistry* 43, 721-775.
- Chopra I. (2007) Bacterial RNA polymerase: a promising target for the discovery of new antimicrobial agents. *Current Opinion in Investigational Drugs (London, England : 2000)* 8, 600-607.
- Clatworthy A. E., Pierson E., Hung D. T. (2007) Targeting virulence: a new paradigm for antimicrobial therapy. *Nature Chemical Biology* 3, 541-548.
- Cooper M. A. (2002) Optical biosensors in drug discovery. *Nature Reviews Drug Discovery* 1, 515-528.
- Cormack B. (2001) Directed mutagenesis using the polymerase chain reaction. *Current protocols in Molecular Biology* Chapter 8, Unit 8.5.

- Costa G. L., Bauer J. C., McGowan B., Angert M., Weiner M. P. (1996) Site-directed mutagenesis using a rapid PCR-based method. *Methods in Molecular Biology (Clifton, N.J.)* 57, 239-248.
- Cramer P. (2002) Multisubunit RNA polymerases. *Current Opinion in Structural Biology* 12, 89-97.
- D'Costa V. M., King C. E., Kalan L., Morar M., Sung W. W. L., Schwarz C., Froese D., Zazula G., Calmels F., Debruyne R., Golding G. B., Poinar H. N., Wright G. D. (2011) Antibiotic resistance is ancient. *Nature* 477, 457-461.
- Danley D. E. (2006) Crystallization to obtain protein-ligand complexes for structure-aided drug design. *Acta Crystallographica. Section D, Biological Crystallography* 62, 569-575.
- Darst S. A. (2004) New inhibitors targeting bacterial RNA polymerase. *Trends in Biochemical Sciences* 29, 159-160.
- Davies J. (2006) Where have all the antibiotics gone? *The Canadian Journal of Infectious Diseases & Medical Microbiology* 17, 287-290.
- Doundoulakis T., Xiang A. X., Lira R., Agrios K. A., Webber S. E., Sisson W., Aust R. M., Shah A. M., Showalter R. E., Appleman J. R., Simonsen K. B. (2004) Myxopyronin B analogs as inhibitors of RNA polymerase, synthesis and biological evaluation. *Bioorganic & Medicinal Chemistry Letters* 14, 5667-5672.
- Dubey A. K., Baker C. S., Romeo T., Babitzke P. (2005) RNA sequence and secondary structure participate in high-affinity CsrA-RNA interaction. *RNA (New York, N.Y.)* 11, 1579-1587.
- Dubey A. K., Baker C. S., Suzuki K., Jones A. D., Pandit P., Romeo T., Babitzke P. (2003) CsrA Regulates Translation of the *Escherichia coli* Carbon Starvation Gene, *cstA*, by Blocking Ribosome Access to the *cstA* Transcript. *Journal of Bacteriology* 185, 4450-4460.
- Ebright R. H. (2000) RNA polymerase: structural similarities between bacterial RNA polymerase and eukaryotic RNA polymerase II. *Journal of Molecular Biology* 304, 687-698.
- Edelheit O., Hanukoglu A., Hanukoglu I. (2009) Simple and efficient site-directed mutagenesis using two single-primer reactions in parallel to generate mutants for protein structure-function studies. *BMC Biotechnology* 9, 61.
- Elalaoui A., Divita G., Maury G., Imbach J.-L., Goody R. S. (1994) Intrinsic tryptophan fluorescence of bovine liver adenosine kinase, characterization of ligand binding sites and conformational changes. *European Journal of Biochemistry* 221, 839-846.
- Epps D. E., Raub T. J., Caiolfa V., Chiari A., Zamai M. (1999) Determination of the Affinity of Drugs toward Serum Albumin by Measurement of the Quenching of the Intrinsic Tryptophan Fluorescence of the Protein. *Journal of Pharmacy and Pharmacology* 51, 41-48.

- European Centre for Disease prevention and Control/European Medicines Agencies (ECDC/EMA). (2009) The bacterial challenge: time to react. A call to narrow the gap between multidrug-resistant bacteria in the EU and the development of new antibacterial agents. *ECDC/EMA Joint Technical Report. Stockholm.*
- Fang Y. (2012) Ligand-receptor interaction platforms and their applications for drug discovery. *Expert Opinion on Drug Discovery* 7, 969-988.
- Feklistov A., Mekler V., Jiang Q., Westblade L. F., Irschik H., Jansen R., Mustaev A., Darst S. A., Ebright R. H. (2008) Rifamycins do not function by allosteric modulation of binding of Mg<sup>2+</sup> to the RNA polymerase active center. *Proceedings of the National Academy of Sciences of the United States of America* 105, 14820-14825.
- Feldman H. A. (1972) The beginning of antimicrobial therapy: introduction of the sulfonamides and penicillins. *The Journal of Infectious Diseases* 125, Suppl:22-46.
- Floss H. G., Yu T.-W. (2005) Rifamycin-mode of action, resistance, and biosynthesis. *Chemical Reviews* 105, 621-632.
- Gourse R. L., Ross W., Rutherford S. T. (2006) General pathway for turning on promoters transcribed by RNA polymerases containing alternative sigma factors. *Journal of Bacteriology* 188, 4589-4591.
- Graef F., Gordon S., Lehr C.-M. Anti-infectives in Drug Delivery—Overcoming the Gram-Negative Bacterial Cell Envelope. In Springer (Hg.) 2016-Current Topics in Microbiology and Immunology, pp. 1–22.
- Greer J., Erickson J. W., Baldwin J. J., Varney M. D. (1994) Application of the Three-Dimensional Structures of Protein Target Molecules in Structure-Based Drug Design. *Journal of Medicinal Chemistry* 37, 1035-1054.
- Gutiérrez P., Li Y., Osborne M. J., Pomerantseva E., Liu Q., Gehring K. (2005) Solution structure of the carbon storage regulator protein CsrA from *Escherichia coli*. *Journal of Bacteriology* 187, 3496-3501.
- Häbich D., Nussbaum F. von. (2009) Lost in transcription--inhibition of RNA polymerase. *Angewandte Chemie International Edition* 48, 3397-3400.
- Hansen S. B., Radic' Z., Talley T. T., Molles B. E., Deerinck T., Tsigelny I., Taylor P. (2002) Tryptophan fluorescence reveals conformational changes in the acetylcholine binding protein. *The Journal of Biological Chemistry* 277, 41299-41302.
- Heeb S., Kuehne S. A., Bycroft M., Crivii S., Allen M. D., Haas D., Cámara M., Williams P. (2006) Functional analysis of the post-transcriptional regulator RsmA reveals a novel RNA-binding site. *Journal of Molecular Biology* 355, 1026-1036.

- Henkin T. M. (1996) Control of transcription termination in prokaryotes. *Annual Review of Genetics* 30, 35-57.
- Heroven A. K., Böhme K., Dersch P. (2012) The Csr/Rsm system of *Yersinia* and related pathogens: a post-transcriptional strategy for managing virulence. *RNA Biology* 9, 379-391.
- Heroven A. K., Böhme K., Rohde M., Dersch P. (2008) A Csr-type regulatory system, including small non-coding RNAs, regulates the global virulence regulator RovA of *Yersinia pseudotuberculosis* through RovM. *Molecular Microbiology* 68, 1179-1195.
- Heurlier K., Williams F., Heeb S., Dormond C., Pessi G., Singer D., Camara M., Williams P., Haas D. (2004) Positive Control of Swarming, Rhamnolipid Synthesis, and Lipase Production by the Posttranscriptional RsmA/RsmZ System in *Pseudomonas aeruginosa* PAO1. *Journal of Bacteriology* 186, 2936-2945.
- Hiraishi N., Tochio N., Kigawa T., Otsuki M., Tagami J. (2013) Monomer-collagen interactions studied by saturation transfer difference NMR. *Journal of Dental Research* 92, 284-288.
- Holdgate G. A., Anderson M., Edfeldt F., Geschwindner S. (2010) Affinity-based, biophysical methods to detect and analyze ligand binding to recombinant proteins: matching high information content with high throughput. *Journal of Structural Biology* 172, 142-157.
- Hsu L. M. (2002) Promoter clearance and escape in prokaryotes. *Biochimica et Biophysica Acta (BBA) - Gene Structure and Expression* 1577, 191-207.
- Hüsecken K., Hinsberger S., Elgaher W. A. M., Hauptenthal J., Hartmann R. W. (2014) Surface plasmon resonance--more than a screening technology: insights in the binding mode of  $\sigma 70$ :core RNAP inhibitors. *Future Medicinal Chemistry* 6, 1551-1565.
- Hüsecken K., Negri M., Fruth M., Boettcher S., Hartmann R. W., Hauptenthal J. (2013) Peptide-based investigation of the *Escherichia coli* RNA polymerase  $\sigma(70)$ :core interface as target site. *ACS Chemical Biology* 8, 758-766.
- Igarashi K., Ishihama A. (1991) Bipartite functional map of the *E. coli* RNA polymerase  $\alpha$  subunit. Involvement of the C-terminal region in transcription activation by cAMP-CRP. *Cell* 65, 1015-1022.
- Infectious Diseases Society of America. (2008) No ESKAPE! New Drugs Against MRSA, Other Superbugs Still Lacking. <[www.sciencedaily.com/releases/2008/12/081201105706.htm](http://www.sciencedaily.com/releases/2008/12/081201105706.htm)>. *ScienceDaily*.
- Irschik H., Augustiniak H., Gerth K., Höfle G., Reichenbach H. (1995) Antibiotics from gliding bacteria. No. 68. The Ripostatins, Novel Inhibitors of Eubacterial RNA Polymerase Isolated from Myxobacteria. *J. Antibiot.* 48, 787-792.
- Irschik H., Gerth H., Höfle G., Kohl W., Reichenbach H. (1983) The myxopyronins, new inhibitors of bacterial RNA synthesis from *Myxococcus fulvus* (Myxobacterales). *J. Antibiot.* 36, 1651-1658.

- Irschik H., Jansen R., Höfle G., Gerth K., Reichenbach H. (1985) The coralopyronins, new inhibitors of bacterial RNA synthesis from Myxobacteria. *J. Antibiot.* 38, 145-152.
- Jin D. J., Gross C. A. (1988) Mapping and sequencing of mutations in the *Escherichia coli* rpoB gene that lead to rifampicin resistance. *Journal of Molecular Biology* 202, 45-58.
- Jishage M, Iwata A, Ueda S, Ishihama A. (1996) Regulation of RNA polymerase sigma subunit synthesis in *Escherichia coli*: intracellular levels of four species of sigma subunit under various growth conditions. *Journal of Bacteriology* 178, 5447-5451.
- Jonas K., Edwards A. N., Ahmad I., Romeo T., Römling U., Melefors O. (2010) Complex regulatory network encompassing the Csr, c-di-GMP and motility systems of *Salmonella* Typhimurium. *Environmental Microbiology* 12, 524-540.
- Kay B. K., Thai S., Volgina V. V. (2009) High-Throughput Biotinylation of Proteins. In High throughput protein expression and purification. Methods and protocols, S.A. Doyle, ed. (Totowa, NJ: Humana Press), pp. 185–198.
- Lamers R. P., Cavallari J. F., Burrows L. L. (2013) The efflux inhibitor phenylalanine-arginine beta-naphthylamide (PA $\beta$ N) permeabilizes the outer membrane of gram-negative bacteria. *PloS One* 8, e60666.
- Landick R., Geszvain K. (2005) The Structure of Bacterial RNA Polymerase. In The Bacterial Chromosome, N.P. Higgins, ed. (American Society of Microbiology), pp. 283–296.
- Lepre C. A., Moore J. M., Peng J. W. (2004) Theory and applications of NMR-based screening in pharmaceutical research. *Chemical Reviews* 104, 3641-3676.
- Lewis K. (2013) Platforms for antibiotic discovery. *Nature Reviews Drug Discovery* 12, 371-387.
- Ling M. M., Robinson B. H. (1997) Approaches to DNA mutagenesis: an overview. *Analytical Biochemistry* 254, 157-178.
- Lira R., Xiang A. X., Doundoulakis T., Biller W. T., Agrios K. A., Simonsen K. B., Webber S. E., Sisson W., Aust R. M., Shah A. M., Showalter R. E., Banh V. N., Steffy K. R., Appleman J. R. (2007) Syntheses of novel myxopyronin B analogs as potential inhibitors of bacterial RNA polymerase. *Bioorganic & Medicinal Chemistry Letters* 17, 6797-6800.
- Ludwig C., Günther U. L. (2009) Ligand based NMR methods for drug discovery. *Front Biosci* Volume, 4565.
- Marden J. N., Diaz M. R., Walton W. G., Gode C. J., Betts L., Urbanowski M. L., Redinbo M. R., Yahr T. L., Wolfgang M. C. (2013) An unusual CsrA family member operates in series with RsmA to amplify posttranscriptional responses in *Pseudomonas aeruginosa*. *Proceedings of the National Academy of Sciences of the United States of America* 110, 15055-15060.

- Mariani R., Maffioli S. I. (2009) Bacterial RNA Polymerase Inhibitors: An Organized Overview of their Structure, Derivatives, Biological Activity and Current Clinical Development Status 16, 430-454.
- Matteelli A., Roggi A., Carvalho A. C. (2014) Extensively drug-resistant tuberculosis: epidemiology and management. *Clinical Epidemiology* 6, 111-118.
- Mayer M., Meyer B. (1999) Characterization of ligand binding by saturation transfer difference NMR spectroscopy. *Angewandte Chemie International Edition* 38, 1784-1788.
- McClure W. R. (1985) Mechanism and control of transcription initiation in prokaryotes. *Annual Review of Biochemistry* 54, 171-204.
- McClure WR C. C. L. (1978) On the mechanism of rifampicin inhibition of RNA synthesis. *J Biol Chem.* 253.
- McPhillie M. J., Trowbridge R., Mariner K. R., O'Neill A. J., Johnson A. P., Chopra I., Fishwick C. W. G. (2011) Structure-based ligand design of novel bacterial RNA polymerase inhibitors. *ACS Medicinal Chemistry Letters* 2, 729-734.
- Minakhin L., Bhagat S., Brunning A., Campbell E. A., Darst S. A., Ebright R. H., Severinov K. (2001) Bacterial RNA polymerase subunit omega and eukaryotic RNA polymerase subunit RPB6 are sequence, structural, and functional homologs and promote RNA polymerase assembly. *Proceedings of the National Academy of Sciences of the United States of America* 98, 892-897.
- Monnet D. L. (2005) Antibiotic development and the changing role of the pharmaceutical industry. *International Journal of Risk & Safety in Medicine* 17, 133-145.
- Moore J. M. (1999) NMR screening in drug discovery. *Current Opinion in Biotechnology* 10, 54-58.
- Moy T. I., Daniel A., Hardy C., Jackson A., Rehrauer O., Hwang Y. S., Zou D., Nguyen K., Silverman J. A., Li Q., Murphy C. (2011) Evaluating the activity of the RNA polymerase inhibitor myxopyronin B against *Staphylococcus aureus*. *FEMS Microbiology Letters* 319, 176-179.
- Mukhopadhyay J., Das K., Ismail S., Koppstein D., Jang M., Hudson B., Sarafianos S., Tuske S., Patel J., Jansen R., Irschik H., Arnold E., Ebright R. H. (2008) The RNA polymerase "switch region" is a target for inhibitors. *Cell* 135, 295-307.
- Mulcahy H., O'Callaghan J., O'Grady E. P., Maciá M. D., Borrell N., Gómez C., Casey P. G., Hill C., Adams C., Gahan C. G. M., Oliver A., O'Gara F. (2008) *Pseudomonas aeruginosa* RsmA plays an important role during murine infection by influencing colonization, virulence, persistence, and pulmonary inflammation. *Infection and Immunity* 76, 632-638.
- Orts J., Tuma J., Reese M., Grimm S. K., Monecke P., Bartoschek S., Schiffer A., Wendt K. U., Griesinger C., Carlomagno T. (2008) Crystallography-independent determination of ligand binding modes. *Angewandte Chemie International Edition* 47, 7736-7740.

- O'Shea R., Moser H. E. (2008) Physicochemical properties of antibacterial compounds: implications for drug discovery. *Journal of Medicinal Chemistry* 51, 2871-2878.
- Pellecchia M., Bertini I., Cowburn D., Dalvit C., Giralt E., Jahnke W., James T. L., Homans S. W., Kessler H., Luchinat C., Meyer B., Oschkinat H., Peng J., Schwalbe H., Siegal G. (2008) Perspectives on NMR in drug discovery: a technique comes of age. *Nature Reviews Drug Discovery* 7, 738-745.
- Powers J. H. (2004) Antimicrobial drug development--the past, the present, and the future. *Clinical Microbiology and Infection* 10 Suppl 4, 23-31.
- Rasko D. A., Sperandio V. (2010) Anti-virulence strategies to combat bacteria-mediated disease. *Nature Reviews Drug Discovery* 9, 117-128.
- Revelles O., Millard P., Nougayrède J.-P., Dobrindt U., Oswald E., Létisse F., Portais J.-C. (2013) The carbon storage regulator (Csr) system exerts a nutrient-specific control over central metabolism in *Escherichia coli* strain Nissle 1917. *PLoS One* 8, e66386.
- Rice L. B. (2008) Federal funding for the study of antimicrobial resistance in nosocomial pathogens: no ESKAPE. *The Journal of Infectious Diseases* 197, 1079-1081.
- Rife C., Schwarzenbacher R., McMullan D., Abdubek P., Ambing E., Axelrod H., Biorac T., Canaves J. M., Chiu H.-J., Deacon A. M., DiDonato M., Elsliger M.-A., Godzik A., Grittini C., Grzechnik S. K., Hale J., Hampton E., Han G. W., Haugen J., Hornsby M., Jaroszewski L., Klock H. E., Koesema E., Kreuzsch A., Kuhn P., Lesley S. A., Miller M. D., Moy K., Nigoghossian E., Paulsen J., Quijano K., Reyes R., Sims E., Spraggon G., Stevens R. C., van den Bedem H., Velasquez J., Vincent J., White A., Wolf G., Xu Q., Hodgson K. O., Wooley J., Wilson I. A. (2005) Crystal structure of the global regulatory protein CsrA from *Pseudomonas putida* at 2.05 Å resolution reveals a new fold. *Proteins* 61, 449-453.
- Rivkin A., Gim S. (2011) Rifaximin: new therapeutic indication and future directions. *Clinical Therapeutics* 33, 812-827.
- Roehrl M. H. A., Wang J. Y., Wagner G. (2004) Discovery of Small-Molecule Inhibitors of the NFAT–Calcineurin Interaction by Competitive High-Throughput Fluorescence Polarization Screening. *Biochemistry* 43, 16067-16075.
- Romeo T. (1998) Global regulation by the small RNA-binding protein CsrA and the non-coding RNA molecule CsrB. *Mol Microbiol* 29, 1321-1330.
- Ross W., Ernst A., Gourse R. L. (2001) Fine structure of *E. coli* RNA polymerase-promoter interactions: alpha subunit binding to the UP element minor groove. *Genes & Development* 15, 491-506.
- Sahner J. H., Brengel C., Storz M. P., Groh M., Plaza A., Müller R., Hartmann R. W. (2013a) Combining in silico and biophysical methods for the development of *Pseudomonas aeruginosa*

- quorum sensing inhibitors: an alternative approach for structure-based drug design. *Journal of Medicinal Chemistry* 56, 8656-8664.
- Sahner J. H., Groh M., Negri M., Hauptenthal J., Hartmann R. W. (2013b) Novel small molecule inhibitors targeting the "switch region" of bacterial RNAP: structure-based optimization of a virtual screening hit. *European Journal of Medicinal Chemistry* 65, 223-231.
- Sánchez-Pedregal V. M., Reese M., Meiler J., Blommers M. J. J., Griesinger C., Carlomagno T. (2005) The INPHARMA method: protein-mediated interligand NOEs for pharmacophore mapping. *Angewandte Chemie International Edition* 44, 4172-4175.
- Scarano S., Mascini M., Turner A. P. F., Minunni M. (2010) Surface plasmon resonance imaging for affinity-based biosensors. *Biosensors & Bioelectronics* 25, 957-966.
- Schubert M., Lapouge K., Duss O., Oberstrass F. C., Jelesarov I., Haas D., Allain F. H.-T. (2007) Molecular basis of messenger RNA recognition by the specific bacterial repressing clamp RsmA/CsrA. *Nature Structural & Molecular Biology* 14, 807-813.
- Sears P., Ichikawa Y., Ruiz N., Gorbach S. (2013) Advances in the treatment of *Clostridium difficile* with fidaxomicin: a narrow spectrum antibiotic. *Annals of the New York Academy of Sciences* 1291, 33-41.
- Severinov K., Soushko M., Goldfarb A., Nikiforov V. (1994) RifR mutations in the beginning of the *Escherichia coli* rpoB gene. *Molec. Gen. Genet.* 244.
- Skjærven L., Codutti L., Angelini A., Grimaldi M., Latek D., Monecke P., Dreyer M. K., Carlomagno T. (2013) Accounting for conformational variability in protein-ligand docking with NMR-guided rescoring. *Journal of the American Chemical Society* 135, 5819-5827.
- Spellberg B. (2012) New Antibiotic Development: Barriers and Opportunities in 2012. *Alliance for the Prudent Use of Antibiotics (APUA) Clinical Newsletter* 30, 8-10.
- Spellberg B., Powers J. H., Brass E. P., Miller L. G., Edwards J. E. (2004) Trends in antimicrobial drug development: implications for the future. *Clinical Infectious Diseases : An Official Publication of the Infectious Diseases Society of America* 38, 1279-1286.
- Spoto G., Minunni M. (2012) Surface Plasmon Resonance Imaging. What Next? *J. Phys. Chem. Lett.* 3, 2682-2691.
- Srivastava A., Talaue M., Liu S., Degen D., Ebright R. Y., Sineva E., Chakraborty A., Druzhinin S. Y., Chatterjee S., Mukhopadhyay J., Ebright Y. W., Zozula A., Shen J., Sengupta S., Niedfeldt R. R., Xin C., Kaneko T., Irschik H., Jansen R., Donadio S., Connell N., Ebright R. H. (2011) New target for inhibition of bacterial RNA polymerase: 'switch region'. *Current Opinion in Microbiology* 14, 532-543.

- Suzuki K., Babitzke P., Kushner S. R., Romeo T. (2006) Identification of a novel regulatory protein (CsrD) that targets the global regulatory RNAs CsrB and CsrC for degradation by RNase E. *Genes & Development* 20, 2605-2617.
- Suzuki K., Wang X., Weilbacher T., Pernestig A.-K., Melefors O., Georgellis D., Babitzke P., Romeo T. (2002) Regulatory Circuitry of the CsrA/CsrB and BarA/UvrY Systems of *Escherichia coli*. *Journal of Bacteriology* 184, 5130-5140.
- Tamma P. D., Cosgrove S. E. (2011) Antimicrobial Stewardship. *Infectious Disease Clinics of North America* 25, 245-260.
- Tavares L. S., Silva C. S. F., Souza V. C. de, da Silva V. L., Diniz C. G., Santos M. O. (2013) Strategies and molecular tools to fight antimicrobial resistance: resistome, transcriptome, and antimicrobial peptides. *Frontiers in Microbiology* 4, 412.
- Tee K. L., Wong T. S. (2013) Polishing the craft of genetic diversity creation in directed evolution. *Biotechnology Advances* 31, 1707-1721.
- Tenover F. C. (2006) Mechanisms of antimicrobial resistance in bacteria. *American Journal of Infection Control* 34, S3-10; discussion S64-73.
- Thillaivinayagalingam P., Gommeaux J., McLoughlin M., Collins D., Newcombe A. R. (2010) Biopharmaceutical production: Applications of surface plasmon resonance biosensors. *Journal of Chromatography. B, Analytical Technologies in the Biomedical and Life Sciences* 878, 149-153.
- Timmermans J., van Melderen L. (2010) Post-transcriptional global regulation by CsrA in bacteria. *Cellular and Molecular Life Sciences* 67, 2897-2908.
- US Department of Health and Human Services. Centers for Disease Control and Prevention. (2013) "Antibiotic resistance threats in the United States, 2013." Atlanta.
- van Assche E., van Puyvelde S., Vanderleyden J., Steenackers H. P. (2015) RNA-binding proteins involved in post-transcriptional regulation in bacteria. *Frontiers in Microbiology* 6, 141.
- Vassylyev D. G., Sekine S.-i., Laptenko O., Lee J., Vassylyeva M. N., Borukhov S., Yokoyama S. (2002) Crystal structure of a bacterial RNA polymerase holoenzyme at 2.6 Å resolution. *Nature* 417, 712-719.
- Venugopal A. A., Johnson S. (2012) Fidaxomicin: a novel macrocyclic antibiotic approved for treatment of *Clostridium difficile* infection. *Clinical Infectious Diseases : An Official Publication of the Infectious Diseases Society of America* 54, 568-574.
- Villain-Guillot P., Bastide L., Gualtieri M., Leonetti J.-P. (2007) Progress in targeting bacterial transcription. *Drug Discovery Today* 12, 200-208.

- Wang Y.-S., Liu D., Wyss D. F. (2004) Competition STD NMR for the detection of high-affinity ligands and NMR-based screening. *Magnetic Resonance in Chemistry* 42, 485-489.
- Wei B. L., Brun-Zinkernagel A.-M., Simecka J. W., Prüß B. M., Babitzke P., Romeo T. (2001) Positive regulation of motility and flhDC expression by the RNA-binding protein CsrA of *Escherichia coli*. *Molecular Microbiology* 40, 245-256.
- Wiesler S. C., Burrows P. C., Buck M. (2012) A dual switch controls bacterial enhancer-dependent transcription. *Nucleic Acids Research* 40, 10878-10892.
- Wilson D. S., Keefe A. D. (2001) Random mutagenesis by PCR. *Current protocols in Molecular Biology* Chapter 8, Unit8.3.
- Wright A. J. (1999) The penicillins. *Mayo Clinic Proceedings* 74, 290-307.
- Yakhnin A. V., Baker C. S., Vakulskas C. A., Yakhnin H., Berezin I., Romeo T., Babitzke P. (2013) CsrA activates flhDC expression by protecting flhDC mRNA from RNase E-mediated cleavage. *Molecular Microbiology* 87, 851-866.
- Yakhnin H., Pandit P., Petty T. J., Baker C. S., Romeo T., Babitzke P. (2007) CsrA of *Bacillus subtilis* regulates translation initiation of the gene encoding the flagellin protein (hag) by blocking ribosome binding. *Molecular Microbiology* 64, 1605-1620.
- Zheng L., Baumann U., Reymond J.-L. (2004) An efficient one-step site-directed and site-saturation mutagenesis protocol. *Nucleic Acids Research* 32, e115.

## 6 Supporting information

### 6.1 Supporting Information for Publication A

Full supporting information is available online:

<http://pubs.acs.org/doi/suppl/10.1021/cb5005433>

#### 6.1.1 Supplemental experimental procedures

##### **Intrinsic fluorescence quenching assay.**

Intrinsic fluorescence quenching assay was performed as described by *Mukhopadhyay et al.* (1) with slight modifications.

Fluorescence emission intensities of RNAP core enzyme in TB [100  $\mu$ l; 50 mM Tris-HCl (pH 8.0), 100 mM KCl, 10 mM MgCl<sub>2</sub>, 1 mM dithiotreitol, 0.01 % Tween 20, 5% glycerol] were measured before and 10 min after addition of the inhibitors [10  $\mu$ l; TB, 50% DMSO]. Employing a Polarstar Omega (BMG Labtech, Ortenberg, Germany) 280 nm and 350 nm were chosen as excitation and emission wavelengths, respectively. The observed reductions of intrinsic fluorescence at each inhibitor concentration were corrected for dimethyl sulfoxide/buffer dilution and the inner-filter effect using N-acetyltryptophanamide.

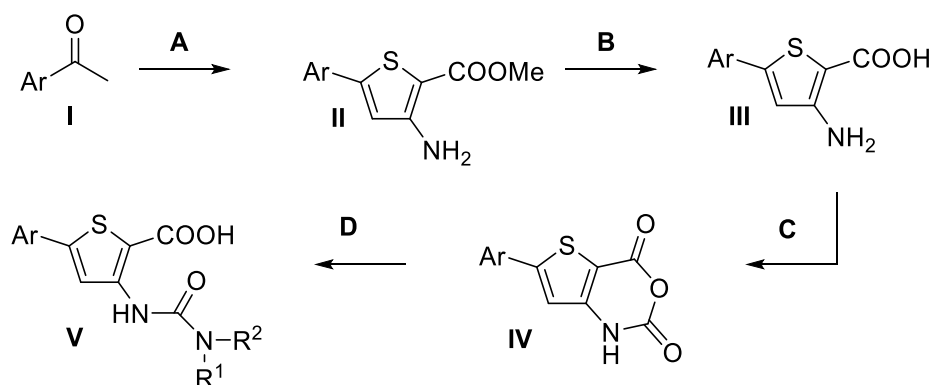
Data were plotted as percent quenching of the intrinsic fluorescence in dependence of inhibitor concentration. The highest observed quenching was set at 100%. Data are means of three independent determinations. For non-linear regression analysis GraphPad Prism 5 (GraphPad Software, La Jolla, CA, USA) was used. Experimental data of rifampicin was fitted to a one-site binding model, whereas data of compound **6**, which showed a biphasic quenching, was fitted to a two-affinity model (2) as demonstrated by *Döppenschmitt et al.* (3) earlier.

## Synthesis of compound 13.

### Materials and methods

Starting materials were purchased from commercial suppliers and used without further purification. Column flash chromatography was performed on silica gel (40–63  $\mu\text{M}$ ), and reaction progress was monitored by TLC on TLC Silica Gel 60 F<sub>254</sub> (Merck). All moisture-sensitive reactions were performed under nitrogen atmosphere using oven-dried glassware and anhydrous solvents. <sup>1</sup>H and <sup>13</sup>C NMR spectra were recorded on Bruker Fourier spectrometers (300 or 75 MHz) at ambient temperature with the chemical shifts recorded as  $\delta$  values in ppm units by reference to the hydrogenated residues of deuteriated solvent as internal standard. Coupling constants (*J*) are given in Hz and signal patterns are indicated as follows: s, singlet; d, doublet; dd, doublet of doublets; t, triplet; m, multiplet, br., broad signal. The purity of the final compounds was measured by HPLC. The Surveyor LC system consisted of a pump, an autosampler, and a PDA detector. Mass spectrometry was performed on a MSQ electrospray mass spectrometer (ThermoFisher, Dreieich, Germany). The system was operated by the standard software Xcalibur. A RP C18 NUCLEODUR 100-5 (125 mm x 3 mm) column (Macherey-Nagel GmbH, Düren, Germany) was used as the stationary phase. All solvents were HPLC grade. In a gradient run the percentage of acetonitrile (containing 0.1% trifluoroacetic acid) was increased from an initial concentration of 0% at 0 min to 100% at 15 min and kept at 100% for 5 min. The injection volume was 10  $\mu\text{L}$ , and flow rate was set to 800  $\mu\text{L}/\text{min}$ . MS analysis was carried out at a spray voltage of 3800 V and a capillary temperature of 350 °C and a source CID of 10 V. Spectra were acquired in positive mode from 100 to 1000 *m/z* at 254 nm for the UV trace.

### Synthesis and spectroscopic data of compound 13



**Scheme S1:** Synthesis of 5-aryl-3-ureidothiophene-2-carboxylic acids.

*Method A, general procedure for the synthesis of 5-aryl-3-amino-2-carboxylic acid methylester (II) (7)*

POCl<sub>3</sub> (26.1 g, 0.17 mol) was added dropwise to DMF (24.9 g, 0.34 mol) maintaining the temperature below 25 °C (cooling in ice bath) and stirred for additional 15 min. The acetophenone **I** (85.0 mmol) was added slowly and the temperature was kept between 40 and 60 °C. After complete addition, the mixture was stirred for 30 minutes at room temperature. Hydroxylamine hydrochloride (23.6 g, 0.34 mol) was carefully added portionwise (exothermic reaction!) and the reaction was stirred for additional 30 min without heating. After cooling to room temperature, the mixture was poured into ice water (300 mL). The precipitated β-chloro-cinnamionitrile was collected by filtration, washed with H<sub>2</sub>O (2 x 50 mL) and dried under reduced pressure over CaCl<sub>2</sub>. In the next step sodium (1.93 g, 84.0 mmol) was dissolved in MeOH (85 mL) and methylthioglycolate (6.97 g, 65.6 mmol) was added to the stirred solution. The β-chloro-cinnamionitrile (61.1 mmol) was added and the mixture was heated to reflux for 30 min. After cooling to room temperature, the mixture was poured in ice water (300 mL). The precipitated solid was collected by filtration, washed with H<sub>2</sub>O (2 x 50 mL) and dried under reduced pressure over CaCl<sub>2</sub>. If necessary, recrystallisation was performed from EtOH.

*Method B, general procedure for the synthesis of 5-aryl-3-amino-2-carboxylic acid (III):*

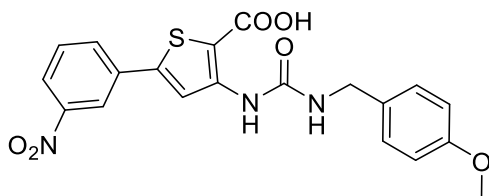
The 5-aryl-3-amino-2-carboxylic acid methyl ester **II** (16.6 mmol) was added to a solution of KOH (60 mL, 0.6M in H<sub>2</sub>O) and MeOH (60 mL). The mixture was heated to reflux for 3 h, concentrated, and washed with EtOAc (2 x 50 mL). The aqueous layer was cooled with ice and acidified with a saturated aqueous solution of KHSO<sub>4</sub>. The precipitated solid was collected by filtration, washed with H<sub>2</sub>O (2 x 30 mL) and dried under reduced pressure over CaCl<sub>2</sub>.

*Method C, general procedure for the synthesis of 5-aryl-2-thiaisatoic-anhydrid (IV) (8, 9)*

To a solution of the 5-aryl-3-amino-2-carboxylic acid (**III**) (5.28 mmol) in THF (50 mL) a solution of phosgene (6.10 mL, 20 wt% in toluene, 11.6 mmol) was added dropwise over a period of 30 min. The reaction mixture was stirred for 2 h at room temperature, followed by the addition of saturated aqueous solution of NaHCO<sub>3</sub> (30 mL) and H<sub>2</sub>O (50 mL). The resulting mixture was extracted with EtOAc/THF (1:1, 3 x 100 mL). The organic layer was washed with saturated aqueous NaCl (100 mL), dried (MgSO<sub>4</sub>) and concentrated. The crude material was suspended in a mixture of *n*-hexane/EtOAc (2:1, 50 mL) heated to 50 °C and after cooling to room temperature separated via filtration.

*Method D, general procedure for the synthesis of of 5-aryl-3-ureidothiophene-2-carboxylic acid (V)(10)*

The 5-aryl-2-thiaisatoic-anhydrid (**IV**) (0.46 mmol) was suspended in water (7.5 mL) and the appropriate amine (4.60 mmol) was added. The reaction mixture was stirred, heated to 100 °C and then cooled to room temperature. The reaction mixture was poured into a mixture of concentrated HCl and ice (1:1) and extracted with EtOAc/THF (1:1, 60 mL). The organic layer was washed with aqueous HCl (2M), followed by saturated aqueous NaCl (2 x 50 mL), dried (MgSO<sub>4</sub>) and concentrated. The crude material was suspended in a mixture of *n*-hexane/EtOAc (2:1, 20 mL) heated to 50 °C and after cooling to room temperature separated via filtration.

**3-(3-(4-Methoxybenzyl)ureido)-5-(3-nitrophenyl)thiophene-2-carboxylic acid**

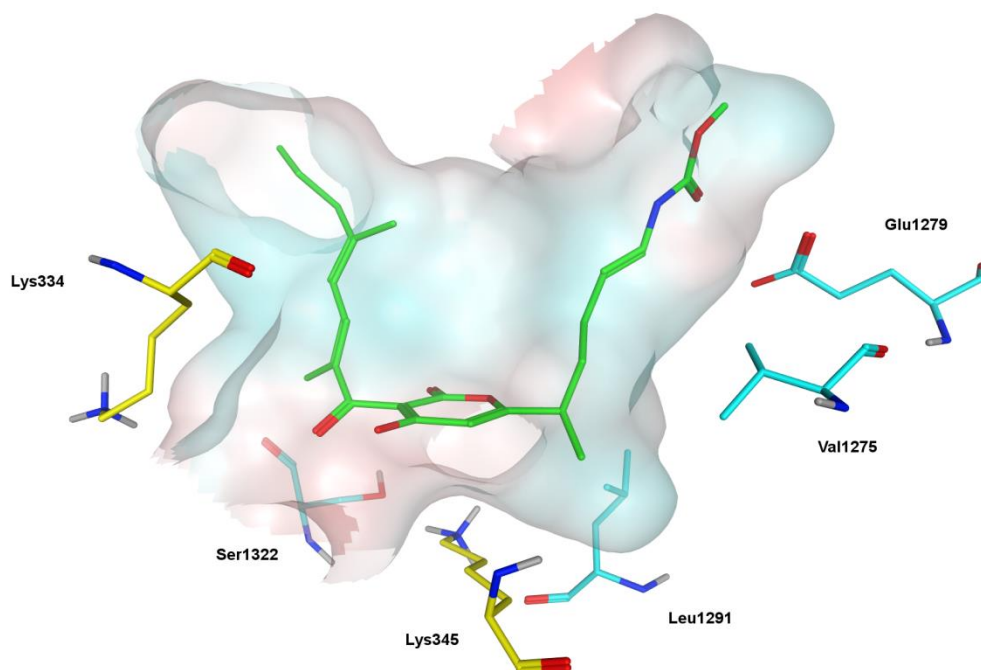
The title compound was prepared from 3'-nitroacetophenone according to the general procedures A-D.

$^1\text{H}$  NMR (DMSO- $d_6$ , 300 MHz):  $\delta$  = 13.22 (br. s, 1H), 9.41 (s, 1H), 8.44 (s, 1H), 8.37 (t,  $J$  = 1.7 Hz, 1H), 8.23 (dd,  $J$  = 1.7, 8.1 Hz, 1H), 8.09 – 8.20 (m 2H), 7.75 (t,  $J$  = 8.1 Hz, 1H), 7.24 (d,  $J$  = 8.6 Hz, 2H), 6.90 (d,  $J$  = 8.6 Hz, 2H), 4.24 (d,  $J$  = 5.6 Hz, 2H), 3.73 (s, 3H) ppm.

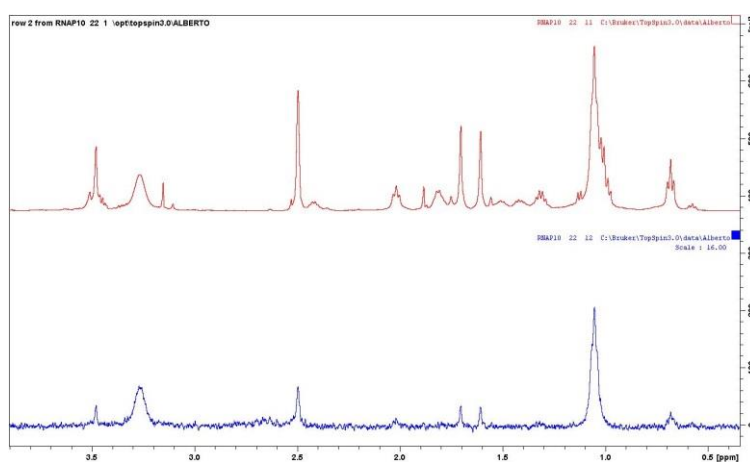
$^{13}\text{C}$  NMR (DMSO- $d_6$ , 75 MHz):  $\delta$  = 164.5, 158.3, 153.8, 148.4, 146.1, 143.8, 134.2, 131.9, 131.6, 131.0, 128.7, 123.5, 119.8, 119.6, 113.7, 107.9, 55.0, 42.5 ppm.

HPLC-Purity: 96.3 %

## 6.1.2 Supplemental figures



**Figure S1.** Myx binding pocket including mutated amino acids. Myxopyronin A is colored in green.  $\beta$  subunit amino acids are colored in turquoise,  $\beta'$  subunit amino acids are colored in yellow.

**Figure S2. STD NMR competition experiments with 6 and Cor/ Rip**

**Figure S2 (A).** Off-resonance spectrum of compound **6** in presence of core RNAP (colored in red). Corresponding STD NMR spectrum of **6** in presence of core RNAP is colored in blue.

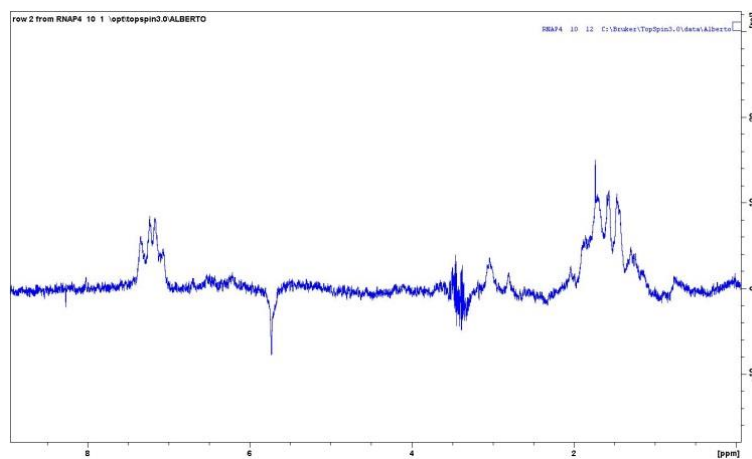


**Figure S2 (B).** STD NMR spectrum of Rip in presence of core RNAP.

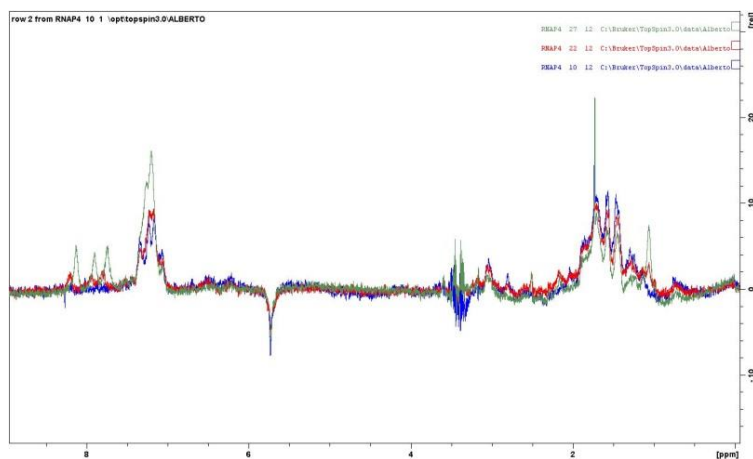


**Figure S2 (C).** STD NMR competition of Rip and **6** in presence of core RNAP. STD spectrum of Rip in presence of core RNAP colored in blue. Corresponding spectra upon addition of 1:1 equivalent of **6** (red) and 1:2 equivalents of **6** (green).

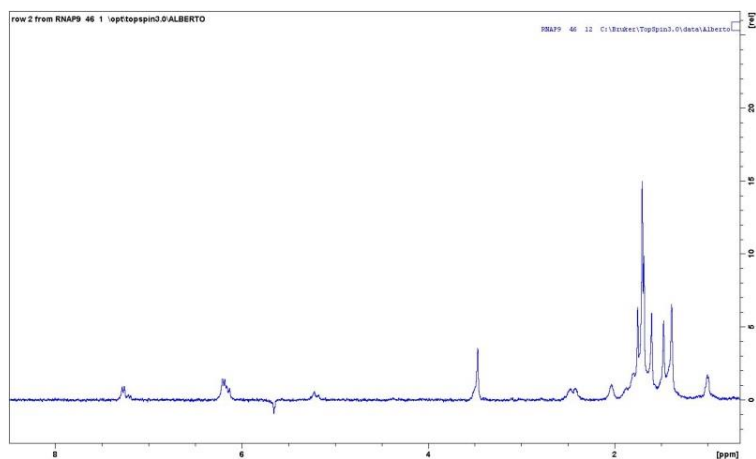


**Figure S2 (D).** STD NMR spectrum of Cor in presence of core RNAP.

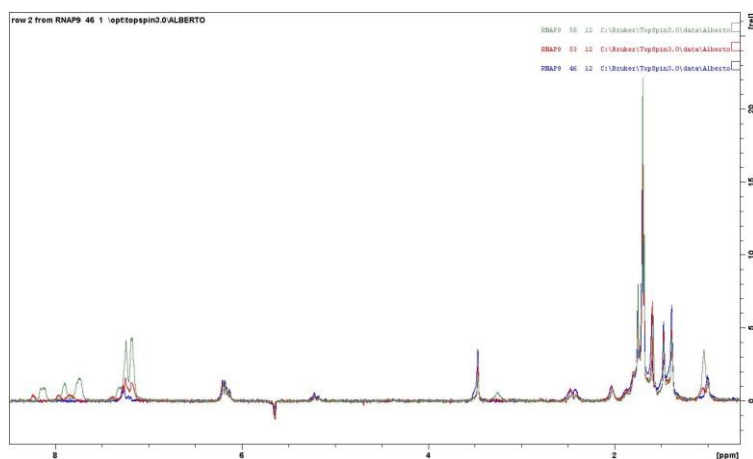


**Figure S2 (E).** STD NMR competition of Cor and **6** in presence of core RNAP. STD spectrum of Cor in presence of core RNAP colored in blue. Corresponding spectra upon addition of 1:1 equivalent of **6** (red) and 1:3 equivalents of **6** (green).

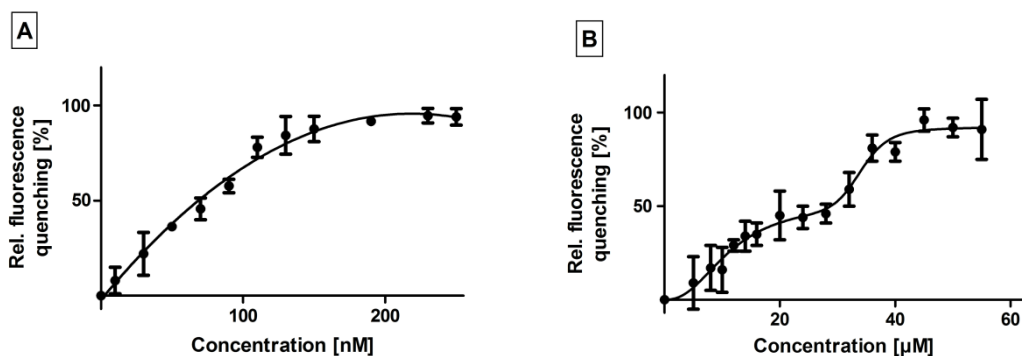


**Figure S3.** Effect of increasing inhibitor concentrations on the intrinsic fluorescence of RNAP. (A) rifampicin (B) **6**

For rifampicin, as expected and as already shown for myxopyronin (**1**), a monophasic curve progression was obtained, meaning that the compound is binding to a single binding site.

In contrast, **6** exhibits a biphasic character of the curve indicating that the compounds bind to more than one single binding site.

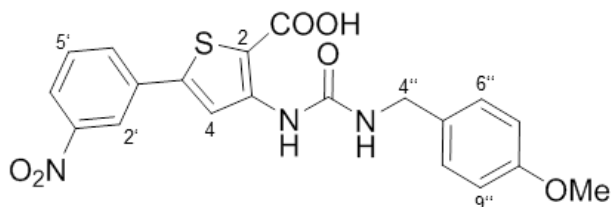


**Figure S4.** Numbering of atoms of compound **13**.

### 6.1.3 Supplemental tables

**Table S1.** Antibiogram of the MRSA strains

Antibiotic / MRSA	COL	USA300 Lac	5191	R44
ampicillin	R	R	R	R
oxacillin	R	R	R	R
gentamicin	S	S	S	S
ciprofloxacin	S	R	R	S
moxifloxacin	S	I	R	S
erythromycin	S	R	R	R
clindamycin	S	S	R	R
linezolid	S	S	S	S
daptomycin	S	S	S	S
vancomycin	S	S	S	S
tetracyclin	R	S	S	R
tigecycline	S	S	S	S
fosfomicin	S	S	R	S
fusidinsäure	S	S	S	S
rifampicin	S	S	S	S
trimethoprim/sulfamethoxazol	S	S	S	R

R, resistant; I, intermediary resistant; S, susceptible

**Table S2.** MIC value determination in *Ec* TolC switch region mutants

Compd	<i>Ec</i> TolC							
	wild type	$\beta'$ K334G	$\beta'$ K334E	$\beta'$ K345T	$\beta'$ K345N	$\beta$ V1275M	$\beta$ E1279K	$\beta$ L1291F
	MIC [ $\mu\text{g/ml}$ ]							
<b>A1</b>	12.5–25	25	> 25	>25	25	25	25	25
<b>A2</b>	25	12.5	> 25	12.5–25	25	25	25	12.5–25
<b>A4</b>	25	50	> 50	25–50	50	25	25	25
<b>A5</b>	12.5	25	> 25	12.5–25	12.5	25	12.5	12.5
<b>A7</b>	25	25	> 50	25–50	25	25	25	25
<b>Myx</b>	1.25	10	> 10	> 25	> 25	> 25	> 25	2.5
<b>Rif</b>	6.25	6.25	6.25	12.5	12.5	12.5	6.25–12.5	6.25–12.5

**Table S3.** *In vitro* transcription assay with wild type/ mutant RNAPs

Compd	RNAP	RNAP	RNAP	RNAP	RNAP	RNAP
	wild type	$\beta$ S1322E	$\beta'$ $\Delta$ 334–5	$\beta'$ K334A	$\beta'$ K334E	$\beta'$ K345A
	IC <sub>50</sub> [ $\mu$ M]					
<b>A1</b>	21.3 $\pm$ 0.1	18.7 $\pm$ 0.9	22.1 $\pm$ 1.8	23 $\pm$ 0.1	21.6 $\pm$ 1.3	16.6 $\pm$ 2
<b>A5</b>	18.8 $\pm$ 1.9	17.9 $\pm$ 1.3	21.7 $\pm$ 3.9	20.5 $\pm$ 2.9	nd <sup>a</sup>	12.2 $\pm$ 0.5
<b>A7</b>	35.4 $\pm$ 0.8	34.8 $\pm$ 2.5	35.3 $\pm$ 2.3	32.8 $\pm$ 5.2	33.6 $\pm$ 0.3	27.5 $\pm$ 4.9
<b>A8</b>	11.6 $\pm$ 0.7	9.4 $\pm$ 1.9	10.3 $\pm$ 0.5	9.9 $\pm$ 0.5	7.7 $\pm$ 0.1	7.3 $\pm$ 1.2
<b>A10</b>	22.6 $\pm$ 0.1	20.7 $\pm$ 0.8	22.1 $\pm$ 0.8	21.5 $\pm$ 1.8	24 $\pm$ 4.7	19.6 $\pm$ 1.6
<b>A11</b>	16.5 $\pm$ 2.9	12.5 $\pm$ 0.1	15.7 $\pm$ 0.6	15.6 $\pm$ 0.8	nd <sup>a</sup>	12.8 $\pm$ 0.3
<b>B2</b>	16.5 $\pm$ 1.3	13.9 $\pm$ 0.7	15.5 $\pm$ 1.5	14.8 $\pm$ 2.4	13.3 $\pm$ 1.5	12.6 $\pm$ 0.5
<b>Myx</b>	0.28 $\pm$ 0.02	5.4 $\pm$ 0.1	0.63 $\pm$ 0.09	0.13 $\pm$ 0.02	0.49 $\pm$ 0.10	> 4
<b>Rif</b>	33.6 $\pm$ 2.3 <sup>b</sup>	> 500 <sup>b</sup>	12.5 $\pm$ 1.6 <sup>b</sup>	21 $\pm$ 0.6 <sup>b</sup>	nd <sup>a</sup>	19 $\pm$ 1 <sup>b</sup>

<sup>a</sup> nd: not determined, <sup>b</sup>: IC<sub>50</sub> [nM]

**Table S4.** Plasmid details. Plasmid pVS10, the pIA-derivatives and MF10 encode the *E. coli* rpoA-rpoB -rpoC [His6] and rpoZ ORFs under control of a T7 promoter (4). Plasmid pRL663 encodes C-terminally hexahistidine-tagged *E. coli* RNAP  $\beta'$  subunit under control of a  $\beta$  tac promoter (5). Plasmid pRL706 encodes C-terminally hexahistidine-tagged *E. coli* RNAP  $\beta$  subunit. under control of a trc promoter (6).

Plasmid	Amino Acid Substitution	RNAP subunit
pVS10	-	-
pIA878	S1322E	$\beta$
pIA879	K334A	$\beta'$
pIA882	K345A	$\beta'$
pIA883	$\Delta$ 334-5	$\beta'$
MF10	K334E	$\beta'$
pRL663 derivative	K345N	$\beta'$
pRL663 derivative	K345T	$\beta'$
pRL706 derivative	V1275M	$\beta$
pRL706 derivative	L1291F	$\beta$

#### 6.1.4 Supplemental references

1. Mukhopadhyay, J., Das, K., Ismail, S., Koppstein, D., Jang, M., Hudson, B., Sarafianos, S., Tuske, S., Patel, J., Jansen, R., Irschik, H., Arnold, E., and Ebright, R.-H. (2008) *Cell* 135, 295–307.
2. J. W. Wells. Analysis and interpretation of binding at equilibrium. In: E. C. Hulme (ed.) *Receptor-Ligand Interactions*, IRL Press, Oxford (1992), 288–349.
3. Döppenschmitt, S., Spahn-Langguth, H., Regårdh C.-G., Langguth, P. (1998) *Pharm. Res.* 15 (7), 1001–6.
4. Belogurov, G.-A., Vassilyeva, M.-N., Svetlov, V., Klyuyev, S., Grishin, N.-V., Vassilyev, D.-G., and Artsimovitch, I. (2007) *Mol. Cell* 26, 117–129.
5. Wang, D., Meier, T., Chan, C., Feng, G., Lee, D., and Landick, R. (1995) *Cell* 81 (3), 341–350.
6. Severinov, K., Mooney, R., Darst, S.-A., and Landick, R. (1997) *J. Biol. Chem.* 272 (39), 24137–24140.
7. Hartmann, H., Liebscher, J. (1984) *Synthesis* 3, 275–276.
8. Fabis, F., Jolivet-Fouchet, S., Robba, M., Landelle, H., Rault, S. (1998) *Tetrahedron* 54, 10789–10800.
9. Foulon, L., Braud, E., Fabis, F., Lancelot, J.-C., and Rault, S. (2003), *Tetrahedron* 59, 10051–10057.
10. Le Foulon, F.-X., Braud, E., Fabis, F., Lancelot, J.-C., and Rault, S. (2005) *J. Comb. Chem.* 7, 253–257.

## 7 Appendix

### 7.1 Curriculum Vitae

#### PERSÖNLICHE DATEN

Name	Martina Frauke Fruth
Geburtsdaten	24.10.1984 in Saarbrücken
Familienstand	ledig
Nationalität	deutsch

#### WISSENSCHAFTLICHER WERDEGANG

02/2011 - 10/2015 **Promotion** unter Anleitung von Prof. Dr. Rolf Hartmann am Helmholtz-Institut für Pharmazeutische Forschung Saarland (HIPS), Abteilung Drug Discovery and Optimization (DDOP), Saarbrücken  
 Titel der Dissertation: „Biophysical and biochemical analysis of protein-ligand interactions in anti-infective drug discovery“

#### AUSBILDUNG

12/2010 **Approbation als Apothekerin**, Saarbrücken  
 05/2010 – 10/2010 **Pharmaziepraktikum**, Fa. Hoffmann-La Roche, Basel  
 Preformulation R&D  
 11/2009 – 04/2010 **Pharmaziepraktikum**, Bellevue-Apotheke, Saarbrücken  
 10/2005 – 09/2009 **Studium der Pharmazie**, Universität des Saarlandes  
 Abschluss: 2. Staatsexamen (Note: 2,0)  
 08/1995 – 06/2004 **Allgemeine Hochschulreife**, Gymnasium am Rotenbühl, Saarbrücken, Abschluss: Abitur (Note: 1,6)

#### MITGLIEDSCHAFTEN

Deutsche Pharmazeutische Gesellschaft DPhG e.V.

## 7.2 Poster presentations

1. Maurer, C. K.\*; Fruth, M.\*, Empting, M.; Herrmann, J., Müller, R.; Dersch, P.; Hartmann, R. W. Discovery of the first small-molecule CsrA-RNA interaction inhibitors as potential anti-infectives using surface plasmon resonance and fluorescence polarization-based screening. *DPhG Annual Meeting* September **2015** “*I3- Interactions, Integrations and Innovations*”. Düsseldorf, Germany.
2. Fruth, M., Sahner, J. H., Plaza, A., Hauptenthal, J., Müller, R., Hartmann, R. W. Discovery of novel RNA polymerase inhibitors targeting the switch region and characterization of the binding mode by saturation transfer difference NMR and INPHARMA. *4<sup>th</sup> International HIPS-Symposium* June **2014** Saarbrücken, Germany.
3. Fruth, M., Sahner, J. H., Plaza, A., Hauptenthal, J., Hartmann, R. W. Discovery of novel RNA polymerase inhibitors targeting the switch region and characterization of the binding mode by saturation transfer difference NMR and INPHARMA. *Discovery Chemistry Congress* February **2014** Barcelona, Spain.
4. Hinsberger, S.; Negri, M.; Groh, M.; Hauptenthal, J.; Fruth, M.; Hartmann, R.W. Development of new, potent bacterial RNA polymerase inhibitors with anthranilate core. *2nd International HIPS-Symposium* June **2012** Saarbrücken, Germany.

## 8 Acknowledgments

Zuallererst möchte ich Prof. Dr. Rolf W. Hartmann aufrichtig danken, für die Möglichkeit diese Arbeit unter seiner Anleitung anfertigen zu dürfen, für die Vergabe des interessanten Dissertationsthemas, für seine Unterstützung sowie den gewährten Freiraum bei der wissenschaftlichen Bearbeitung der Themengebiete.

Des Weiteren möchte ich mich herzlich bei folgenden Personen bedanken, die maßgeblich zum Gelingen dieser Arbeit beigetragen haben:

Prof. Dr. Dr. h.c. Hans H. Maurer für die Übernahme des Koreferats und die wissenschaftlichen Diskussionen im Rahmen der Thesis Committee Meetings.

Dr. Jörg Haupenthal für die Betreuung, die Einarbeitung in molekularbiologische Methoden, seine stets offene Tür und seine Zeit, die er sich genommen hat, mich bei jeglichen Anliegen und Problemen zu unterstützen.

Ich bin Dr. Alberto Plaza zu großem Dank verpflichtet für sein unermüdliches Engagement und seine Expertise, die ausschlaggebend für das Gelingen der ligand-basierten NMR Experimente waren. Außerdem möchte ich ihm herzlich dafür danken, dass er mich stets aufzuheitern wusste und für seine Freundschaft.

Den Mitgliedern des RNAP-Teams für zahlreiche wissenschaftliche Diskussionen und konstruktive Anregungen. Insbesondere möchte ich Dr. Jan Henning Sahner, Dr. Stefan Hinsberger, Dr. Matthias Negri, Dr. Matthias Groh und Walid Elgaher für die erfolgreiche Zusammenarbeit danken.

Dr. Christine Maurer für das super Teamwork und die freundschaftliche Arbeitsatmosphäre im CsrA-Projekt. Zudem möchte ich ihr herzlichst für ihre stete Hilfsbereitschaft und ihren Humor danken, der so manche Rückschläge und Verzögerungen innerhalb des Projekts erträglicher gemacht hat.

Dr. Martin Empting für seine hilfreichen wissenschaftlichen Anregungen, für die Durchführung der Modelling Experimente und für die gute Zusammenarbeit im CsrA-Projekt.

Unseren allzeit hilfsbereiten und gut gelaunten TAs, insbesondere Jeannine Jung und Jannine Ludwig für ihre exzellente Arbeit in der biologischen Wirkstofftestung. Jeannine Jung danke ich zudem für die Einarbeitung in den RNAP Transkriptionsinhibitions-Assay.

Katrin Schmitt, Martina Schwarz und May Küffner für ihre Hilfe bei administrativen und organisatorischen Dingen, sowie Lothar Jager für die schnelle und kompetente Behebung diverser technischer Probleme.

Dr. Martin Frotscher, Dr. Stefan Boettcher, Sebastian Krug und Dr. Elisabeth Weidel für die gute Zusammenarbeit und die tolle Zeit während der gemeinsamen Betreuung des Instrumentelle Analytik Praktikums.

Recht herzlich bedanken möchte ich mich bei meinen lieben Kollegen aus Büro 1.31 sowie darüber hinaus bei allen ‚guten Leuten‘, insbesondere Dr. Christine Maurer, Ines Joachim, Benjamin Kirsch, Dr. Stefan Boettcher, Dr. Kristina Hüsecken, Dr. Martin Empting, Dr. Roman Sommer, Juliette Emmerich, Dr. Nina Hanke, Dr. Marco Gargagno, Andreas Kany und Andreas Thomann für die vielen kleinen Aufheiterungen im Büro- und Laboralltag, die vielen gemeinsamen Unternehmungen, für den guten Zusammenhalt sowie die schöne Zeit während und nach der Arbeitszeit.

Dr. Michael Storz, Dr. Stefan Hinsberger, Dr. Elisabeth Weidel und Michael Zender danke ich für ihren treuen Beistand in allen Lebenslagen, ihre wissenschaftlichen Denkanstöße sowie ihre gute und zuverlässige Freundschaft! Stefan sei zudem gedankt für zahlreiche inspirierende Kaffeepausen und für die großartige Zeit in Barcelona sowie darüber hinaus. Lilli gebührt ein großes Dankeschön für die kompetente praktische Einarbeitung in das Themengebiet der SPR-Spektroskopie sowie für die schöne Zeit in New York. Michael danke ich darüber hinaus für die vielen guten und langen Gespräche bei einem Glas Wein sowie dafür, dass er mich sowohl wissenschaftlich als auch privat gelegentlich durch einen kleinen Schubser auf den richtigen Weg gebracht hat.

Ines Joachim danke ich dafür, dass sie immer sehr bemüht war mich für sportliche Aktivitäten zu motivieren, für ihre Hilfsbereitschaft und die regenerativen kurzen Pausen an der frischen Luft bei aufkommenden Nachmittagstiefs.

Allen jetzigen und ehemaligen Mitgliedern des AK Hartmanns sei gedankt für das sehr angenehme Arbeitsklima, was das Erstellen dieser Arbeit sehr erleichtert hat. Ich werde diese Zeit in schöner Erinnerung behalten.

Ein besonderer Dank geht an Dr. Christine Maurer, Dr. Michael Storz und Dr. Stefan Hinsberger für das aufmerksame Korrekturlesen dieser Arbeit.

Ganz herzlich möchte ich mich außerdem bei meinen Freunden bedanken, insbesondere bei Lena, Neda, Russalina und Eva, die mich jederzeit tatkräftig unterstützt haben, mich stets aufbauten und für die erforderliche Abwechslung sorgten.

Gar nicht genug danken kann ich meiner Mutter Monika, meinem Bruder Michael, sowie Guisi, Giorgia und Amelie für ihre Fürsorge, ihr Verständnis und ihre bedingungslose Unterstützung.

Von Herzen danke ich Christian Brengel, der mir bei allen Sorgen und Problemen beratend zur Seite stand und mir durch seine liebevolle Unterstützung ein sehr großer Rückhalt war.